FORECASTING THE CONSEQUENCES OF THE FAILURE OF THE EASTERN RIM OF CRATER LAKE, MOUNT RUAPEHU

A thesis presented in partial fulfilment of the requirements for the degree of

Master of Science

In

Earth Science

at Massey University, Palmerston North, New Zealand.

MASSEY UNIVERSITY

Emma Phillips

2011

ABSTRACT

A numerical code for simulating dry flows of granular material, Titan2D, was used to model a range of possible collapse scenarios and resulting debris avalanches from a possible failure of the eastern crater rim of Mount Ruapehu, New Zealand. The eastern rim of Crater Lake, Mount Ruapehu consists of a stratigraphic sequence of intercalating volcaniclastic diamictons, pyroclastics and lavas, some of which are highly hydrothermally altered. This rim is under outward pressure from Crater Lake and constitutes one of the steepest parts of the active volcano. Its sudden failure could involve up to 50 million m^3 of rock material, almost certainly generating a debris avalanche and/or a break-out lahar up to 9 times the size of the March 2007 event. A failure of hydrothermally altered flank materials on this side of the volcano has already occurred (c. 4600 yrs Mangaio Fm. (Donoghue & Neall, 2001)). A quantitative hazard and risk analysis of this scenario has never been undertaken, despite ongoing hydrothermal alteration and considerable sapping of both the inside and outside of the rim from explosive eruptions and base surges during the 1995/1996 and 2007 eruptions. New stratigraphic data were integrated with existing high-resolution topographic information and aerial photography to produce a detailed map of the eastern rim to highlight the distribution of contrasting stratigraphic sequences and the distribution of those units with the largest degree of alteration. This information was used as the first step towards defining the likelihood of different failure volumes and geometries to be tested in numerical hazard simulations. A quantitative scenario-based hazard forecast for partial or full collapse of the crater rim and subsequent events was determined. Simulated data of flow run out, inundation, diversion, velocity and mass transport were analysed to identify the resulting hazards for the Whangaehu and Tongariro River catchments. The results of this research suggest that the Mangatoetoenui, Upper Waikato, Tongariro and Whangaehu River catchments could be greatly affected by a sudden collapse of the eastern rim and any subsequent lahar events.

ACKNOWLEDGEMENTS

I would like to sincerely thank Dr. Jon Procter, Dr. Gert Lube and Prof. Shane Cronin for their time, guidance and patience throughout this project. I am grateful to have worked with a bunch of people with such a wide range of expertise.

I am greatly appreciative for the assistance from all of the staff in the Soils and Earth Sciences group who have shared their knowledge, time and skills, especially Kate Arentsen, Prof. Vince Neall, Bob Stewart, Anja Möbis, Mike Bretherton, and Glenys Wallace.

I am grateful to the Geosciences Society of New Zealand, Massey University, and the Tongariro Natural History Society for their financial assistance from the S.J. Hastie Research Award, Massey University Masterate Scholarship and Tongariro Natural History Society Memorial Award.

I would like to thank the Team at GNS Science (Margaret Low, Chris Massey and Graham Hancox) and Harry Keys from DOC for discussion of ideas, and access to publications and photographs.

Thanks to the students of the Earth Science department who assisted in the field, laboratory and who just stopped by to have a talk or laugh. Special thanks to Amanda MacDonald-Creevey and Simon Vale, who have made this journey with me right from first year, for your friendship, humour and competitiveness.

Finally, very special thanks to my family and friends who supported me and took an interest in my studies. Pranil, thanks for your support, encouragement and willingness to climb up Ruapehu with me in the snow when no one else could go. Mum, you kept me focussed and supported me and every way throughout this process and for that I will always be grateful.

TABLE OF CONTENTS

LIST OF FIGURES

LIST OF TABLES

Chapter 1: INTRODUCTION

The eastern rim of Crater Lake, Mount Ruapehu (2797m) consists of a stratigraphic sequence of highly hydrothermally altered deposits of intercalating volcaniclastic diamictons, pyroclastics, and lavas. This rim is under outward pressure from Crater Lake and constitutes one of the steepest parts of the active volcano. The sudden failure of this ~50 million m^3 rim would generate a debris avalanche and/or, a break-out lahar that could be 8-9 times the size of the March 2007 event. Geological evidence shows that a similar failure of hydrothermally altered flank material on this side of the volcano has occurred before (at c. 4600 yrs BP Donoghue & Neall, 2001). A quantitative hazard and risk analysis of this scenario has never been undertaken, despite an apparent increasing likelihood of its occurrence due to ongoing hydrothermal alteration and erosion of the inside and outside of the rim caused by explosive eruptions and wet surges from Crater Lake during 1995/1996 and 2007. The increasingly precarious rim could fail with a range of triggers, including: a new magmatic intrusion, an explosive eruption, increased seismicity, or even elevated pore-water pressure, especially along weak strata.

1.1 Thesis Objectives:

The focus of this study is the eastern rim of Mount Ruapehu's Crater Lake, particularly Pyramid Peak. The main objective of this research was to carry out a quantitative scenario-based hazard forecast for partial or full collapse of the crater rim and the likely subsequent events. The main research aim was to forecast a possible lahar hazard on the Whangaehu and Tongariro River catchments, using computational modelling techniques.

The specific objectives of this study were to:

1) Establish a new detailed map of the stratigraphy of the Eastern Flank (in particular Pyramid Peak)

2) Quantify the 3D geometry, state of alteration and failure conditions of key geologic units composing the eastern rim to define and characterise potential failure blocks.
3) To determine the volumes of collapsing material and define possible scenarios of collapse.
4) Apply the Titan2D flow model to compute flow run out, diversion, inundation, velocity and mass transport collapse volumes, for the range of likely collapse scenarios.

The main outputs of the thesis are:

1) Geological map of research area
2) Simulations of potential debris avalanches.
3) Hazard assessment from collapse scenarios.

1.2 Thesis Structure:

Chapter 1. Introduction

Chapter one contains an introduction to the study area, including the regional geology, volcanic history and a summary of previous work done on the Tongariro Volcanic Centre, in particular Mount Ruapehu.

Chapter 2. Geology of the eastern rim

Chapter two describes the stratigraphy, structure and stability of the eastern rim of Crater Lake. It includes geological maps, cross-sections and defined areas and volumes of possible collapse scenarios to be simulated.

Chapter 3. Titan modelling and parameter testing

Chapter three gives a brief overview of the wide range of computational model types that currently exist to simulate volcanic and non-volcanic mass flows. Detailed information is provided for the Titan2D modelling program used in this study, along with previous examples of Titan2D mass flow simulations. The remainder of chapter three describes initial tests conducted to obtain physical input parameters for the

modelling of debris avalanches at Ruapehu; the results from a systematic series of debris avalanche simulations, as well as their subsequent analysis and interpretation.

Chapter 4. Hazard implications

This chapter examines the possible hazard implications the resulting debris avalanche scenarios will have on the surrounding area, in particular the Whangaehu and Tongariro River catchments.

Chapter 5. Discussion and conclusions

In chapter five the overall study is discussed along with conclusions and ideas for future research.

1.3 Methodology:

Field Work

The initial part of this study involved collecting data from the field between March and May 2010. The exposed stratigraphy of Pyramid Peak was described and photographed. The position of exposures and sample locations were identified using a Garmin eTrex Vista® HCx hand held Geographical Positioning System (GPS), with an accuracy of 5-10 meters, and the NZMS 260 T20 topographical map.

Laboratory Work

Several stratigraphic units contained within the Pyramid Peak complex were systematically sampled. Grain-size analysis was carried out on these samples to determine the percentage of clay using standard sieving techniques and the *Partica* Laser Scattering, Particle Size Distribution Analyser (PSDA). In order to characterise the state of alteration of various stratigraphic units on Pyramid Peak, the types of clay minerals present were determined using X-Ray Diffraction (XRD) analysis.

Geological Mapping

New stratigraphic data collected in the field were integrated with existing high-resolution topographic information and aerial photography, supplied by Graham

Hancox, Institute of Geological and Nuclear Sciences (GNS) and Harry Keys, Department of Conservation (DOC), to produce a geological map and cross-section of the eastern rim complex. The new geological map and cross-section helped highlight the distribution of contrasting stratigraphic sequences and the probable distribution of those units with the largest degree of alteration. This information was used to define the likelihood of different failure volumes and geometries tested in numerical hazard simulations.

Numerical Modelling

Granular continuum computational modelling techniques were applied to simulate a range of initial collapse volumes and locations resulting in multiple debris avalanche scenarios from the eastern rim of Crater Lake, Mount Ruapehu. The flow model used to simulate the collapse scenarios was Titan2D (Patra *et al*., 2005). Titan2D is a free software application developed by the Geophysical Mass Flow Group at the State University of New York (SUNY) at Buffalo. Titan2D was developed for the purpose of simulating granular flows (primarily geological mass flows such as volcanic debris avalanches) over Digital Elevation Models (DEMs) of natural terrain.

Geographic information System (GIS) and software used

The site maps and the geological map of the study area were created using a variety of software. The geological map was created using Arc View (ESRI Inc., 2011) and Adobe Illustrator (Adobe Systems Inc., 2011). The maps created and images used are all displayed using the New Zealand Map Grid (NZMG). The outputs of the Titan2D runs were modified using a text editor, Ultra Edit 32 (IDM Computer Solutions Inc., 2011) and a user created script, PLTPROC and converted to text files. The text files were imported into Arc View and converted into vector points and then into raster files. The output data were displayed with numerous datasets such as: roads, rivers, land use and places. The final maps were then exported as JPG files.

Arc View

Arc View (ESRI Inc., 2011) is a desktop GIS package. In Arc View, geographical spatial data can be both created and analysed, in a vector format. Data can be created in the

form of a point, line or polygon. These data have geographical attributes as well as an attached table, which contains information about geographic characteristics. The data created can be displayed individually or combined and overlaid. Displayed data can be queried and analysed (spatially) to show relationships between different data sets. Arc View can also be used to create and display maps.

Adobe Illustrator

Adobe Illustrator (Adobe Systems Inc., 2011) is a vector-based imaging program. It creates vector graphics made of lines and curves defined by mathematical objects (vectors). This program was used to create a cross-section and the geological map.

Other software

Ultra Edit 32 (IDM Computer Solutions Inc., 2011) and PLTPROC are text file editors, used to modify datasets. TecPlot 360 (Tecplot Inc., 2011) is a Computational Fluid Dynamics (CFD) and numerical simulation software package used in post-processing simulation results. TecPlot 360 was used to create videos of the debris avalanche scenarios simulated by Titan2D.

Imagery and Data sets

The scanned topomap NZMS 260 T20 was the main image used for mapping, digitizing and map display. It was used as a reference and also a backdrop for output maps.

A Digital Elevation Model (DEM) at 20m resolution of the central North Island from Land Information New Zealand (LINZ) was used for image display, but a DEM at 10m resolution was created from contour and spot height data from various Real Time Kinematic Global Positioning system (RTK GPS) surveys to provide more detail of the eastern rim area and the eastern flank area. This was used as an input for Titan2D.

An orthophoto of the eastern crater rim from Massey University and GNS Science was also used; this was acquired during a Light Detection and Ranging airborne laser scan (LiDAR) of Mount Ruapehu. The LiDAR was acquired in April 2007, after the 18th March

dam break lahar, and used in this study as a base image for numerous figures representing the study site and volume scenarios.

1.4 Study Area:

The study area (fig. 1.1) covers ~ 0.6 km^2 of the eastern rim of Crater Lake, Mount Ruapehu. It is bounded by the Crater Lake to the west, the Whangaehu Glacier to the north and the Whangaehu River to the south. The area is generally considered to be Pyramid Peak with an approximate volume of 50 million m^3.

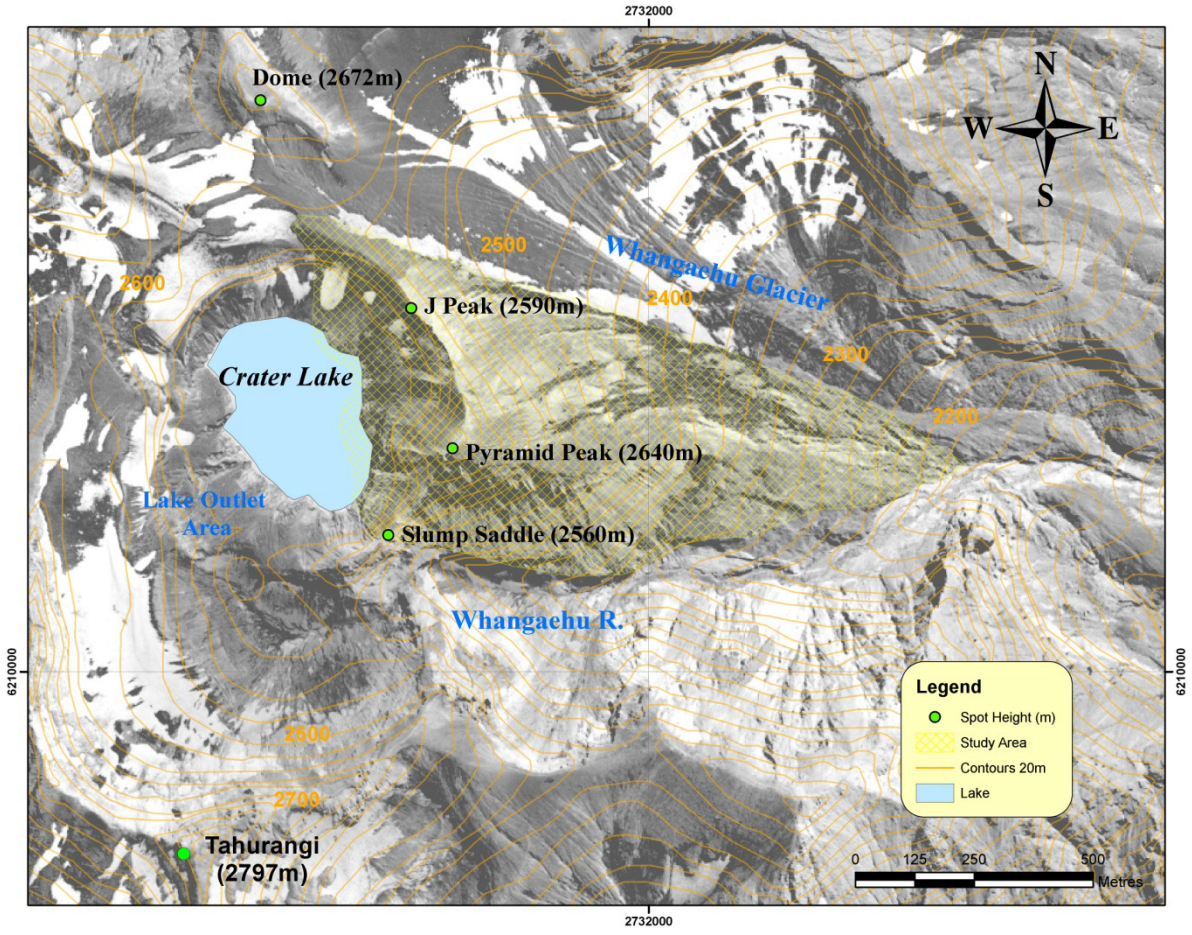

Figure 1.1: Study area, eastern rim complex.

Geography

The main geographic features on the eastern flank of Mount Ruapehu are the Tukino Ski field and village (fig. 1.2), and the Alpine Club (Whangaehu) Hut. The popular 'Round the Mountain Track' (RTMT) along which lies the DOC Rangipo Hut is located at the base of the volcano. Several streams and rivers originate from the eastern flanks of

the volcano; Mangatoetoenui Stream, Upper Waikato Stream, Whangaehu River, Makahikatoa Stream, and Wahianoa River. The first two are upper tributaries for the Tongariro River, which flows north through the township of Turangi before entering Lake Taupo. The Tongariro River is one the most important fishing rivers in New Zealand and is also home to the Tongariro National Trout Centre (DOC, 1999). The Tongariro Power Scheme, which produces 4% of the country's total electricity generation (Genesis Energy, 2010), uses water sourced from Tongariro and Ruapehu volcanoes. A number of power scheme structures are also situated along or near the Tongariro River and State Highway 1, such as the Aqueduct and the Rangipo Power Station and Dam. Two out of the four sections of the Tongariro Power Scheme are situated on the eastern side of Mount Ruapehu: the Eastern Division and Tongariro (Genesis Energy, 2010). In the Eastern Division, water is taken from the Wahianoa River through the Wahianoa Aqueduct (8,400 m long) and is transported eastward under the Whangaehu River and State Highway 1 into the Mangaio Tunnel (Genesis Energy, 2010). The water ends up in the Mangaio Power Station or Lake Moawhango (Genesis Energy, 2010). The Rangipo Dam is situated in the Tongariro section of the Tongariro Power Scheme (Genesis Energy, 2010). The dam is located on the Tongariro River at a head pond. Below the dam is a Blue Duck habitat (Genesis Energy, 2010). The dam is also used for sporting activities. The Rangipo Power Station (120 MW) is situated underground in the Kaimanawa Forest Park (Genesis Energy, 2010). The closest populated area is the township of Waiouru. Waiouru is located southeast of the study area and is the site of the New Zealand Army Helwan Camp and Army Museum. Mount Ruapehu's ring plain is occupied by the Karioi Forest to the south and the Rangipo Desert to the east, which itself is largely occupied by the New Zealand Army. The area north of the Rangipo Desert falls within the Tongariro National Park boundaries. State Highway 1, the main highway of the country, is located east of the ring plain. Mount Ruapehu supports a number of small permanent glaciers and snowfields and has a more extensive snow cover in the winter months (Kilgour *et al*., 2010). The main glacier on the upper eastern flank is the Whangaehu Glacier, which partially retreats over the summer months. Mount Ruapehu is situated in a temperate zone with prevailing westerly winds that gather moisture from the Tasman Sea and travel across the North Island. Mount Ruapehu, Ngauruhoe, and Tongariro are

significant topographic obstructions in the central North Island and receive high amounts of rainfall (~2200 mm/yr) (AMG, 2009). There is a small noticeable rain shadow effect in the Rangipo Dessert on the eastern side of Mount Ruapehu.

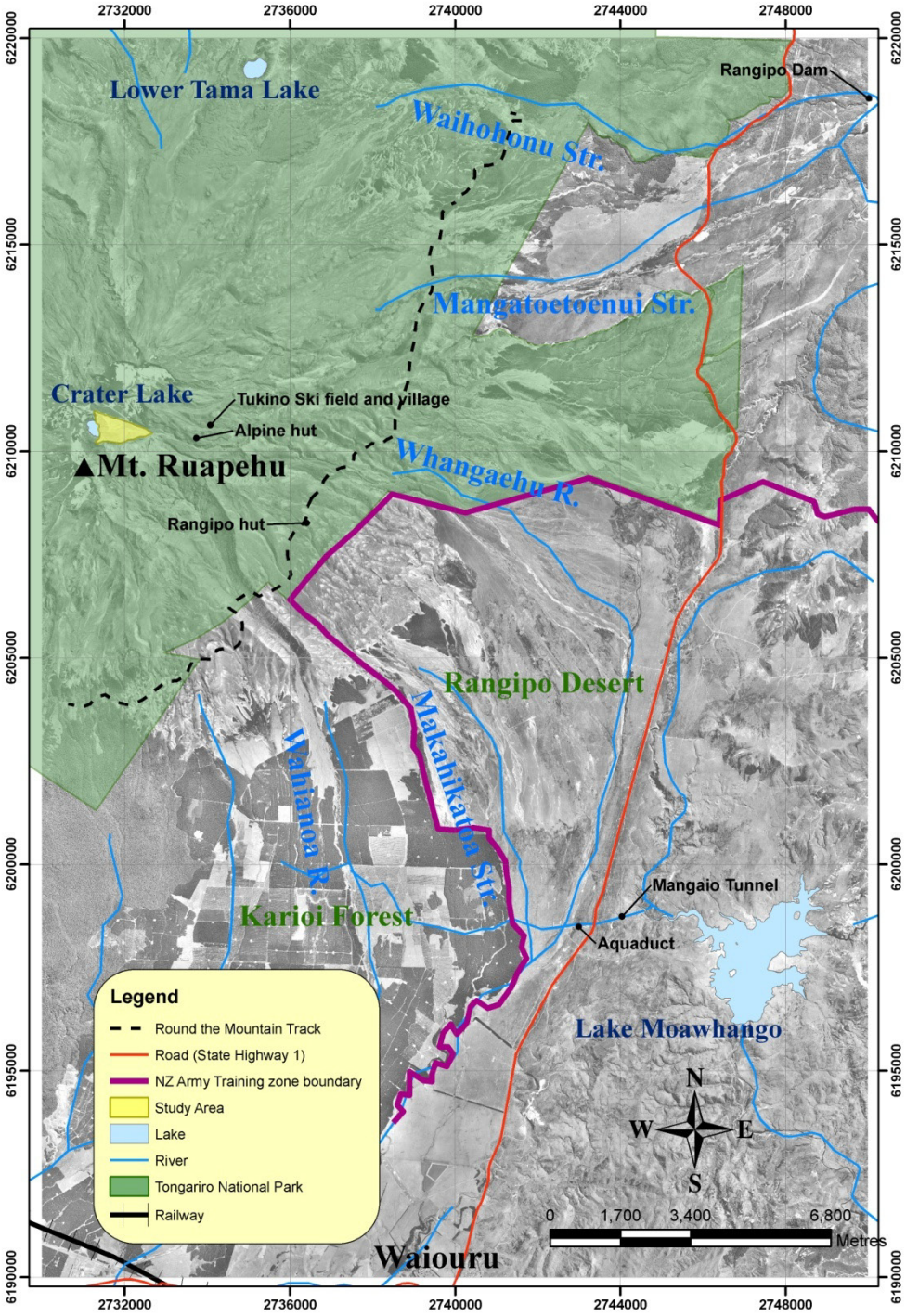

Figure 1.2: Study location and surrounding geography.

In winter there is snow to about 1500 m and annual temperatures vary dramatically between ~25°C and -10°C (AMG, 2009). In the last glaciation (~23-13 ka BP) (Pillans *et al*., 1993), however, the climate in the central North Island of New Zealand was generally drier, colder, and there was an increase in seasonality and extremes of climate (Drost *et al*., 2007).

1.5 Regional Geology:

New Zealand is situated at the boundary between the Pacific and Australian Plates. The geology of the North Island of New Zealand is dominated by its position in relation to the subduction zone, where the oceanic crust of the Pacific Plate to the east is subducting beneath continental crust of the Australian Plate to the west (Cole, 1990; Graham *et al*., 1995). The Hikurangi subduction margin beneath the North Island accommodates oblique motion between the Pacific and Australian Plates (Nicol & Wallace, 2007). This margin occupies the transition from subduction, with backarc extension along the Tonga-Kermadec margin, to continental collision along the Alpine Fault (Nicol & Wallace, 2007). Subduction becomes increasingly oblique to the south until the continental crust (Chatham Rise) of the Pacific Plate is obducted onto the continental crust of the Australian Plate in the zone of transpression under the South Island about 10 km wide (Cole, 1990; Graham *et al*., 1995). Reverse-dextral movement on the Alpine Fault accommodates much of the movement in this zone (Cole, 1990; Graham *et al*., 1995). Due to the clockwise rotation of the forearc there are rapid lateral changes in subduction styles that occur in the central North Island (Reyners *et al*., 2006). This is accommodated in the backarc extension of the Taupo Volcanic Zone (TVZ) in the north and by the compression of the Wanganui Basin in the south (Reyners *et al*., 2006).

Subduction has led to numerous geomorphic and tectonic features in the North Island (fig. 1.3); however the most prominent is the backarc volcanism in the central North Island. This zone of volcanism extends approximately 300 km north-northeast across the North Island from Ohakune to White Island and beyond to the edge of the continental shelf (Graham & Hackett, 1987; Wilson *et al*., 1995).

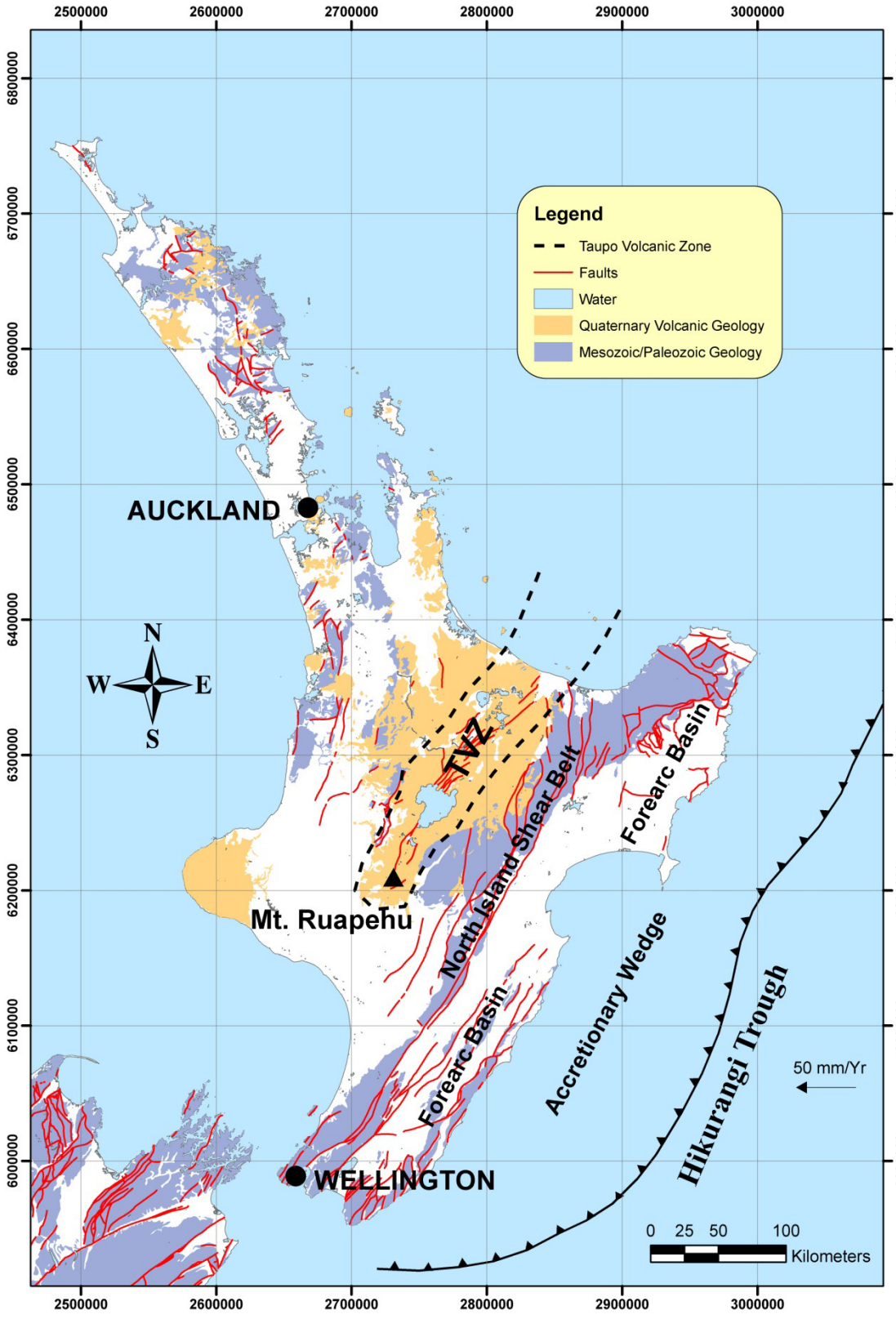

Figure 1.3: Mount Ruapehu's location in the Taupo Volcanic Zone in the Central North Island of New Zealand.

The term Taupo Volcanic Zone (TVZ) is used to describe this north-northeast to south-southwest trending zone of active volcanism, which is up to 50 km wide in the central part and narrows both northwards and southwards (Stern, 1986; Graham & Hackett, 1987; Cole, 1990). Wilson *et al*. (1995) defined the TVZ as the area enclosed by an envelope drawn around all caldera structural margins and individual vent sites associated with the north-northeast to south-southwest orientated Kermadec subduction system. The TVZ is the principal location of the Late Pliocene and Quaternary volcanic activity in New Zealand (Wilson *et al*., 1995; Villamor & Berryman, 2001; Allan *et al*., 2008) (fig. 1.4), and is said to encompass the active portion of a wedge-shaped area of dominantly Quaternary rhyolitic-andesitic volcanism termed the Central Volcanic Region (CVR) (Graham *et al*., 1995). The CVR was geologically defined by the area of preserved ignimbrites deposits, yet this area does not reflect either their original extent or include any defined vent areas (Wilson *et al*., 1995). The most obvious section of the volcanic arc is at the southern (Tongariro Volcanic Centre) propagating tip of the TVZ represented by the young andesitic and basaltic volcanism. Arc expression is the least obvious in the east, which is mainly represented by dacitic volcanism (Cole, 1990). Backarc basin volcanism occurs dominantly in the central section of the TVZ and is comprised of bimodal rhyolite and high-alumina basalt eruptives (Cole, 1990).

The present day TVZ began around 2 Ma with early andesitic volcanism (Rowland *et al*., 2010). This was accompanied and swamped by intensive and volumetrically dominant rhyolitic activity from 1.6 Ma onwards (Wilson *et al*., 1995; Rowland *et al*., 2010). At this time the central portion of the TVZ was the largest and most frequently active rhyolitic magmatic system on Earth (Wilson *et al*., 1995), producing up to 15,000 km^3 of rhyolitic magma (Allan *et al*., 2008).

1.6 Tongariro Volcanic Centre:

The Tongariro Volcanic Centre (TgVC) is located at the southern end of the Taupo Volcanic Zone (TVZ) (fig. 1.4) and includes four large predominantly andesitic volcanoes: Kakaramea, Pihanga, Tongariro (including Ngauruhoe) and Ruapehu (Cole,

1990; Cassidy *et al*., 2009). The TgVC also includes a number of eroded centres (Mangakatote and Hauhungatahi), a satellite cone and associated flows (Pukeonake) and four craters near Ohakune (Cole *et al*., 1986; Graham & Hackett, 1987; Cole, 1990; Cassidy *et al*., 2009). The large volcanoes are surrounded by a ring plain constructed mainly of re-deposited volcaniclastic material (Cole *et al*., 1986; Cole, 1990; Donoghue *et al*., 1995). The regional basement is metamorphosed greywacke of Mesozoic age (Cassidy *et al*., 2009).

Structurally, Pihanga, Kakaramea and older Tongariro vents define an old northwest-trending lineament. The younger multiple vents of Tongariro and Ruapehu define a north-northeast-trending lineament which parallels the present day regional trend of the Taupo fault belt (Graham & Hackett, 1987). The main structural control on recent vent location is a system of high-angle normal faults, which extend to the Bay of Plenty (Graham & Hackett, 1987). Active faults in the TgVC are all normal, with fault planes usually dipping towards eruptive centres (Cole, 1990). There are three major structures in this region: the north northeast trending Mount Ruapehu Graben; the east-west to east southeast-west northwest-trending Ohakune-Raetihi Fault set; and the northeast-trending Karioi Fault set (Villamor & Berryman, 2006). The Mount Ruapehu Graben is situated at the southern end of the modern Taupo Rift, and has been created as a result of backarc extension related to the Hikurangi subduction margin (Villamor & Berryman, 2006). The extension rate in this area is estimated to be around 2.3±1.2 mm/yr (Villamor & Berryman, 2006). The other two structures strike perpendicular to the Taupo Rift at the southern end (Villamor & Berryman, 2006). The complicated structure in the southern end of the Taupo Rift is related to the block rotations in the Hikurangi subduction margin (Villamor & Berryman, 2006).

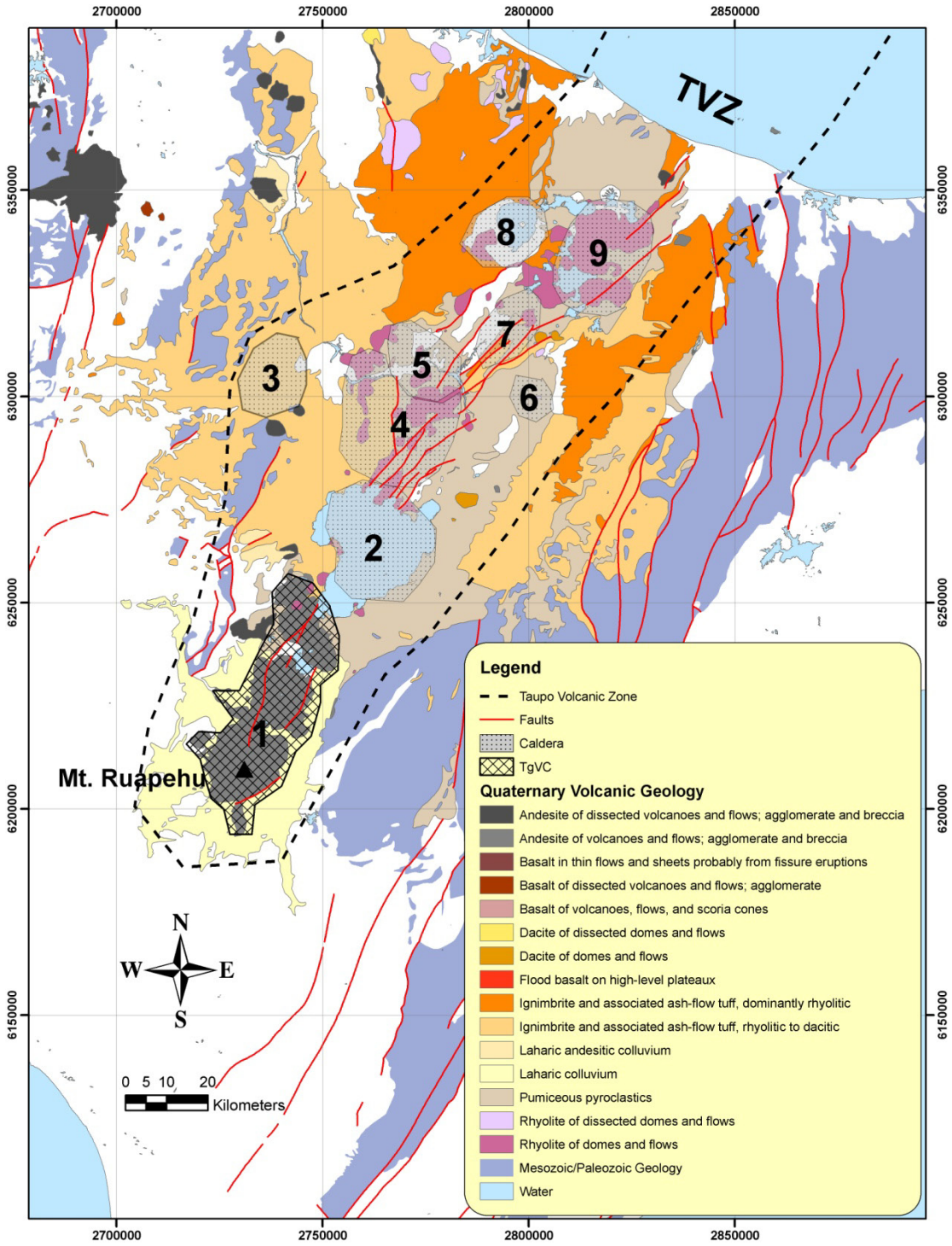

Figure 1.4: Quaternary volcanic geology of the Taupo Volcanic Centre. Volcanic centres and calderas: 1-Tongariro, 2-Taupo, 3-Mangakino, 4-Whakamaru, 5-Maroa, 6-Reporoa, 7-Kapenga, 8-Rotorua, 9-Okataina. Derived from Wilson *et al*. (1995).

There is no certainty about the maximum age of the TgVC; however, the oldest materials that have been dated are pebbles of andesite that were found in the Lower Pleistocene conglomerates in the marine sequences of the Wanganui District dated at

c. 1.7 Ma (Cole *et al*., 1986; Williams, 1986, Donoghue, 1991). The next oldest dates are that of lavas from Tongariro (0.27 Ma) (Cassidy *et al*., 2009), Ruapehu (0.3 Ma) (Gamble *et al*., 2003), and Kakaramea (0.22 Ma) (Cole *et al*., 1986). The TgVC is still very active today with the latest phreatomagmatic eruption occurring at Crater Lake, Ruapehu in 2007 (Lube *et al.*, 2009; Christenson *et al.*, 2010).

Tongariro volcano is a complex of cones and craters that comprise 17 volcano-stratigraphic units (Cassidy *et al*., 2009). The youngest and most active of which is Ngauruhoe (around 4.7 ka BP onwards) (Möbis, 2010), with the latest eruption occurring in 1976 (Donoghue, 1991). The oldest units of Tongariro volcano are dated from 275 ka (Hobden *et al*., 1996), and are exposed in the Tama Lakes area (Cassidy *et al*., 2009). The massif has been divided by older (> 20 ka) and younger (< 20 ka) lavas (Cole *et al*., 1986). The older group is represented by lavas that have been greatly eroded and show little original topographic expression (Cole, 1978). The younger group erupted from a series of vents trending NNE-SSW. The major period of explosive activity was around 9.7 ka, with eruptions from Tama Lakes, Blue Lake and North Crater, producing Mangamate Tephra and several flows (Nairn *et al*., 1998). The most recent activity has been from Te Mari, Red Crater and Ngauruhoe (Cole, 1978; Cole *et al*., 1986).

Other vents in the TgVC include Maungakatote, Pukeonake, and Hauhungatahi. Maungakatote is located around 10-15 km WNW of Lake Rotoaira, and is made up of two coalescing cones, Maungakatote and Maungaku (Cole *et al*., 1986). The two cones are considered to be partly younger than 0.32 Ma (Cole, 1978). 5.6 km west of Ngauruhoe lays a 143 m high scoria cone, Pukeonake (Cole *et al*., 1986). Pukeonake lies on an N-S trending fissure and has produced voluminous lava flows that cover an area of 55 km^2 to the west of the cone (Cole, 1978). The Kawakawa tephra (27±0.9 ka) (Lowe *et al*., 2008) that mantles the scoria cone suggest that Pukeonake was formed before ~27 ka (Cole *et al*., 1986). Hauhungatahi is situated 12 km NW of Ruapehu. The low eroded cone overlies Miocene marine siltstones and is thought to be one of the oldest vents within the TgVC, around 0.5 Ma or older (Cole, 1978; Cole *et al*., 1986). The Ohakune Craters are the southernmost vents of the TgVC and occur 19 km SW of

Ruapehu, near Ohakune. Two explosion craters, now occupied by the Rangatau Lakes, are located 4.5 km SW of Ohakune. 1 km NW of Ohakune lay at least five craters (Cole, 1978; Cole *et al*., 1986).

The TgVC lavas range in composition from basalt to dacite (53-63% SiO_2), with the bulk being andesite (Cole *et al*., 1986; Gamble *et al*., 2003). The lavas are nearly all porphyritic and are not considered to be truly representative of a magmatic liquid, meaning there may be mixing between magmas (Gamble *et al*., 1999). This was concluded due to the lavas containing glomercrysts, igneous nodules, disequilibrium phenocryst assemblages, or xenoliths (Cole *et al*., 1986; Gamble *et al*., 1999). Price *et al*. (2005) suggests that the andesite lavas are generated through the interaction of mantle-derived magmas with lower crustal melts.

1.7 Mount Ruapehu:

Mount Ruapehu is a large andesitic stratovolcano associated within a convergent plate boundary, and is the largest composite volcano within the central North Island of New Zealand (Graham & Hackett, 1987; Hackett & Houghton, 1989; Kilgour *et al*., 2010). Ruapehu has been active since ~300 ka (Gamble *et al*., 2003), producing voluminous lava, tephra and lahars (Graham & Hackett, 1987). The eruptive styles have ranged from subplinian, strombolian, phreatomagmatic, vulcanian and dome-related explosive eruptions, to extrusion of lava flows and domes (Hackett & Houghton, 1989). The oldest age (0.3 Ma) for the volcano was recorded from Te Herenga Formation lavas in the Whakapapanui gorge (Gamble *et al*., 2003). The volcano rises to an elevation of 2797 m and is comprised of a series of overlapping craters that have been active at various times during the Holocene (Hackett & Houghton, 1989; Kilgour *et al*., 2010). Four major cone-building episodes have occurred from a variety of summit, flank and satellite vents over the 300 ka. Four formations have been correlated with each episode and named by Hackett (1985) and are displayed in table 1.1 below. From oldest to youngest the formations are Te Herenga, Wahianoa, Mangawhero, and Whakapapa (fig. 1.5) (Graham & Hackett, 1987; Hackett & Houghton, 1989), with contacts between each formation being unconformable (Cole *et al*., 1986).

Formation	Approximate age (ka)	Estimated original volume (km^3)	Location of vents	Composition	Approximate output rate (km^3/ka)
Whakapapa	0 – 15	2.6	Summit and flanks of modern cone	Andesite-dacite (57-66% SiO_2)	0.17
Mangawhero	15 – 60	35	Summit region of Ruapehu	Basalt to dacite (52-64% SiO_2)	0.78
Wahianoa	60 – ~134	45	SE quadrant of Ruapehu	Andesite (54-61% SiO_2)	0.75
Te Herenga	> 120 – ~300	65	N and NW Ruapehu	Andesite (54-59% SiO_2)	<0.50

Table 1.1: Lithostratigraphy of Ruapehu composite volcano after Hackett and Houghton (1989) and ages after Gamble *et al*. (2003).

Te Herenga Formation is the oldest at around ~300 ka (Gamble *et al*., 2003), consisting of lava flows, autoclastic breccias, plugs and dikes exposed principally on the north-western flank of Ruapehu (Hackett & Houghton, 1989). The eroded Wahianoa Formation (*ca*. 60 - ~134 ka (Gamble *et al*., 2003)) is exposed on the south-eastern side of Ruapehu. It contains lava flows, autoclastic breccias and lahar deposits. Mangawhero Formation (*ca*. 15 - 60 ka) forms the present high peaks and main cone of Ruapehu and it predominately comprises lavas and pyroclasts. Whakapapa, the youngest formation (*ca*. < 15 ka), has been erupted from six vents across the massif (four flank and two summit vents) and is characterized by young block lavas, autoclastic breccias and pyroclastic units (Hackett & Houghton, 1989).

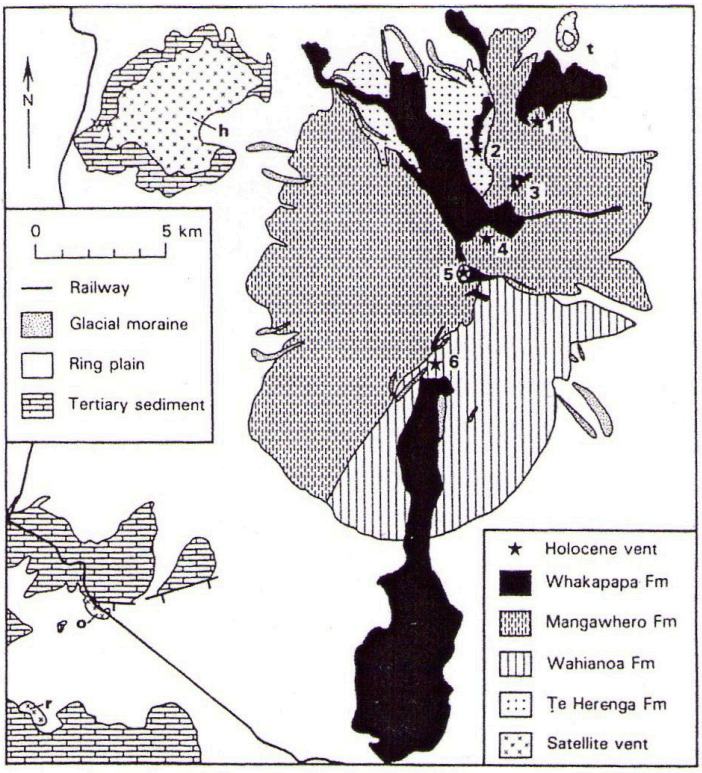

Figure 1.5: Sketch map of the geology of Mount Ruapehu and proximal surrounding area (Hackett & Houghton, 1989). *t* Lower Tama Lake, *h* Hauhangatahi, *o* Ohakune craters, *r* Rangitau Lakes. ★Holocene vents: 1) Tama, 2) Pinnacle Ridge, 3) Tama, 4) Iwikau, 5) Crater Lake, and 6) Rangataua.

The volcanic complex is made up of two parts: a composite cone 110 km^3 in volume, surrounded by an equally voluminous ring plain of ~100 km^3 (Hackett & Houghton, 1989). Cone-forming sequences are dominated by sheet and autobrecciated lava flows, which seldom reach the ring plain (Hackett & Houghton, 1989). The ring plain is composed of lahar and debris avalanche deposits (Palmer, 1991; Palmer *et al*., 1993; Cronin *et al*., 1996; Lecointre *et al*., 1998; Donoghue & Neall, 2001), medial to distal pyroclastic fall (Topping, 1973; Donoghue & Neall, 1996; Donoghue *et al*., 1997), and material fluvially reworked from the cone. Lavas and pyroclastic rocks from Ruapehu range from porphyritic basaltic andesites, andesites and rare dacites (Gamble *et al*., 2003). The phenocryst assemblage of these rocks is dominated by plagioclase, with minor components of clinopyroxene and orthopyroxene and Fe-Ti oxides (Gamble *et al*., 2003). Both olivine and amphibole are rare, but are not entirely absent from Ruapehu lavas and tephras (Gamble *et al*., 2003). Ruapehu is a dynamic volcanic-sedimentary system, characterised by high accumulation rates and by rapid lateral and vertical changes in facies (Hackett & Houghton, 1989). Four distinctive associations of

lithofacies have been defined by Hackett and Houghton (1989): (1) the central and flank vent, (2) the proximal cone, (3) the distal ring plain, and (4) the satellite vent associations. These are described in table 1.2 below.

Association	Principal lithofacies	Minor lithofacies	Other notable features
Central and flank vent	Irregular lava domes and plug like intrusions – welded fall deposits – vent breccias	Thin lavas – lahar deposits	Tectonically oversteepened dips – alteration
Proximal cone-building	Massive and autobrecciated lava flows – lahar deposits	Fall tephra – reworked sediments – dikes – block and ash flow deposits	Complex gully-filling morphology – numerous apparent stratigraphic inversions
Distal ring plain	Hyperconcentrated and normal stream deposits – lahar deposits – fall deposits	Debris avalanche deposits – lava flows - loess	Fall deposits strongly wind-influenced
Satellite vent	Strombolian bomb beds – phreatomagmatic surge and fall deposits – aa lava flows	Reworked sediments – distal fall deposits from composite volcano	Relatively primitive chemical composition

Table 1.2: Lithofacies associations for Ruapehu composite volcano, Derived from Hackett and Houghton (1989) page 55, table 2.

Despite the volume and complexity of volcaniclastic material of Mount Ruapehu's ring plain, it was not initially studied in any detail. More in depth studies of the ring plain by Topping (1973), Donoghue (1991), Hodgson (1993), Palmer *et al*. (1993), Cronin (1996), and Lecointre *et al*. (1998) have found that the ring plain contains a more complete record of the eruptive history of Ruapehu than the volcanic cone itself.

The north-western ring plain of Ruapehu was mapped in detail by Cronin and Neall (1997). Using rhyolitic and andesitic cover-bed stratigraphy Cronin and Neall (1997) defined 15 lahar episodes in the north-eastern Ruapehu ring plain, which ranged in age from > 65-5 ka. They linked two main periods of lahar and fluvial aggradation (c. 75-65 ka and 23-14 ka) with the two coolest periods of the Last Glacial (marine $\delta^{18}O$ stages 4 and 2). It is suggested that the increase in lahar generation was conditioned by a

greater sediment supply and an increased availability of water, which was provided by the cool and stormy climate during these periods (Cronin & Neall, 1997). These lahars could have been triggered by a range of mechanisms such as: sudden Crater Lake rim collapse, releasing large amounts of water inducing debris flows; flank collapse of hydrothermally altered and unstable portions of the cone; phreatic and phreatomagmatic eruptions, generating snow slurry lahars and hyperconcentrated flows; and eruptions that generate large volumes of tephra on snow and ice covered slopes, later remobilized by intense rainfall (Lecointre *et al*., 2004).

Cronin and Neall (1997) discovered that the distribution of lahars on the North-eastern ring plain of Ruapehu was strongly influenced by two events occurring between 23-14.7 ka. Around 23 ka, a large lava flow was emplaced between the present Waihohanu and Oturere Stream separating the eastern Tongariro and Ruapehu ring plains (Cronin & Neall, 1997). Subsequently, during the Last Glacial Maximum, moraines were emplaced along the Upper Whangaehu and Mangatoetoenui valleys, blocking lahars from the upper eastern flanks of Ruapehu to the ring plain between the Upper Waikato and Te Piripiri Streams (Cronin & Neall, 1997). Lahars generated on the eastern flanks of Ruapehu since 14.7 ka have therefore been channelled either to the northeast into the Mangatoetoenui or southeast down the Whangaehu Catchment (Cronin & Neall, 1997). Based on the stratigraphy of the ring plain Cronin and Neall (1997) devised an eruptive history of Ruapehu:

- 75 to 64 ka: moderately frequent (1 per 600 years) large volume and large magnitude eruptions and frequent low volume and low magnitude eruptions
- 64 to 35.8 ka: very low frequency (1 per 7,000 years) large volume and large magnitude eruptions and frequent low volume and low magnitude eruptions
- 35.8 to 22.5 ka: moderate-low frequency (1 per 800 years) large volume and large magnitude eruptions
- 22.5 to 10 ka: moderately frequent (1 per 500 years) large volume and large magnitude eruptions
- 10 ka: 1 large volume and large magnitude eruption including a pyroclastic flow
- 10 to 0.97 ka: infrequent, low volume and low magnitude eruptions

- 0.97 to 0.25 ka: infrequent, low volume and low magnitude eruptions
- 0.25 to 0.18 ka: infrequent, low volume and low magnitude eruptions
- 1800 years ago to present: Frequent (1 every 100 years) low volume and low magnitude eruptions.

The south-eastern ring plain of Ruapehu was mapped in detail by Donoghue (1991). A chronology and stratigraphy of the Late Quaternary volcaniclastic sequences were determined using interbedded local andesitic tephras and distal rhyolitic tephras (Donoghue & Neall, 2001) (table 1.3). The lahar deposits, which dominate these sequences, could be dated back to c. 22,400 yrs BP (Donoghue & Neall, 2001) (fig. 1.6). Five formations were mapped across the south-eastern ring plain: Onetapu Formation (c. 1,850 yrs BP to present), Manutahi Formation (c. 5,370-3,200 yrs BP), Mangaio Formation (4,600 yrs BP), Tangatu Formation (c. 14,700-5,400 yrs BP), and Te Heuheu Formation (>22,600-14,700 yrs BP) (Donoghue & Neall, 2001). Each formation represents periods of aggradation.

Volcanism at Ruapehu has been documented since 1861 (Hancox *et al*., 1997). This activity has consisted of very frequent, relatively small-to-medium phreatic and phreatomagmatic eruptions (e.g. 1895, 1969, 1971, 1975, 1978, 1979, 1980, 1981-1982, 1985, 1987, 1988, 2007) (Gregg, 1960; Houghton *et al*., 1987; Kilgour *et al*., 2010), and more prolonged magmatic eruptions such as occurred in 1945 and 1995-1996 (Nakagawa *et al*., 1999; Cronin *et al*., 2003). Destructive lahars have also accompanied the 1969, 1971, 1975 and 1977 eruptions (Hackett & Houghton, 1989). At least five vents have been active on Ruapehu during the Holocene; however, historically the activity has been confined to the southern crater which is occupied by a hot, acidic crater lake (Christenson & Wood, 1993).

Tephra Layers	Source*	Age (Ka)	Reference to age
Ngauruhoe Tephra	TgV	c. 1.8-0†	Donoghue (1991)
Taupo Tephra (Unit Y)	TVC	1.85‡	Froggatt & Lowe (1990)
Mangatawai Tephra	TgV	2.5-1.85‡	Donoghue (1991)
Waimahia Tephra (Unit S)	TVC	3.3‡	Froggatt & Lowe (1990)
Hinemaiaia Tephra (Units I-R)	TVC	5.2-3.95‡	Wilson (1993)
Motutere Tephra (Units G-H)	TVC	5.8-5.3‡	Wilson (1993)
Mangamate Tephra (Mm), Poutu Lapilli	TgV	c. 9.7†	Topping (1973)
Mm, Wharepu Tephra	TgV	c. 9.7†	Topping (1973)
Poronui Tephra (Unit C)	TVC	9.81‡	Froggatt & Lowe (1990)
Mm, Ohinepango Tephra	TgV	c. 9.7†	Topping (1973)
Mm, Waihohonu Lapilli	TgV	c. 9.7†	Topping (1973)
Mm, Oturere Lapilli	TgV	9.78‡	Topping (1973)
Karapiti Tephra (Unit B)	TVC	10.1‡	Wilson (1993)
Pahoka Tephra	TgV	c. 10-9.8†	Topping (1973)
Bullot Formation (Bt), Pourahu Member	RV	c. 10†	Donoghue (1991)
Waiohau Tephra	OVC	11.85‡	Froggatt & Lowe (1990)
Rotorua Tephra	OVC	13.08‡	Froggatt & Lowe (1990)
Rotoaira Tephra	TgV	13.8‡	Topping (1973)
Rerewhakaaitu Tephra	OVC	14.7‡	Froggatt & Lowe (1990)
Kawakawa Tephra	TVC	22.59‡	Wilson (1993)
Okaia Tephra	TVC	c. 23†	Froggatt & Lowe (1990)
Omataroa Tephra	OVC	28.22‡	Froggatt & Lowe (1990)
Hauparu Tephra	OVC	35.87‡	Froggatt & Lowe (1990)
Rotoehu Ash	OVC	64§	Wilson (1993)

Table 1.3: Tephra marker beds. Derived from Cronin *et al*. (1997).
*TgV = Tongariro volcano, Rv = Ruapehu volcano, TVC = Taupo Volcanic Centre, OVC = Okataina Volcanic Centre. †Estimated ages. ‡Average or single ^{14}C ages on old half-life basis. §Whole rock K-Ar age.

The Crater Lake on Mount Ruapehu has been a feature of the volcano since observations started in 1897; the only exceptions were a brief disappearance in 1945 during a period of extrusive magmatic activity (Christenson & Wood, 1993) and following the 1995 eruptions (Cronin *et al.,* 2003). Since its reestablishment in 1946 it has been a source of numerous phreatic and phreatomagmatic events (Christenson & Wood, 1993). Crater Lake is oval in shape, has a ~500 m diameter and an area of 0.2 km^2. The main overflow discharge from the lake occurs at a single outlet, forming the head waters of the Whangaehu Stream (Christenson & Wood, 1993). Recently recorded bathymetry found the lake to be 134 m deep with an estimated volume of 9.0 million m^3 (Christenson & Wood, 1993).

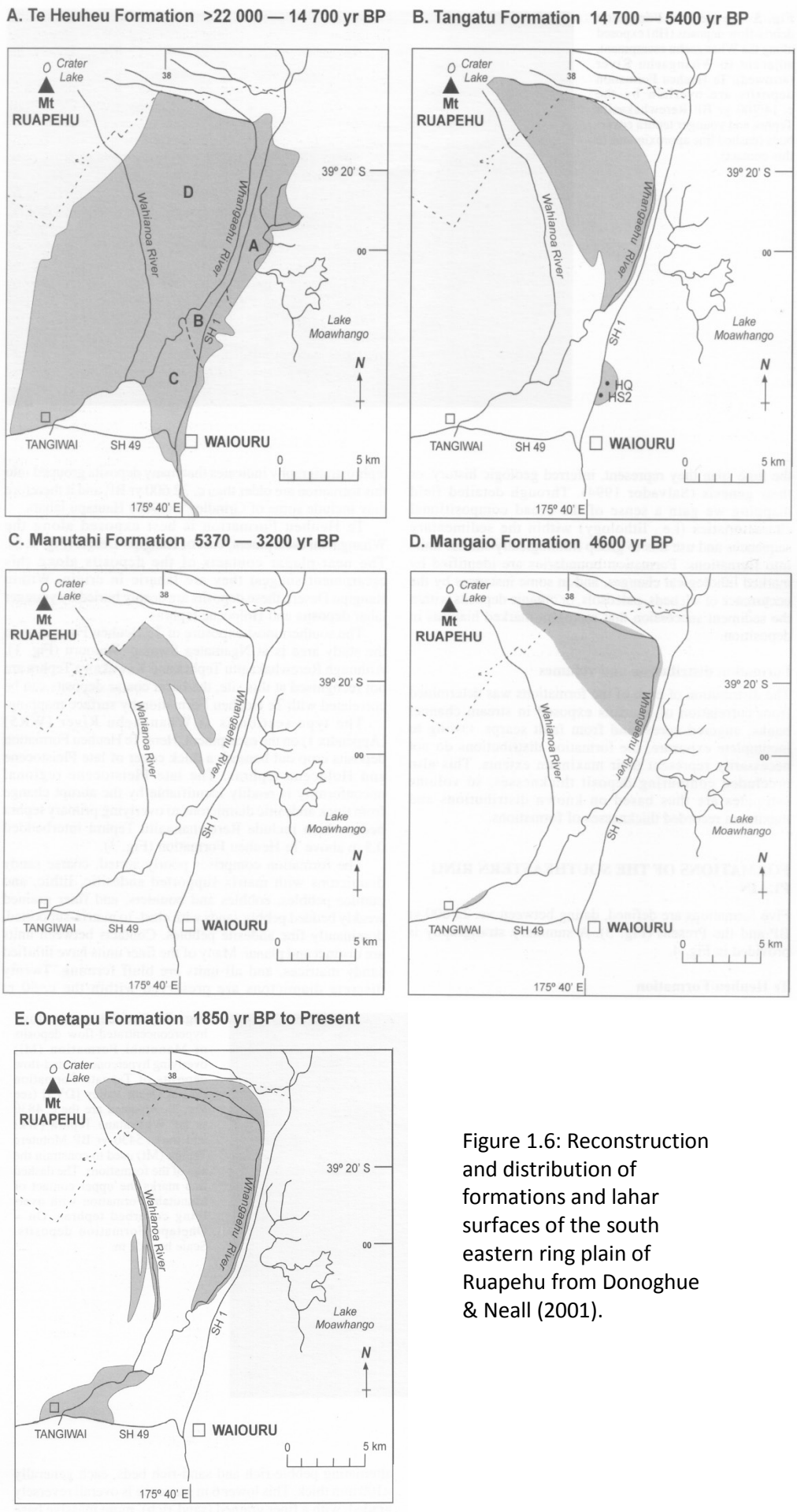

Figure 1.6: Reconstruction and distribution of formations and lahar surfaces of the south eastern ring plain of Ruapehu from Donoghue & Neall (2001).

1.8 Debris avalanches

Eruptions from Ruapehu and resulting hazards (including pyroclastic surges and ballistic fallout) can be disruptive and life threatening to those in the proximal area such as skiers, trampers, and climbers. However, other hazards such as lahars, debris flows, and debris avalanches can reach further distances and have the potential to affect areas well outside the Tongariro National Park boundaries. These hazards may also occur without any volcanic activity. Debris avalanches also have the potential to transform downstream into other types of granular-fluid mass flows by entraining water and/or sediment. The devastation these hazards can cause is demonstrated by the loss of 151 lives in 1953 when a lahar took out the rail bridge over the Whangaehu River at Tangiwai, resulting in a train plunging into the river (O'Shea, 1954).

Debris avalanches are recently recognised volcanic phenomena (Ui *et al*., 2000). Although they were observed and recorded during the 1888 eruption of Bandai in Japan and the 1956 eruption of Bezymianny in Kamchatka. Only after the collapse of the northern sector of Mount St. Helens, and subsequent avalanche deposition in May 1980, was the role of debris avalanches in the evolution of a volcano recognised (Siebert *et al*., 1987; Palmer *et al*., 1991; Ui *et al*., 2000). Before then, debris-avalanche events and deposits had been studied for nearly a century; however, they were often misinterpreted as lahar deposits, pyroclastic flows, lava flows and even glacial moraines (Palmer *et al*., 1991; McGuire, 1996; Ui *et al*., 2000).

A debris avalanche can be defined as the rapid movement of an incoherent, unsorted mass of material mobilised by gravity that originates from the collapse of a volcanic edifice (Palmer & Neall, 1989). The most significant geomorphic feature of debris avalanche deposits is hummocky topography (Siebert *et al*., 1987; Ui *et al*., 2000). The shape of hummocks is variable and irregular; however, the volume and height of hummocks are typically larger in proximal and medial parts of the deposit and decrease towards the distal reaches (Siebert *et al*., 1987; Ui *et al*., 2000). Other diagnostic features of debris avalanches include levees, marginal and distal cliffs, and an amphitheatre at the source (Ui *et al*., 2000). Debris avalanche deposits are composed of debris-avalanche blocks that are transported relatively intact from source

and a matrix, which occurs both within and between debris-avalanche blocks (Palmer & Neall, 1989). Debris avalanche deposits often show lithological and textural zoning pointing towards an incomplete mixing of blocks and matrix proportions during transport (Palmer & Neall, 1989). Avalanche blocks are also strongly fractured and broken. However, individual pieces of a block are often found in close proximity resulting in a 'jig-saw' fracture pattern (McGuire, 1996; Ui *et al*., 2000). The debris avalanche matrix consists of a mixture of smaller volcanic fragments derived from various parts of the source volcano (Ui *et al*., 2000). The matrix material is a result of the collision and fragmentation of the debris avalanche blocks. Materials from other sources (e.g. fluvial gravels, soil layers, and basement rock) are often found to be entrained into the primary debris avalanche matrix (Ui *et al*., 2000). It is the resulting deposit of large avalanche blocks surrounded by a matrix of various materials that creates the characteristic hummocky terrain (Ui *et al*., 2000).

Based on the variable observed processes that form them, three types of debris avalanches are distinguished: Bezymianny, Bandai, and Unzen (Siebert *et al*., 1987; Ui *et al*., 2000). Bezymianny-type debris avalanches are associated with magmatic eruptions (e.g. Mount St. Helens), while Bandai-type debris avalanches occur in conjunction with phreatic eruptions. Unzen-types are not directly related to volcanic activity but are a result of a collapse triggered by an earthquake or other non-volcanic trigger mechanisms (Ui *et al*., 2000). Unstable portions of an edifice may fail in response to internal and external triggers; including magmatic intrusion, overloaded steep slopes, seismic activity, edifice spreading, and precipitation (McGuire, 2003).

The dynamic processes that occur after failure are poorly understood and have only been inferred from analysis of the debris avalanche deposit or from experimental studies (Thompson *et al*., 2010). Currently debris avalanches are suggested to evolve from a stage of initial block sliding involving horst and graben-type extension, to more chaotic conditions further from source as initial material disaggregates and other materials are entrained (Thompson *et al*., 2010). Overall emplacement is interpreted to be non-turbulent as original stratigraphy relationships and fragile jigsaw fracture blocks are generally retained (Thompson *et al*., 2010).

The volume of well-documented debris avalanche deposits varies largely and by many orders of magnitudes from less than 10^{-4} km^3 to several 10s of km^3 (e.g. Hayashi & Self, 1992). Interestingly, a negative correlation exists between the apparent friction of debris avalanches (often expressed as the ratio of fall height to run out distance) and avalanche volume (e.g. Dade & Huppert, 1998; Legros 2002). The relationship is similar to that found for the case of non-volcanic long-runout landslides (Heim 1932) and has provoked a number of models and theories to explain this apparent reduction in flow resistance. These include specific mechanisms potentially responsible for a reduction of bulk flow resistance (e.g. air fluidization, acoustic fluidisation, basal self-lubrication, mechanical fluidization to name a few (Ui *et al*., 2000)) as well as largely contrasting rheological models (including Bingham models and rapid granular flow models). Many workers have used these models and theories (or a combination of them) to interpret specific geometric and sedimentological characteristics of debris avalanche deposits. However, none of these attempts can sufficiently explain all aspects of debris avalanche transport (Ui *et al*., 2000).

Early workers (Gibson & Morgan, 1927; Grange, 1931; Gregg, 1960) in New Zealand recognised that surrounding the two major andesitic stratovolcanoes of Taranaki and Ruapehu was an extensive apron of volcaniclastics. Sections of these aprons or ring plains had distinctive mounds known as hummocks and were recognised as having been emplaced by a gravity-flow mechanism (Palmer *et al*., 1991). After the 1980 Mount St. Helens event, several of the New Zealand ring plain deposits were reinterpreted and as a result a genetic relationship between debris avalanches and lahars in a collapse event was found (Palmer *et al*., 1991).

The Quaternary deposits of volcanic debris avalanches in New Zealand are confined to four andesitic stratovolcanoes: White Island, Tongariro, Ruapehu and Taranaki (Palmer *et al*., 1991). The instability of large stratovolcanoes is conditioned by the inter-layering of mechanically weak and strong materials (pyroclastics and lavas) (McClelland & Erwin, 2003). Instability also increases with weathering by hydrothermal alteration (McClelland & Erwin, 2003). These stratovolcanoes are often built on uneven or weak

surfaces tilted by tectonic processes, adding to instability (McClelland & Erwin, 2003). Ruapehu is comprised of lavas that extend up to 14 km from source, stabilising much of the edifice and leaving only small portions of unconsolidated volcaniclastic deposits exposed (Palmer *et al*., 1991).

Collapses from New Zealand stratovolcanoes occur in different directions, resulting in the ring plains being made up of different aged segments, which are recognised and named separately (Palmer *et al*., 1991). In between periods of ring-plain accumulation are periods of fluvial erosion that incise valleys; this forms new paths to guide younger flows (Palmer *et al*., 1991). The relatively unconfined terrain of the medial material of Ruapehu's ring plain has allowed debris avalanches and lahar events to spread radially outward (Palmer *et al*., 1991). As a result the development of lithofacies distributions is different to those debris-avalanche deposits that were generally deposited in valleys (Palmer *et al*., 1991).

Unconfined debris-avalanche deposits can be divided into three lithofacies (table 1.4) that occupy distinct positions with respect to each other (Palmer *et al*., 1991). These lithofacies represent changes in the nature of flow within the debris avalanche as it travels away from source. Two lithofacies (axial-a and axial-b) are attributed to the debris-avalanche phase of the flow and a third (the marginal lithofacies) represents deposition during a debris-flow phase (Palmer *et al*., 1991). The development and mobility of the marginal lithofacies are conditioned by: hydrothermal alteration, water, allophane and other short-range-order clays (Palmer *et al*., 1991).

Geological evidence shows that at least two debris avalanche events have occurred at Ruapehu. The Murimotu Formation, dated at 9,500 ka, is located on the north-western ring plain of Mount Ruapehu and was triggered by gravitational collapse, probably due to the intrusion of dikes into the hydrothermally weakened Te Herenga Formation (Palmer & Neall, 1989; McClelland & Erwin, 2003).

Lithofacies	Description	Basal and Upper surfaces	Geometry	Interpretation
Axial-A	Framework-supported fabric. Tabular brecciated megaclasts dominate, >10 m. These megaclasts are monolithologic with silty and intraclast matrix of same lithology as megaclast fragments. Primary megaclasts of stratified deposits and hydrothermally altered material to 100 m long. Scarce secondary material. Silty sand interclast matrix. Mounds cored by single and multiple brecciated clasts.	Basal surface not exposed. Surface mounds to 50 m high and basal diameters as large as 500 m. Closely spaced mounds, 150-300/km^2.	Sheet or lobate	Clast and megaclast-rich debris avalanche
Axial-B	Tabular to equant brecciated megaclasts are dominant clast type; stratified megaclasts less common. Secondary megaclasts of stratified sedimentary deposits, and clasts of lignite and tephra. Angular to subrounded clasts, some with rock-flour rims. Silty sand interclast matrix. Mounds cored by single megaclasts.	Planar to irregular, non-scoured to scoured base. Surface mounds <10 m high with basal diameters <25 m. Widely spaced mounds, 20-150/km^2.	Sheet or shoestring	Interclast matrix-rich debris avalanche
Marginal	Matrix-supported fabric, brecciated clasts rare, no stratified primary megaclasts. Secondary component dominates. Stratified secondary clasts and megaclasts common, as high as 100 m long. Secondary clasts of lignite, tephric loess, tephra, and diamicton abundant locally. Subrounded to rounded clasts dominate, some subangular clasts. Allophane-rich sandy mud to sandy, silt interclast matrix.		Sheet or shoestring	Lahar (debris flow)

Table 1.4: Lithofacies in New Zealand debris-avalanche/lahar deposits (Palmer *et al*., 1991).

The Mangaio Formation (fig. 1.6) is located on the south-eastern ring plain of Mount Ruapehu and represents a debris-avalanche event occurring at c. 4,600 yrs BP (Donoghue & Neall, 2001). The Mangaio Formation is characterised by abundant white

hydrothermally altered lithic clasts in a clay-textured matrix (Donoghue & Neall, 2001). This debris avalanche event was inferred to have been derived from the failure in hydrothermally altered flank rocks and not associated with eruption activity due to the absence of tephra directly overlying or underlying the deposit (Donoghue & Neall, 2001). The possible source of this debris avalanche is the highly weathered Wahianoa Formation, which makes up much of the south-eastern flank of Mount Ruapehu (Donoghue & Neall, 2001).

1.9 Past studies on the crater rim of Mount Ruapehu

Hancox *et al.* (1997) looked into the stability of the crater rim after the 1995-1996 eruptions. Significant geomorphic changes were noted at Stump Saddle between 1991 and 1996, including a 25% loss of material from Stump Saddle and an overall steepening of the inner crater wall by up to 20%. These changes, however, were interpreted as insignificant due to the broad nature of the rim (Hancox *et al*., 1997). Further, Hancox *et al.* (1997) concluded that material loss and over-steepening had little effect on the crater wall strength and on the ability to hold Crater Lake at full capacity. The potential of a collapse of the south eastern rim was said to be low. However, it was also noted that previous eruptions (larger than in 1995-96) had triggered partial collapses of portions of the southern and eastern rims and that the possibility of another such collapse could not be ruled out (Hancox *et al*., 1997).

Hales (2000) utilised the low level of the Crater Lake, Ruapehu in 2000 to provide a description of the stratigraphy previously obstructed by water. The study revealed a detailed geological map of the Crater Lake region and provided new clues towards better understanding of the stratigraphy of the area. Importantly, Hales (2000) developed a history of the Crater Lake vent and correlated this information with previous knowledge of its evolution. This resulted in a new system to simplify the hitherto established stratigraphy of the proximal volcanic edifice and in the definition of the Crater Lake Formation and its associated stratigraphic members.

Prior to this study, Manville *et al.* (2003) modelled possible future debris avalanche events from Mount Ruapehu through numerical simulations, using the software LAHARZ. Based on geological evidence, the likely origin of these events was Pyramid Peak, the south-eastern crater rim (Manville *et al*., 2003). Four failure surfaces were determined and volume scenarios calculated. The largest event involved the collapse of the entire Pyramid Peak due to a deep-seated failure reaching the bottom of the lake (Manville *et al*., 2003). They found that the resulting simulation of the debris avalanche that was directed into the main Whangaehu channel produced a proximal hazard zone boundary at the fan apex (~7.5 km from source), with the Rangipo fault scarp diverting it to the south and then travelling 20 km further from source. The largest scenario inundated an area of ~62 km^2 and the smallest ~19 km^2 with average deposit thicknesses of ~4 m and ~2 m, respectively (Manville *et al*., 2003). However, this study did not state any possible hazards these events would have on the surrounding area; instead the study was constructed to test the LAHARZ model.

A collapse event at Mount Ruapehu is an acknowledged hazard and the likelihood of such an event occurring is increasing, with the continual hydrothermal weathering and erosion. Despite this, quantitative hazard and risk analysis of possible collapse scenarios have yet to be undertaken.

Chapter 2: GEOLOGY OF THE EASTERN RIM

2.1 Introduction:

This study concentrates on the eastern rim geology and on defining the structural relationship these units have on the stability of the study area. The studied area (fig. 2.1) is comprised of a section of the eastern crater rim spanning from J Peak to L Peak. This region is bounded by the Whangaehu Glacier to the north, Whangaehu Gorge to the south and Crater Lake to the west. The geology of the eastern rim of Mount Ruapehu has been poorly defined with Hales (2000) being the only study that has attempted to map the geology of the Crater Lake area in any detail. Prior to this study there was only a structural sketch map drawn in conjunction with a hazard assessment for the area after the 1995-1996 eruptions by Hancox *et al*. (1997). There have also been detailed studies of historic eruption deposits from 1945-2007 (Beck, 1950; Healy *et al*., 1978; Nairn *et al*., 1979; Kilgour *et al*., 2010).

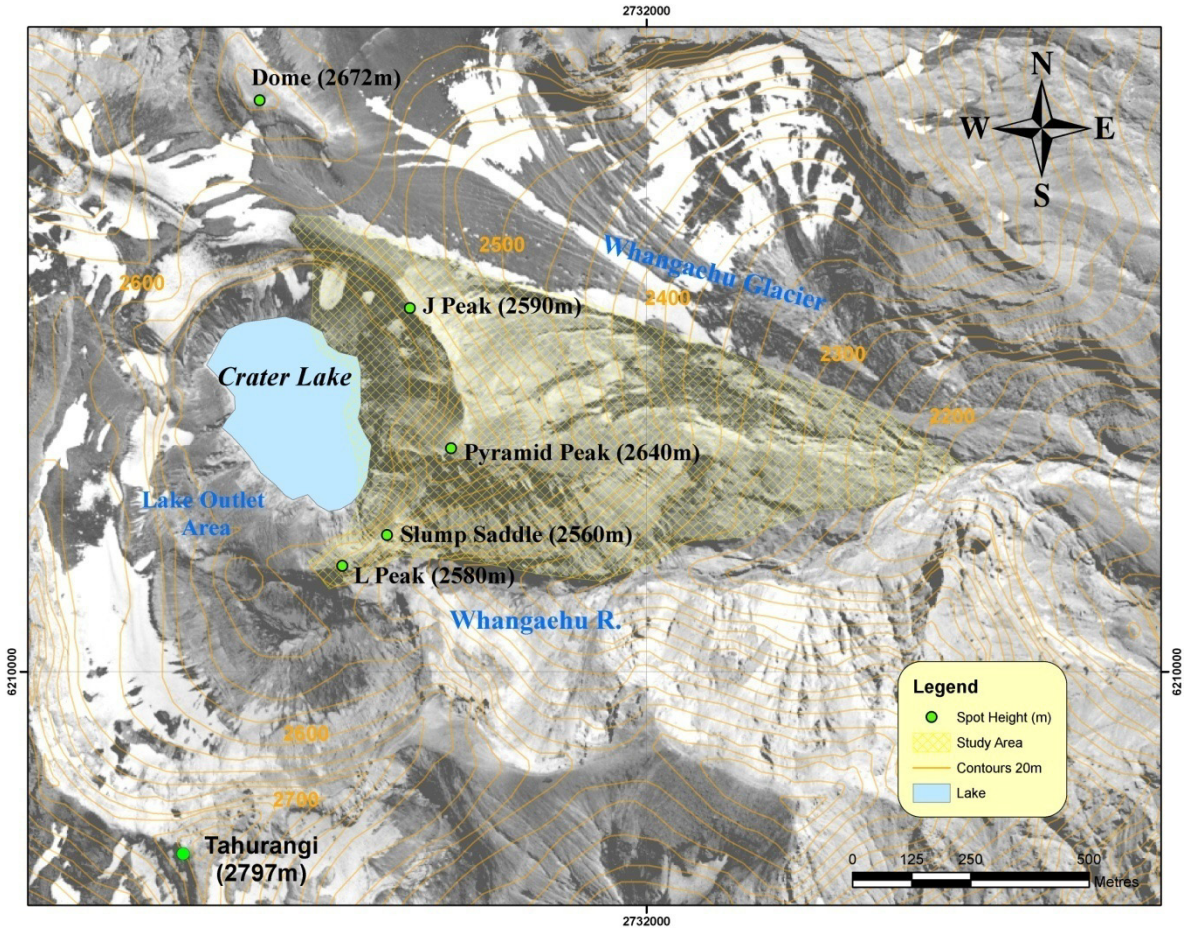

Figure 2.1: Study area, eastern rim complex.

Precise ages for the rocks that make up the eastern rim of Crater Lake have not been determined due to the rocks being too young for radiogenic isotope age dating and also an absence of dateable carbon or fossils. A detailed study of the geology of the Crater Lake area has been difficult because of a lack of exposed outcrops for correlation and also the complex sequence of erosion and collapse between periods of varied deposition (Hales, 2000).

This study aims to construct a map of the stratigraphy of the eastern rim of Mount Ruapehu and quantify the state of alteration and failure conditions of key geological units within the eastern rim of Crater Lake in order to define and characterise potential failure volumes of collapse blocks. From this, the study then aims to define possible volume scenarios of collapsing material and mass flow run out.

2.2 Previous work on the geology of the eastern rim:

Hancox *et al*. (1997) prepared a stability assessment of the crater rim of Mount Ruapehu for DOC following the 1995-1996 eruptions. They describe briefly the structure of the south eastern crater rim to be made up of interbedding lavas and welded and non-welded tephra deposits. The tephra deposits comprise volcanic ash, bombs, and layers of scoriaceous blocks (Hancox *et al*., 1997). On the inside and the crest of the crater rim there are some prominent layers of older blocky lava, compacted ash (tuff), and agglomerate. The tuff and agglomerate layers were found to dip both away from and into the crater rim at 30°-35°, whereas the lava flows appeared to have shallower dips of 5°-15° away from the crater (Hancox *et al*., 1997).

Hales (2000) described the rocks of the Crater Lake area during a period of low lake level. From these descriptions he derived a detailed geological map of the region. The aim was to develop a history of the Crater Lake vent and correlate this information with current knowledge of eruptive deposits in distal areas.

Despite the lack of dateable material, the eastern rim was interpreted to contain deposits of the Crater Lake history that are < 2000 ka (Hales, 2000). Volcanic deposits from Mount Ruapehu associated with this late Holocene period were previously grouped into three mapable formations. The Crater Lake is formed within the Whakapapa Formation (Hackett, 1985) containing a stratigraphic sequence of lava and tephra. The Tufa Trig Formation, described in Donoghue *et al*. (1995), is defined by medial and distal post-Taupo tephra deposits of the ring plain. The Onetapu Formation (Donoghue, 1991; Hodgson, 1993) consists of the post-Taupo lahar stratigraphy of the south eastern ring plain. Ona-1 (>1530±160 ^{14}C yrs BP (Hodgson *et al*., 2007)), the oldest (preserved) lahar unit of the Onetapu Formation, suggests the Crater Lake was emplaced between then and 1717 cal. yrs BP (Lowe *et al*., 2008), which is the age of the Taupo ignimbrite that Ona-1 overlies.

Hales (2000) stated that describing the proximal deposits of the crater rim area in relation to the current terminology would be complicated and impractical. Therefore, he proposed a new system to simplify the proximal stratigraphy. Hales changed the 'Crater Lake member' into the Crater Lake Formation that would include all deposits from Ruapehu that are < 2000 years old. The Tufa Trig formation and the Onetapu Formation were included as two of the 13 members of the Crater Lake Formation; the current and proposed stratigraphy is noted in table 2.1 below. Due to the complexities involved in the spatial distribution and genesis of each formation or member, it is difficult to develop a unified stratigraphic classification.

Ruapehu Lava Stratigraphy after Hackett (1985)	Tongariro Volcanic Centre Medial and Distal Tephra after Donoghue *et al.* (1995)	Revised Ruapehu Stratigraphy including lava and tephra after Hales (2000)
Whakapapa Fm < 10,000 years - Crater Lake Mem (< 2,000 years) - Tama Mem - Rangataua Mem - Iwikau Mem	Tongariro Subgroup - Tufa Trig Fm (Ruapehu derived < 1,800 years) - Ngauruhoe Fm - Mangatawai Fm - Papakai Fm - Mangamate Fm - Pahoka Tephra (10,000 years)	Crater Lake Fm (< 2,000 years) - 1995/1996 Mem - 1945 Mem - Crater Basin Mem - Bench Mem - Pyramid Mem - Outlet Mem - Iridescent Mem - Stalactite Mem - Swimming Bluff Mem - Coffin Mem - Waterfall Mem - *Onetapu Fm?* - *Tufa Trig Mem?* Whakapapa Fm (2,000 to 10,000 years) - Tama Mem - Rangataua Mem - Iwikau Mem
Mangawhero Fm 10,000 to 65,000 years		Mangawhero Fm 10,000 to 65,000 years
Wahianoa Fm 65,000 to 120,000 years		Wahianoa Fm 65,000 to 120,000 years
Te Herenga Fm > 120,000 years		Te Herenga Fm > 120,000 years

Table 2.1: The current stratigraphic system and the proposed revision derived from Hales (2000).

Hales (2000) defined new Crater Lake Formation members using obvious unconformities and other stratigraphic relations (fig. 2.2). During mapping some areas were inaccessible due to rock fall and instability, or covered by tephra from the 1995/1996 eruptions.

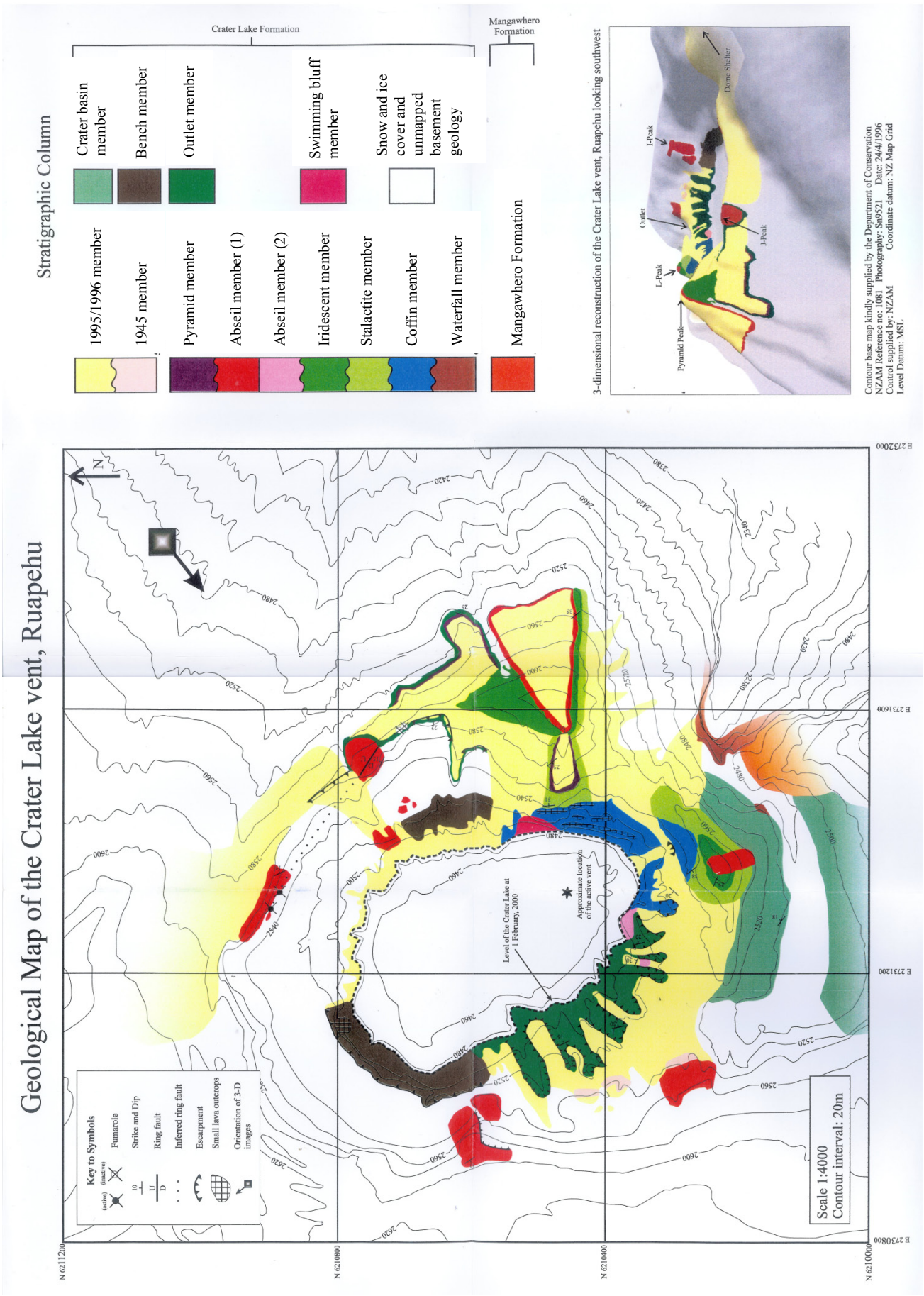

Figure 2.2: Geological map of the Crater Lake vent area, Ruapehu from Hales (2000).

2.3 Geological observations from this study:

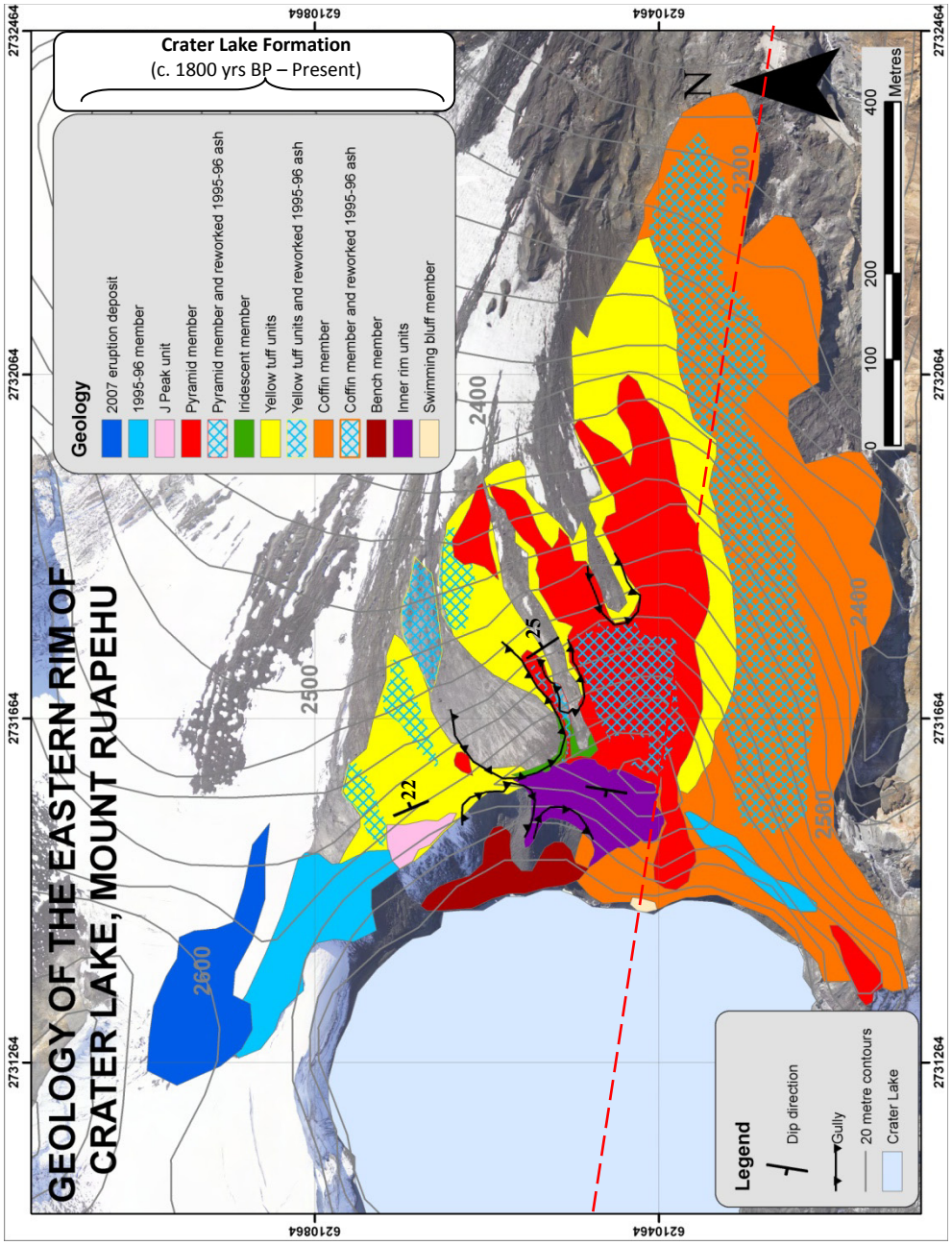

Figure 2.3: Geological map of the eastern crater rim, Mount Ruapehu. Red dashed line represents the location of the cross-section in figure 2.4. Geodetic Datum NZGD 1949, Map Projection NZMG. Topographic data LINZ (Crown copyright reserved).

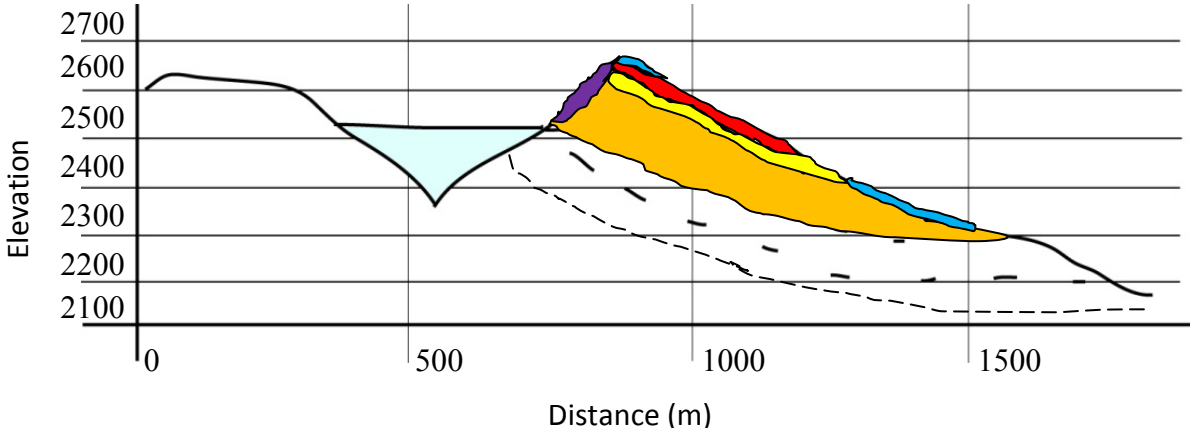

Figure 2.4: Cross-section of constructed geological map in figure 2.3. This represents the resulting overall structure of the eastern rim. The black dashed lines are the inferred structure of the lower units that were obscured.

The eastern rim of Mount Ruapehu is composed of interbedded lavas, tephra deposits and scoriaceous blocks and bombs (Hancox *et al*., 1997). Using field observations, the terminology of Hales (2000), past studies and numerous aerial photographs (provided by Harry Keys, DOC and Graham Hancox, GNS) the upper contrasting units of the eastern crater rim were studied and mapped (fig. 2.3). The major limitation of mapping using aerial photography is that it is indicative and gives only general indications of geology. Purely visual clues such as colour, texture, unconformities and the dip of beds can be used. Bedding is also hard to determine on a highly erodible landscape. Another limitation is that aerial photographs are generally only taken after an eruption, when most of the area is covered in fresh ash that is eroded soon after.

Since the study of Hales (2000) subsequent erosion has exposed more detail than previously observed. Table 2.2 shows the comparison of units defined in this study with those in Hales (2000). Some units described in Hales (2000) were not observed in this study area, while others have been expanded due to differences in geological interpretation.

Hales (2000)	This study
Not observed	2007 eruptive unit
1995/1996 member	Observed, distribution changed
1945 member	Not observed, not within study area
Pyramid member	Observed, distribution extended
Abseil member	Only the Red agglomerate observed from this unit. Mapped as J Peak unit
Iridescent member	Laminated ash layers in this unit observed. Different distribution.
Stalactite member	Not observed, obscured
Coffin member	Observed
Waterfall member	Not observed, not in study area
Crater basin member	Not observed, not in study area
Bench member	Observed
Outlet member	Not observed, not in study area
Swimming bluff member	Observed
Mapped as part of Iridescent member	Yellow tuff unit
Not observed, mapped as 1995/1996 member	Inner rim unit

Table 2.2: Correlation of mapped units used in this study with those used in Hales (2000).

2.3.1 Geological descriptions

2007 eruptive unit

This unit was made up of unconsolidated ash and ballistics. It has a 2-4 cm basal layer of dark grey-brown, fine to medium-grained ash and lapilli, which is overlain by blocks, bombs and lapilli ranging in size from 1 cm to >20 cm, with varied colours and state of alteration. Some were dark to medium grey andesitic lava fragments from previous eruptive episodes. Some andesitic blocks had sulphur filled pores and vesicles (fig. 2.5); these were also seen by Kilgour *et al*. (2010). Other angular blocks were light coloured, fine-grained and possibly cemented vent material. The current extent of the deposit (fig. 2.7) is patchy and in places reworked. Only a small patch remains of the 2007 unit on the north eastern rim, drapping over a portion of the 1995/1996 deposits and the upper Whangaehu Glacier. There are possibly other locations on the eastern crater rim where this deposit is also preserved; however it was hard to discern due to covering scree and reworked deposits.

Figure 2.5: Andesitic block from the 2007 eruption with sulphur filled vesicles (16/03/2010).

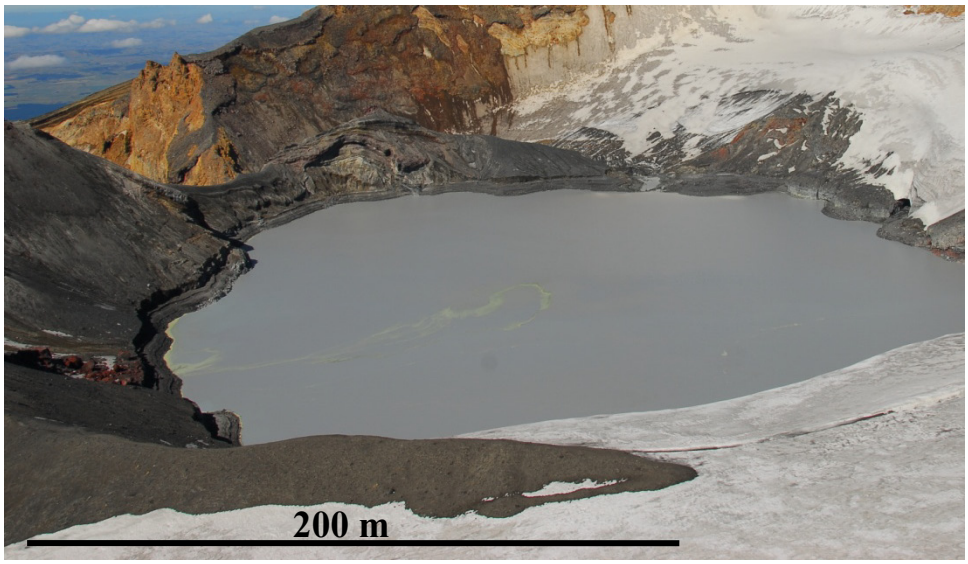

Figure 2.6: North eastern rim of Crater Lake pre-2007 eruption. Photo provided by Graham Hancox, GNS, taken on 23/03/2007.

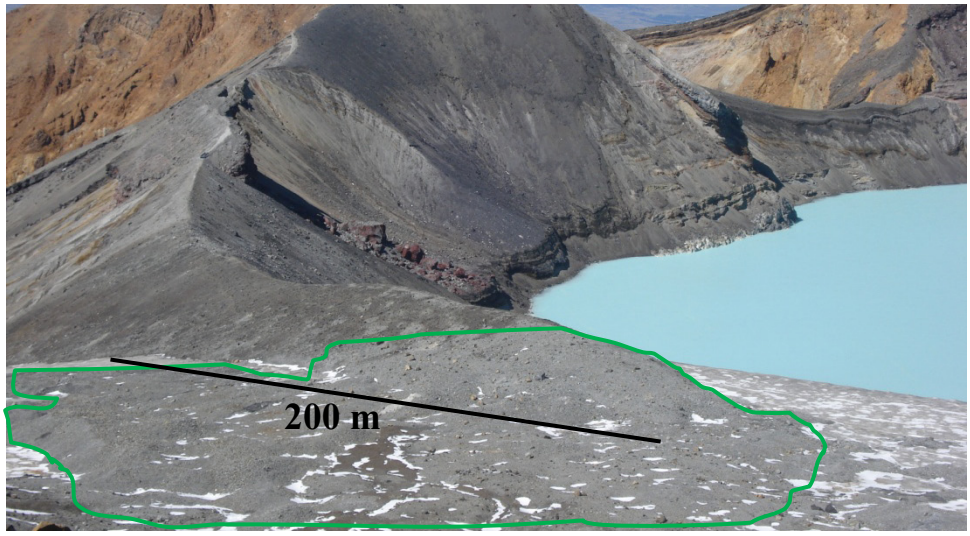

Figure 2.7: North eastern rim of Crater Lake post-2007 eruption (31/03/2010). 2007 surge deposit outlined in green.

1995/1996 member

This unit consists of dark grey and brown layers of poorly sorted sub-rounded to sub-angular matrix supported breccias, with dense lava and scoria clasts, in between layers of grey and brown ash. The lower unit consists of randomly distributed black andesitic bombs within a coarse, dark-brown matrix with finer laminated brown ash at the base. This was distinguished due to its contrasting colour and lithology to the layers below. Similar types of deposits were described in the 1995/1996 member type section in Hales (2000). This unit was observed on the north eastern rim leading up to J Peak (fig.

2.8) and on Stump Saddle (fig. 2.9). Subsequent erosion since 2000 and deposition of 2007 eruptive material has resulted in changes to the extents of this deposit.

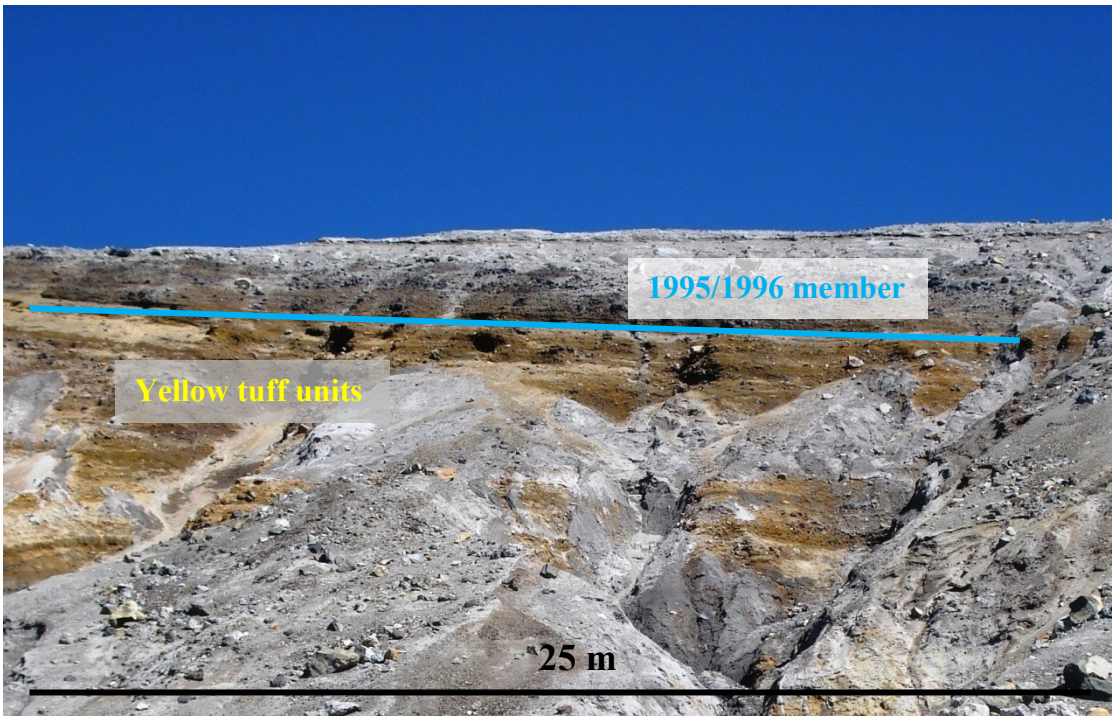

Figure 2.8: 1995/1996 member located on the outer eastern rim near J Peak (Blue line showing the base of the 1995/1996 member) (31/03/2010).

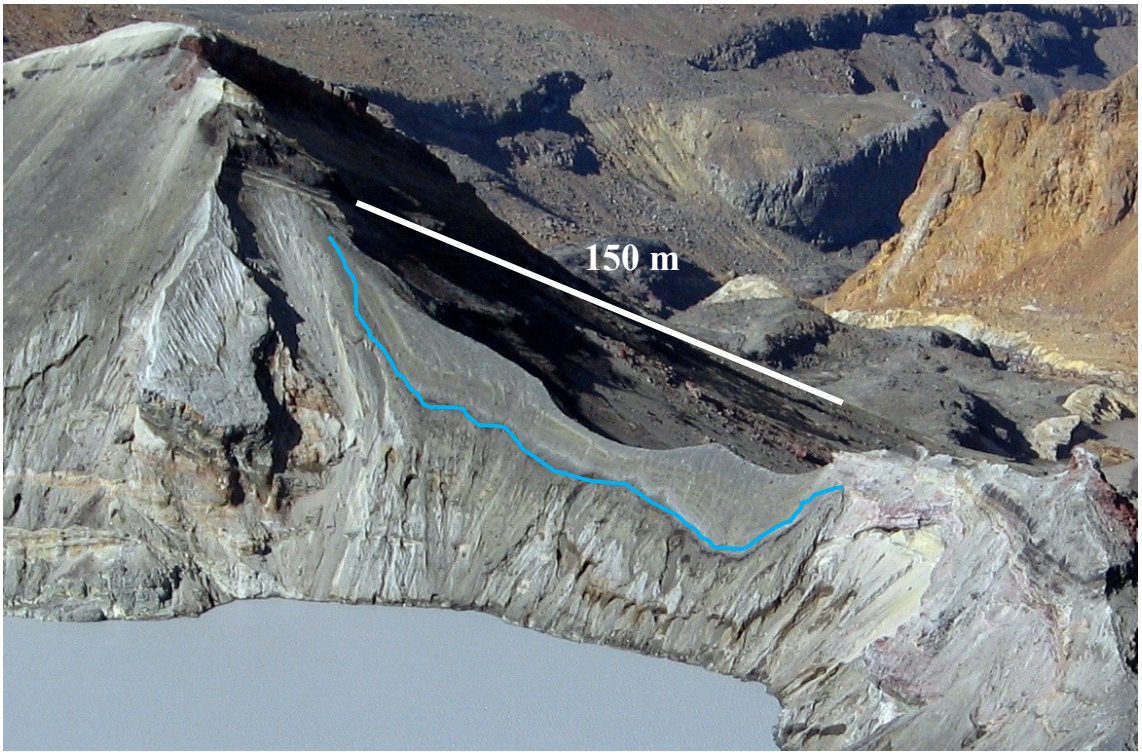

Figure 2.9: 1995/1996 member on Stump Saddle, south eastern crater rim. Photo supplied by Graham Hancox, GNS (22/03/2004).

Iridescent member

Despite the difference in distribution, this unit resembles a section of the Iridescent member described in Hales (2000). This unit is present along the top of Pyramid Peak, containing light to medium grey, medium to fine-grained deposits of cross-bedded and laminar bedded lapilli and ash layers, interbedded with coarse matrix-supported fragmented pebble layers. This is here interpreted as proximal surge and fallout deposits. This unit may be overlain by the 1995/1996 member and subsequent deposits from 2007 but erosion in this unit and subsequent 1995/1996 and 2007 eruptives filling the eroded areas creates a complex stratigraphic relationship. Similarities between ash and surge deposits of this unit and post 1995 deposits also make it hard to define unit boundaries and any unconformities. This unit contains internal faults and offsets and is unconformable with the Inner crater unit (fig. 2.10). This unit is overlain by patches of Pyramid member (fig. 2.10).

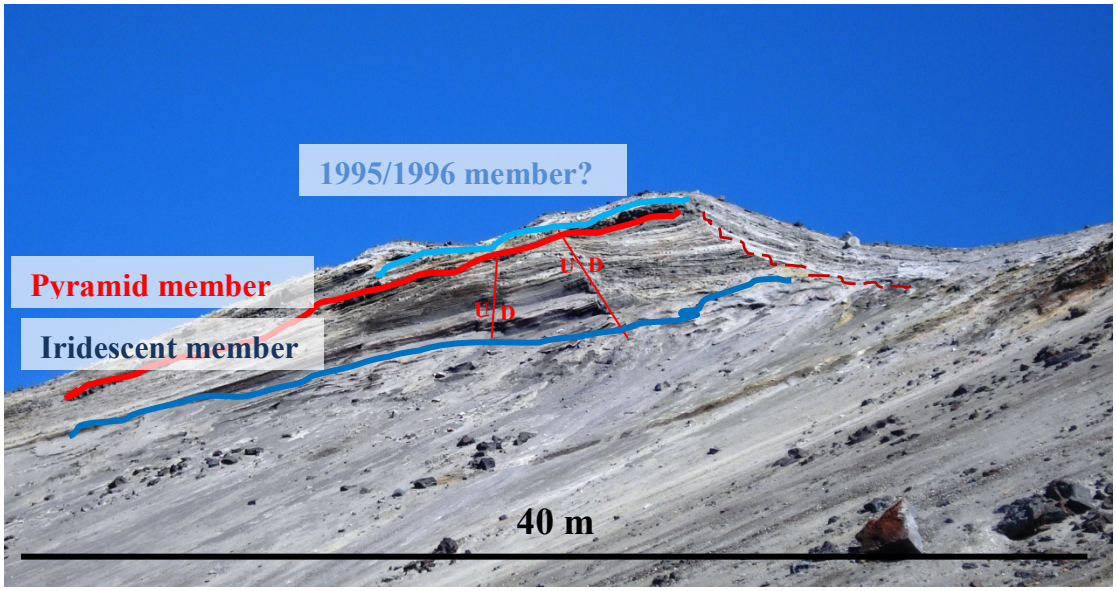

Figure 2.10: Section of the Iridescent member (base lined in dark blue) observed along the crest of the eastern crater rim. Overlying Pyramid member marked in red. The two vertical red lines indicate faults in this unit and the dark red dashed line depicts the unconformity between the outer and inner rim strata (31/03/2010).

J Peak unit

The J Peak unit is best identified by the red agglomerate unit comprising the majority of J Peak. It forms the top of the Peak and is characterised by its deep red colour (fig

2.11). The J Peak unit is coarse-grained, brecciated, scoriaceous agglomerate that has a rough exterior. The exposed surfaces have weathered to a white/pink colour in places. Hales (2000) referred to this unit in the Abseil member.

Figure 2.11: Looking up at J Peak, capped by the J Peak unit. Picture insert is of a fragment from the J Peak unit showing its distinctive red colour (31/03/2010).

Pyramid member

Pyramid member is a complex sequence of lava flows and breccias. It starts with a basal black massive, welded, and vesicular, scoriaceous autobrecciated lava unit with an upper solid grey-black lava flow unit of an average thickness of 2-5 m. It outcrops on the inner and outer rim walls (with a 25° dip) and appears to have been emplaced as a flow that drapes over the underlying units resulting in various dips and dip directions, characteristic of a lava flow. This unit outcrops between J Peak and Pyramid Peak on the outer wall; on top of Pyramid Peak; and also capping L Peak. A portion of this unit also dips into the crater on the inner wall below Pyramid Peak (fig. 2.12).

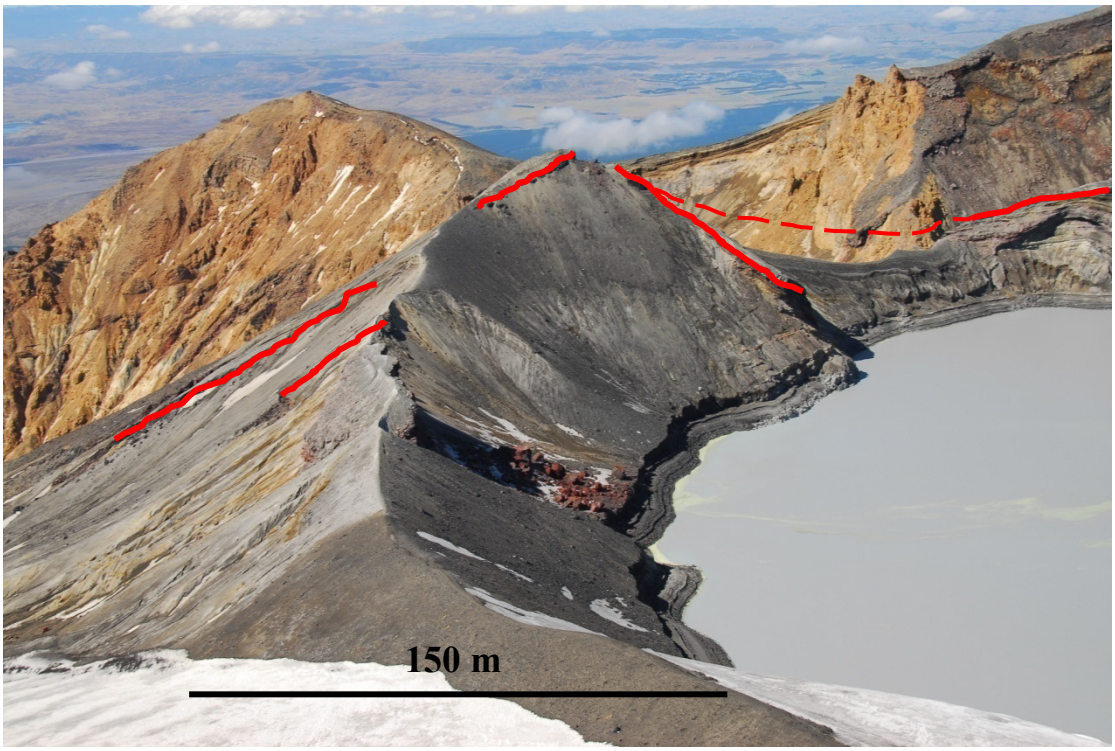

Figure 2.12: Pyramid member exposures (red lines). The dashed line is where this unit existed in 1961 before being eroded (fig. 2.13). Photo looking south, supplied by Graham Hancox, GNS, taken on 23/03/2007.

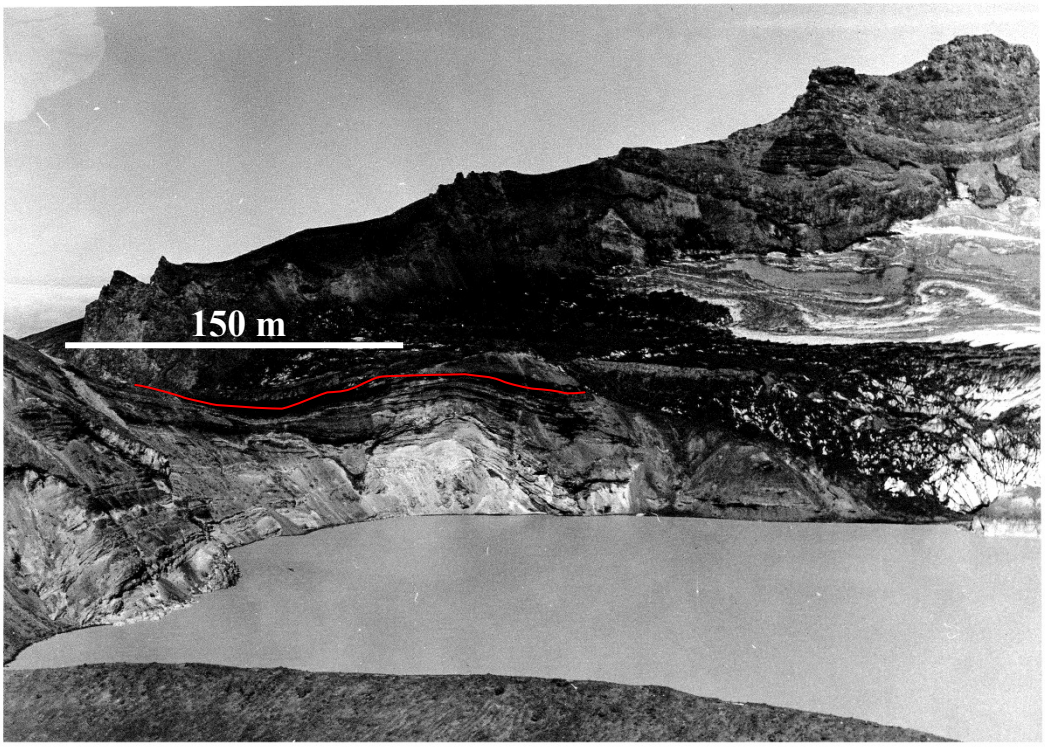

Figure 2.13: Possible past extent of the Pyramid member from Pyramid Peak to L Peak (red line). Photo is looking south, taken on Easter 1961. Photo supplied by Harry Keys, DOC. Red line representing the Pyramid member.

Yellow tuff units

These units are found in a similar location with similar distribution to the Iridescent member described by Hales (2000), but its lithology differs. This unit ranges in exposed thickness from around 2-10 m, and comprises beds of cream, grey and orange/brown tuff that have distinct erosional patterns of rills and lobes (fig. 2.14). The beds in this unit consist of light-grey, fine-grained ash, and cream and brown fine to medium-grained ash layers, and coarse lapilli-sized lithics. In this study the Yellow tuff units are found below the Pyramid member and J Peak member and are mainly exposed on the outer wall, but can be correlated to the inner wall in places.

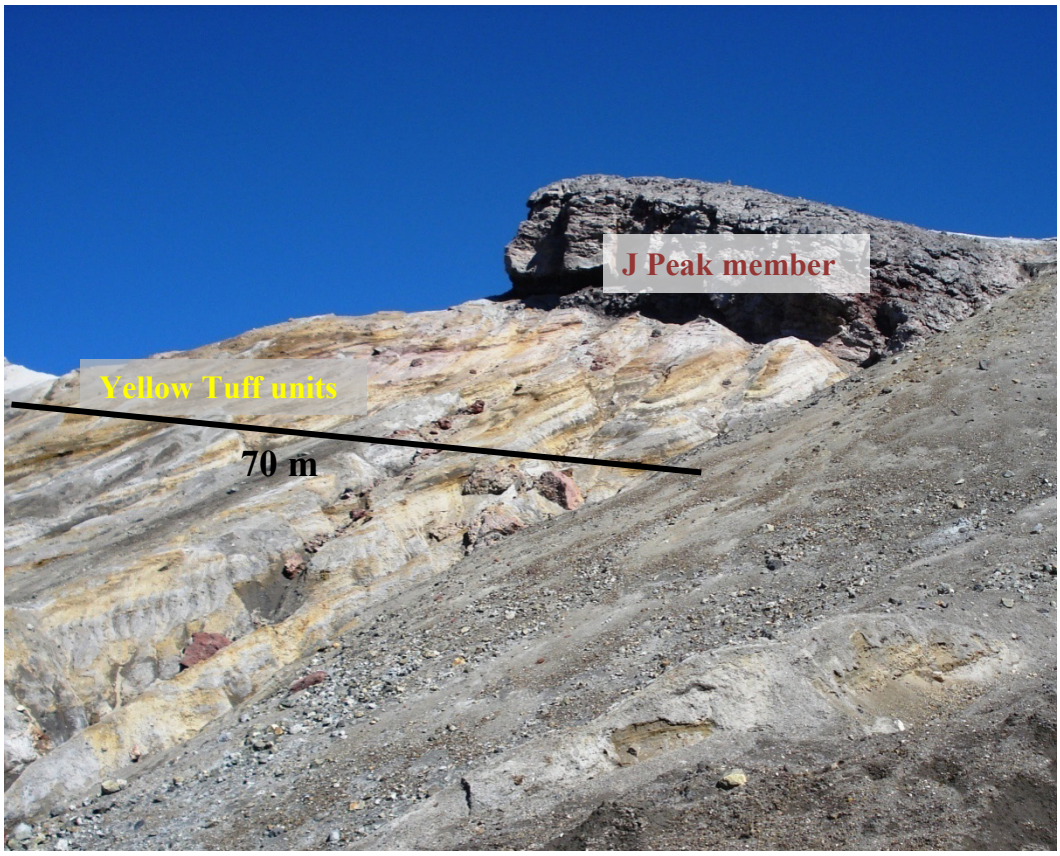

Figure 2.14: Yellow tuff units below J Peak member on the outer rim of the eastern rim of Crater Lake (31/03/2010).

Inner rim unit

This unit occurs on the inner eastern crater wall. The lithology of this unit was not observed by Hales (2000) and was instead mapped as the 1995/1996 member. This unit is made up of laminated and cross-bedded layers of grey, fine to medium-grained ash, with some darker grey, coarse-grained units. It was defined separately from the

Pyramid member and Iridescent member of this study due to the unconformable position of this deposit on the inner wall of the Crater Lake. The inner rim unit dips into the crater and appears to be cemented to the upper inner rim. It was possibly emplaced by one or more wet base surges. Where this unit has been eroded, large gullies have formed under J Peak and above the Bench member (fig. 2.15).

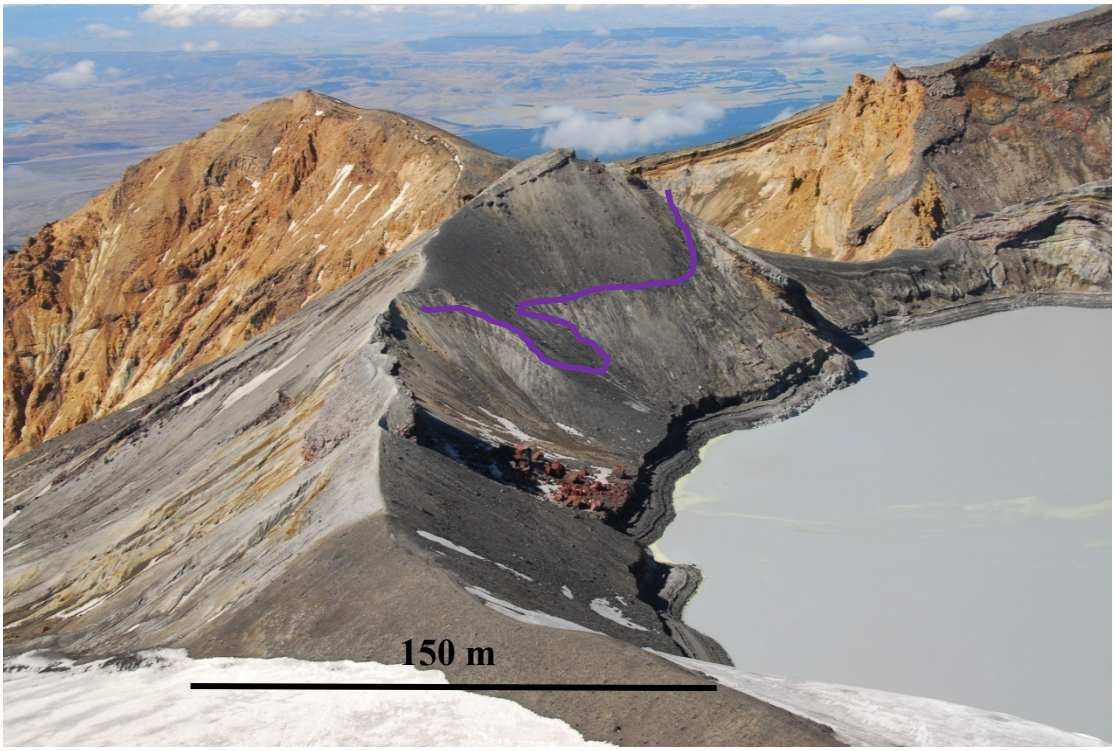

Figure 2.15: Current lower boundary distribution of the inner rim units (purple line). Photo looking south, supplied by Graham Hancox, GNS, taken on 23/03/2007.

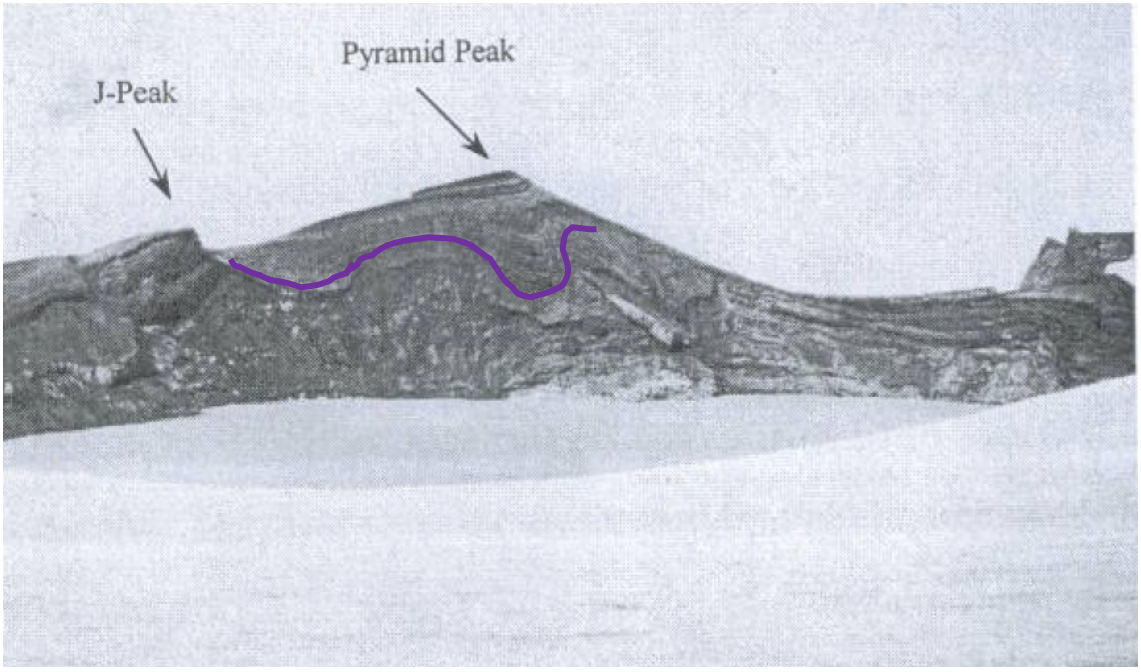

Figure2.16: The possible historic lower boundary distribution of inner rim units (purple line) before the formation of gully erosion to the right of J Peak in this image, seen in figure 2.15 above. Photo from Hales (2000) provided by Harry Keys, taken in 1939.

Coffin member

This unit outcrops at the base of Pyramid Peak below an obvious unconformity on L Peak, and in Stump Saddle. The dominant rock type is grey-brown, poorly sorted, non-welded breccia, interbedded with small lava flows at the base of Pyramid Peak and Stump Saddle. The identification of this unit is primarily based on its distinctive brown colouring and its contrasting near horizontal layering (compared to above units that are on a ~30° dip). It consists of a sequence of lavas, located at the base of Pyramid Peak (fig. 2.17). This may correlated to other lava like units that outcrop in the Whangaehu Gorge on the southern flank or Pyramid Peak (fig. 2.18).

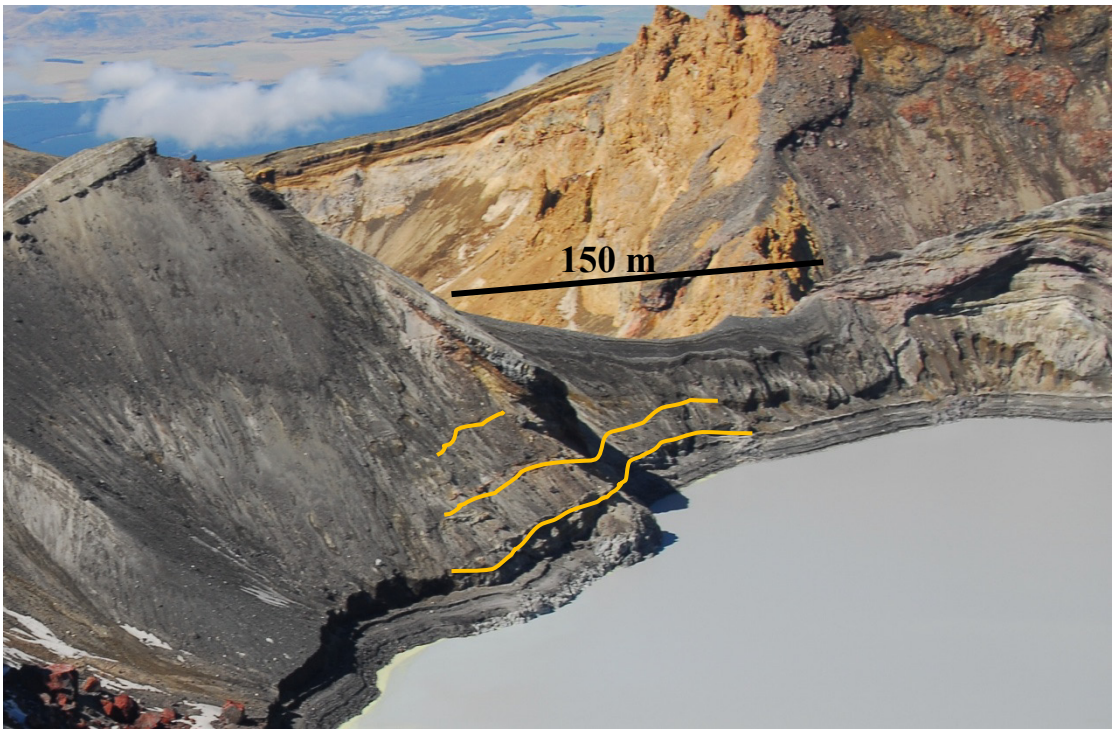

Figure 2.17: Lava sequences of the Coffin member (orange lines) within the south eastern inner crater wall. Photo supplied by Graham Hancox, GNS, taken on 23/03/2007.

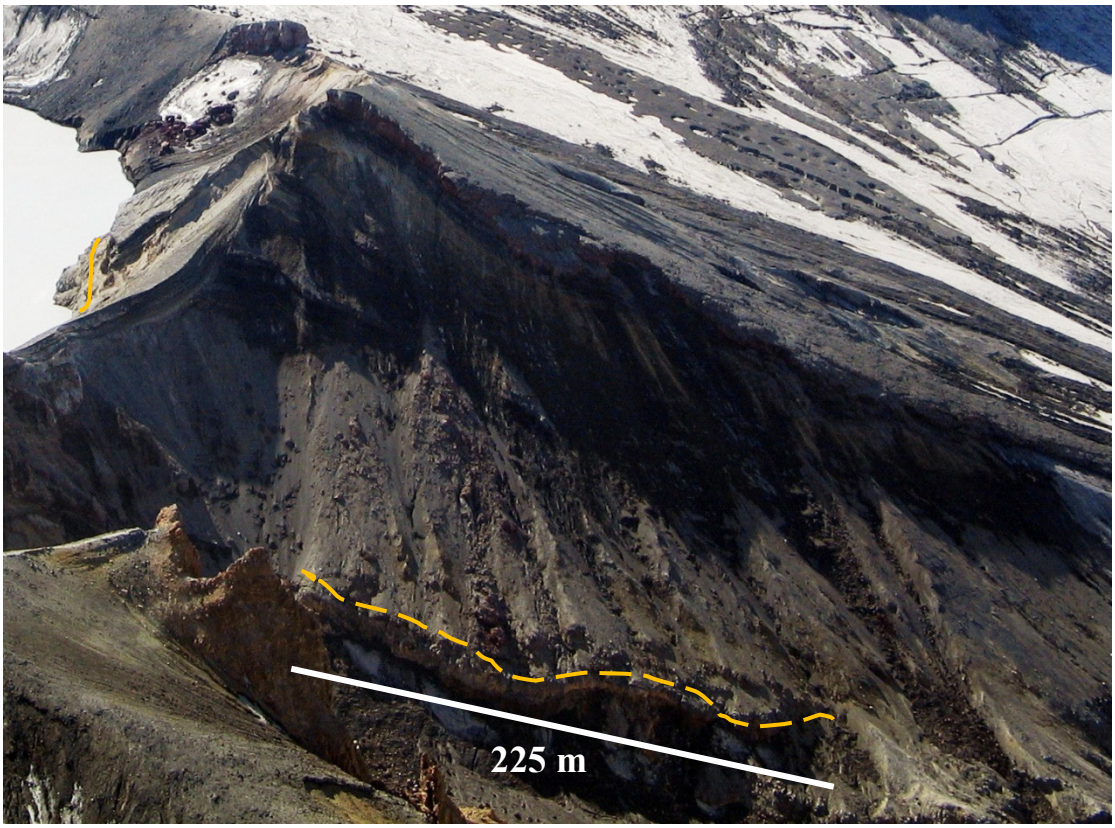

Figure 2.18: Correlation of the Coffin member from the inner crater rim (orange line) to the southern flank of Pyramid Peak, Upper Whangaehu Gorge (orange dashed line). Photo taken looking north (22/03/2004), supplied by Graham Hancox, GNS.

Bench member

This unit is found below J Peak (fig. 2.19). It is thick with sub-angular to rounded, massive, matrix supported agglomerates interbedded with thick, grey, finely laminated muddy deposits. Hales (2000) suggested that this breccia was formed by a debris flow due to the rounded and polylithic clasts.

Figure 2.19: Bench member (represented by brown line) near lake level on the inner crater wall (31/03/2010).

Swimming bluff member

Hales (2000) describes this unit as lava that is geochemically distinct and highly altered. It is exposed at the base of Pyramid Peak and at current lake level below J Peak (fig. 2.20). Hales (2000) found this unit difficult to correlate to other locations in the Crater Lake area and suggested it to be an intrusion. Due to its location and partial submergence by Crater Lake, no extensive lithological description could be made in this study. It was defined by its contrasting near white colouring and columnar like joints.

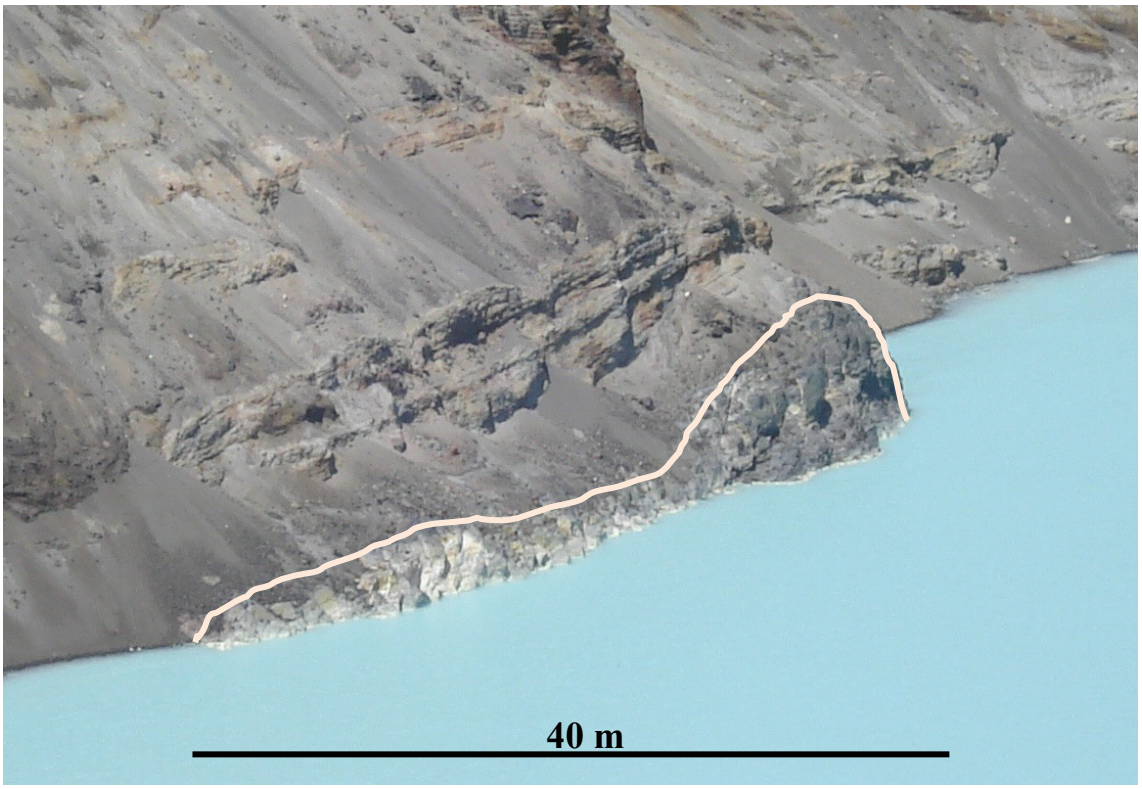

Figure 2.20: Distinctive white appearance and columnar joints of the Swimming Bluff member (top of unit outlined in peach). Base of the inner eastern crater wall (16/03/2010).

2.4 Clay analysis:

Samples were collected from both the inside and outside of the eastern crater rim (fig. 2.21-2.23). The objective was to find the clay content of the samples collected from Pyramid Peak and identify the type of clay minerals and therefore infer the state of alteration.

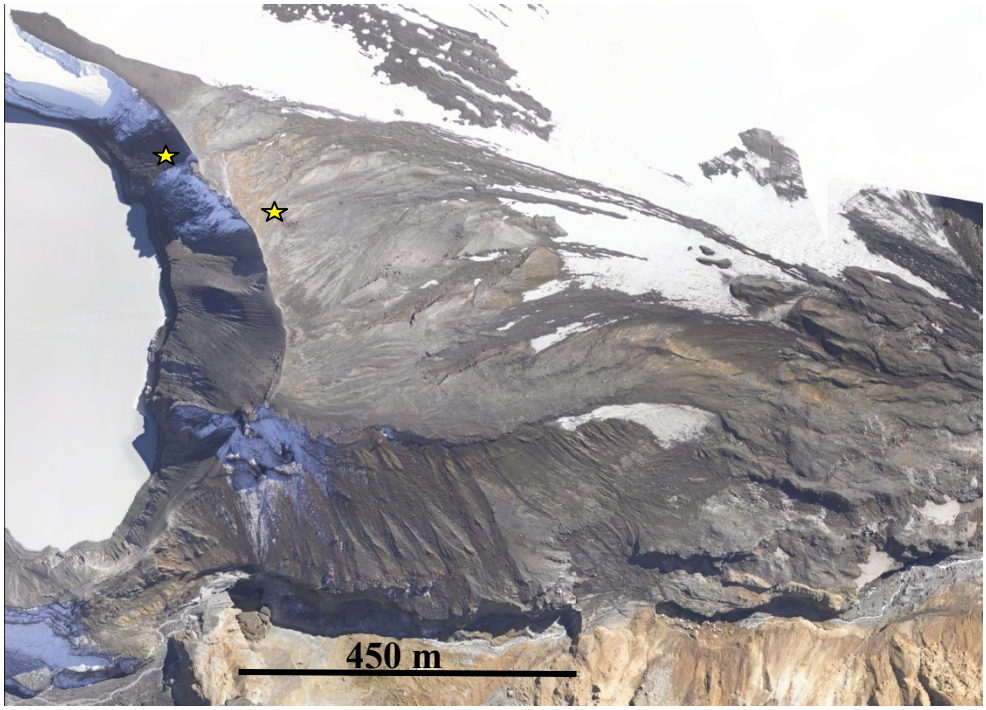

Figure 2.21: Locations of sample collection (depicted by the yellow stars). The Massey University and GNS Science orthophoto, taken April 2007.

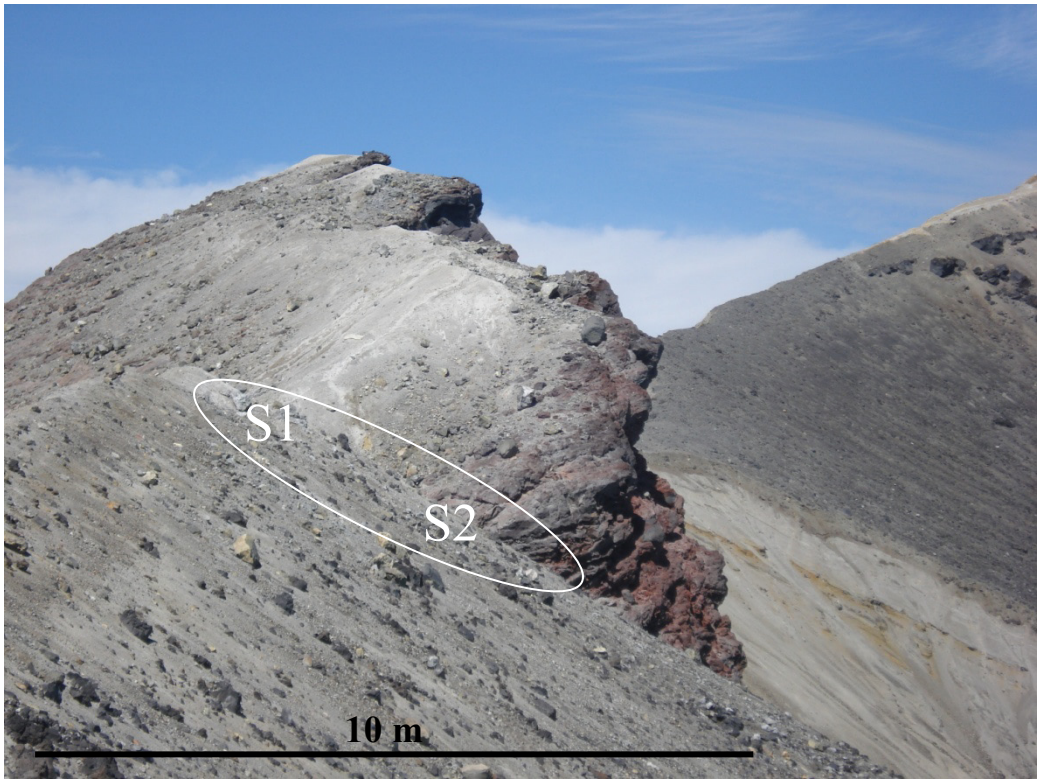

Figure 2.22: A close up of where samples S1 and S2 were collected. Located on the inner eastern crater wall along side J Peak. 16/03/2010.

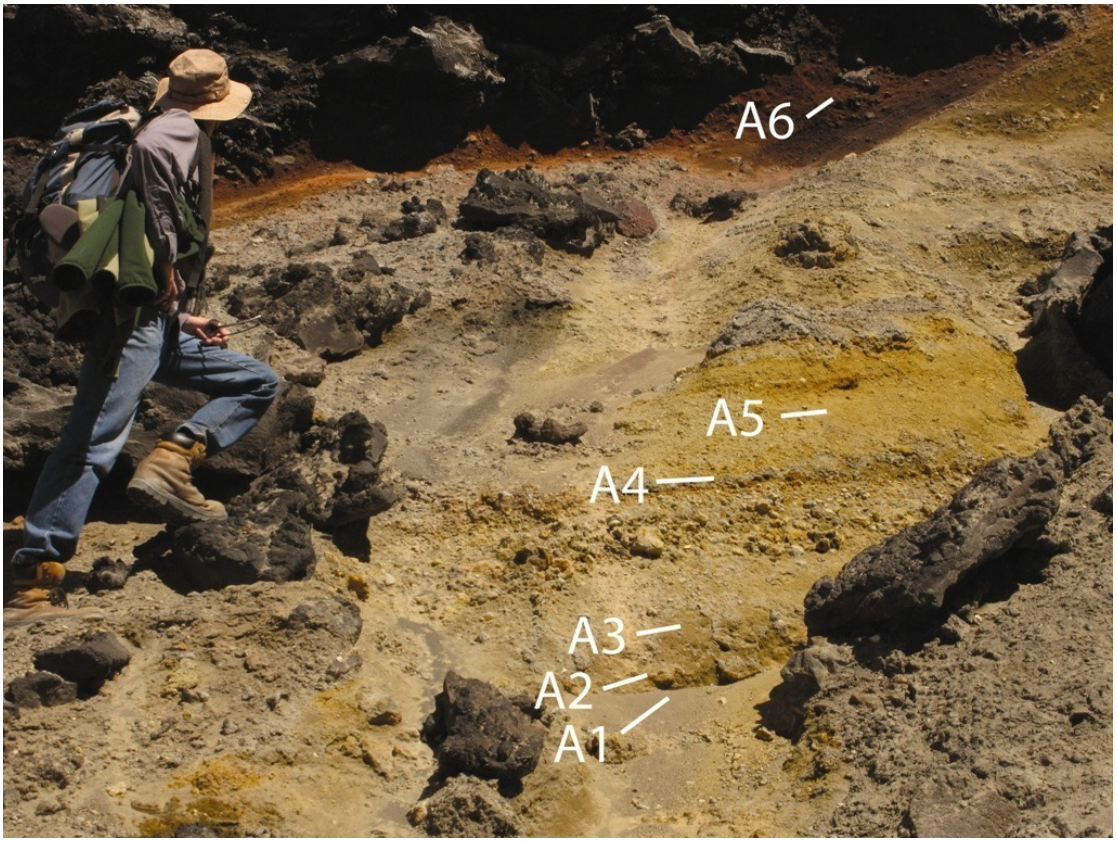

Figure 2.23: Close up of where samples A1-A6 were collected. Located on the outer flank of Pyramid Peak. 16/03/2010.

2.4.1 Clay content

The samples were split into two and weighed. Half of the sample was dried in the oven at 40°C and weighed again. The difference in weight was used to find the moisture content, which was ~8%. The other half of the sample was then sieved to 2 mm (-1.0 phi), using the Wentworth method, using a range of sieves in 0.5 phi intervals. The < 2 mm samples were separated into a ~5 g sub sample. These were then run through the *Partica* Laser Scattering Particle Size Distribution Analyser (PSDA). The results from the > 2 mm sieving and the PSDA were combined and the clay content in percentage weight was recorded (fig. 2.24).

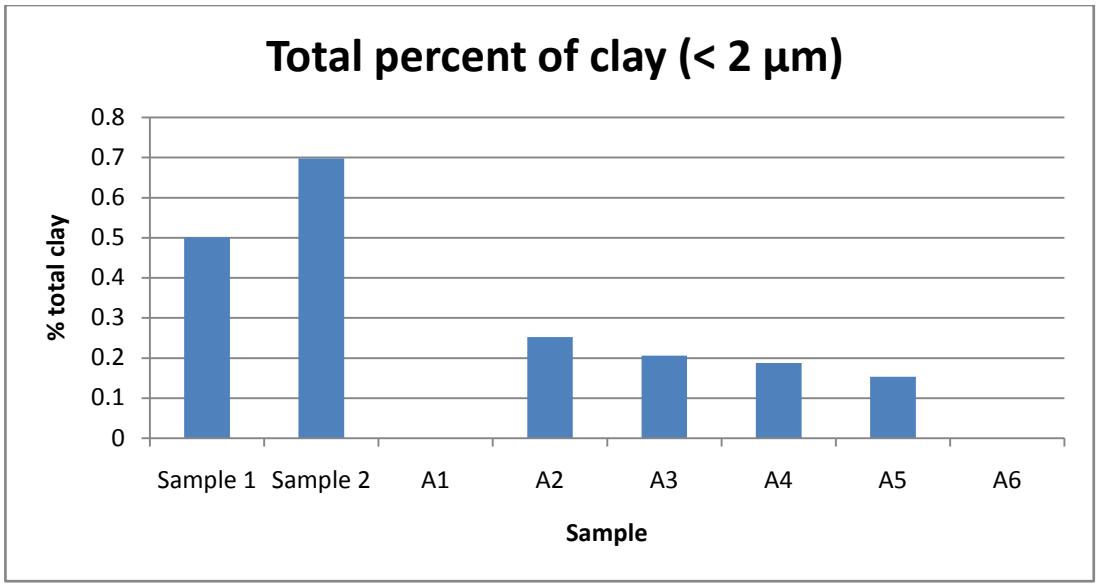

Figure 2.24: Resulting clay content of the collected samples. Sample1 and sample 2, inner crater wall. Sample A1-A6, outer crater wall.

2.4.2 Clay identification

The identification of clay minerals present in the tested samples was carried out using X-Ray Diffraction (XRD) analysis. The analysis was preformed on the GBC *E*MMA instrument and using the software program TracersV6. For XRD sample preparation a small part of each sample was put into suspension for 8 hours along with 4-10 drops of ammonium. The suspended material was separated and dried onto one of the metal chips used for the XRD. Results are presented in table 2.3.

Sample	Clay content
Sample 1	Gypsum, Natroalunite
Sample 2	Natroalunite, Alunite, Halloysite, Kaolinite
A1	Natroalunite, Jarosite, Halloysite
A2	Natroalunite, Jarosite
A3	Alunite, Halloysite
A4	Alunite, Jarosite
A5	Alunite
A6	Natroalunite, Alunite

Table 2.3: Resulting clay content from XRD analysis.

Alunite (including Natroalunite and Jarosite) and Halloysite were the main clay minerals found in the samples collected from the upper eastern crater wall. These clays are all associated with hydrothermal alteration (Grim, 1968; Inoue, 1995). These units contain clay minerals that are typically found in the hydrothermal system and at the base of Crater Lake, therefore this material could have easily become incorporated into eruptions and subsequently deposited in fall and surge beds. Compared to the Mangaio Formation, which represents a debris avalanche event from the failure of highly hydrothermally altered units, that has been found to have a clay content of 10-40% (Lecointre *et al*., 2004), the amounts of clay (< 1%) found in these samples were not significant. This low clay content suggests that hydrothermal alteration of the upper units of the eastern crater rim is not extensive. The samples collected from the inner crater rim have higher amounts of clay than the outer, possibly due to the proximity to the eruptive vent. The inner wall is more likely to be plastered with lake bed clay, through phreatic eruptions and wet surges. It is likely that permeable units further down in the eastern rim sequence with direct contact to percolating Crater Lake water also have larger clay contents due to hydrothermal alteration after emplacement.

2.5 Collapse scenario development:

2.5.1 Previous stability studies on the eastern crater rim

Hancox *et al*. (1997) assessed the stability of the Crater Lake rim of Mount Ruapehu following the 1995-1996 eruptions. From surveying, significant changes were determined in the 'Stump Saddle' area, with a net loss of 25 m of material since 1991 and a gain of 3-5 m of 1996 tephra. 50 m of material was also found to have been removed from the inner eastern crater wall, reducing its average width from 315 m to 250 m at 2450 m elevation. Hancox *et al*. (1997) stated that this was not a significant loss as the crater rim is still quite broad at this level. There was little overall change observed on the outer eastern crater wall, apart from the partial infilling of gullies with loose tephra. There was also some erosion of the Whangaehu channel below the waterfall (Hancox *et al*., 1997).

Due to the broad cross-section of the eastern crater rim Hancox *et al*. (1997) suggested that none of the above changes would result in a significant loss in crater wall strength, or reduce its ability to retain Crater Lake water once it has refilled. Hancox *et al*. (1997) also explained that the eastern crater rim is composed of relatively strong materials, including several supporting bands of strong blocky lava. They concluded that the changes from the 1995-1996 eruptions and future eruptions of similar magnitudes were unlikely to significantly reduce the rim's strength and stability. Hence the potential for a collapse of the eastern rim is currently considered to be low (Hancox *et al*., 1997). However, they did note that the collapse of the current lake outlet has occurred before and that there is a possibility for future collapse of the 1996 tephra dam when the lake refills. This occurred on 18th March 2007, producing a large lahar down the Whangaehu Catchment. Hancox *et al*. (1997) also acknowledged that the entire eastern side of the older South Crater has been destroyed before, with Crater Lake vent subsequently forming in its place. Hence a collapse cannot be ruled out. It was suggested that a collapse could occur from dike intrusion, which was the cause of a collapse at Pinnacle Ridge ~10,000 years ago (Hancox *et al*., 1997). The stability analysis carried out by Hancox *et al*. (1997) concluded that under static conditions the

most likely surfaces of the inner and outer eastern rim to fail would only be superficial, and that the potential for deeper seated failures are very unlikely.

Hancox (2001) assessed of the stability of the J peak area of Ruapehu's crater rim during an inspection for DOC. A crack along the crest of J Peak and the monitoring of continual displacements indicated that it is unstable. Hancox (2001) describes J Peak as a prominent knob of lava and agglomerate on the eastern crater rim between Dome and Pyramid Peak. It is suggested to be a remnant of a more extensive agglomerate/lava layer that has subsequently eroded. These failures of the layer along with local gullies have left J Peak unsupported and vulnerable to translational sliding (Hancox, 2001). No evidence was found to indicate that there is a more deep-seated instability in this area, but if J Peak fails there could be further erosion of the tuff beds below. Hancox (2001) concluded that any failure in this area will most likely be superficial.

Despite ongoing concerns for the stability of the eastern crater rim of Mount Ruapehu, no estimates of collapse volumes were provided and no downstream effects were evaluated.

2.5.2 Current stability assessment

No extremely hydrothermally altered layers could be identified within this study. The resulting clay analysis also supports the lack of strongly hydrothermally altered layers in this area. This could be due to either limited sampling, or the young age of the material which has yet to weather significantly or be hydrothermally altered. These upper units also do not come into contact with the water or hydrothermal system of Crater Lake. The main climatic weathering processes would be wind and rain, freeze and thaw and erosion from eruptive/seismic activity. Therefore, there appears to be no significantly hydrothermally altered layers to affect the stability of the upper flanks of Pyramid Peak. Instead it seems the most important layers that influence stability are the lavas that are draped unconformably over the unconsolidated materials making up Pyramid Peak. The importance of the lava units on the stability of Pyramid Peak was

also mentioned by Hancox *et al*. (1997). The lava units protect the layers below them and hold up the layers above. Where these lavas have fallen away, large gullies have formed, carving back into and exposing readily erodible volcaniclastic materials. The failures of small surficial lava blocks (such as J Peak) are not of much concern in terms of creating large debris avalanches, as they are themselves of low volume. The most coherent lava layers are present on the southern slope of Pyramid Peak, which support a vast amount of material and seem to stabilise this area. The initial failure of this whole section could result in a significant avalanche of material and subsequent minor slips afterwards as the landscape adjusts to the destabilisation. At present this block is being under cut as material erodes from the southern side into the upper Whangaehu catchment and the western side into the lake. This large block is also being eroded into by gullies on the eastern slopes.

Numerous aerial photographs taken between 1920s and 2010 were used as aids in constructing the geological map of the Pyramid Peak area. Changes to the eastern rim are noticeable over this time (fig. 2.25), although Pyramid Peak did not seem to change dramatically. The area with the greatest change is that of Stump Saddle. The Hancox *et al*. (1997) assessment of the south eastern crater rim suggested this also. Working with the older photographs enabled stratigraphic observations that are now no longer available. However, the majority of the photographs were taken shortly after an eruption event where the area was draped in fresh tephra. This obstructed any observation of change and detail of the stratigraphic units, although in some photographs certain units could be seen in areas of the crater rim where erosion has since occurred. This is noticeable especially between L Peak and Pyramid Peak, where material has since been lost from Stump Saddle. Suspected faults were also inferred around the Stump saddle region (fig. 2.25d).

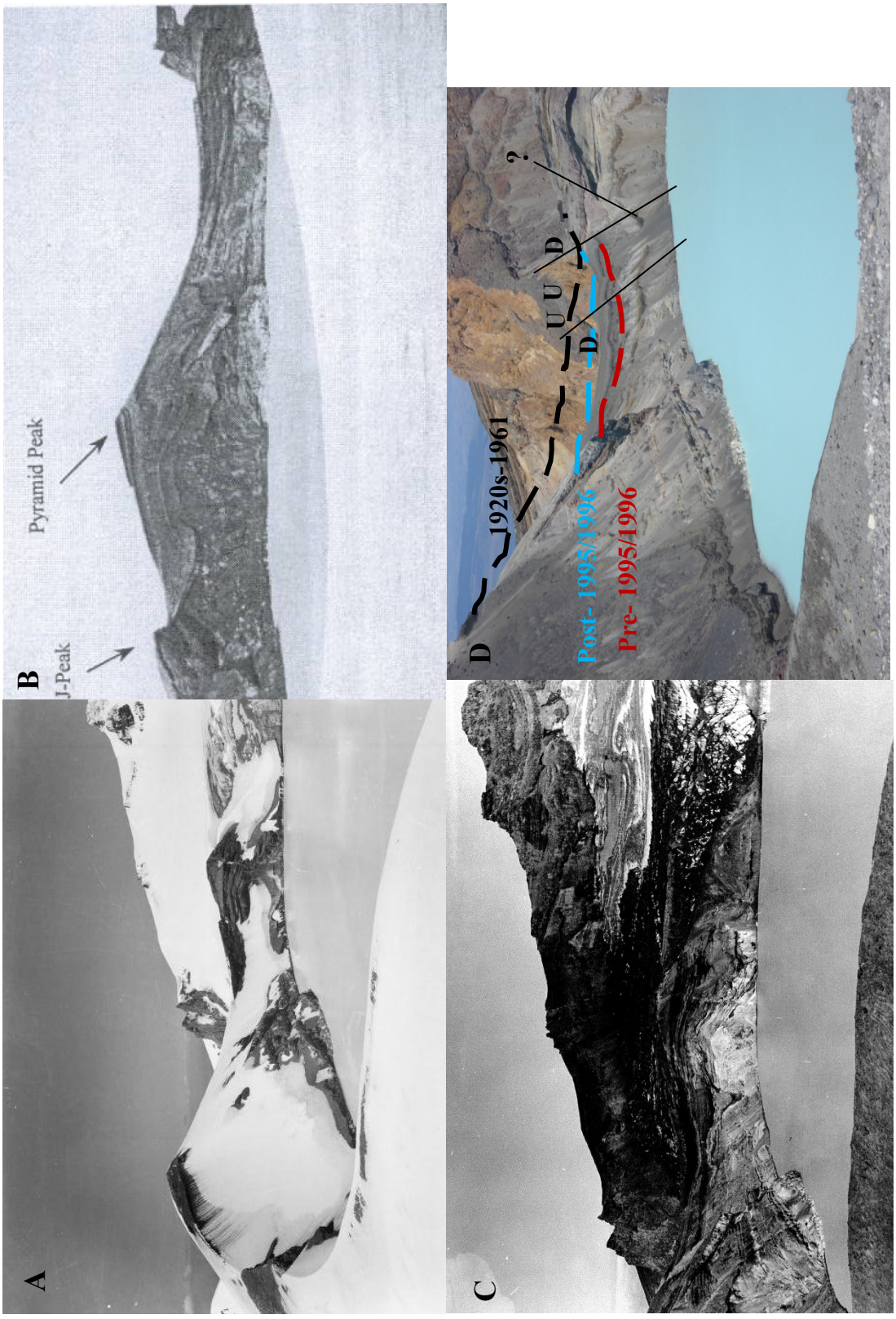

Figure 2.25: Four images ranging from the 1920s-2010 used to help show how the south eastern rim has changed. Stump Saddle was found to have changed the most. A) Photograph of Crater Lake taken in the 1920s by Thorley (1920s). B) Photo from Hales (2000) provided by Harry Keys, taken in 1939. C) Photo provided by Harry Keys, DOC, taken in Easter of 1961. D) Photo of Stump Saddle taken during field work in March 2010.

2.5.3 Scenarios developed:

Four possible failure events have been developed from the observed geology of the eastern crater rim. The possible failure events are based primarily on the boundaries below successive consolidated lava flow units. The varying volume of the scenarios is based on the structure of the eastern crater rim and the factors conditioning its stability. The first two scenarios are based on the failure of the upper flanks of the eastern crater rim, which would be conditioned by the failure of the supporting bands of lava, such as that of the Pyramid Peak and Coffin members. The failure of these units may also result in the rapid erosion of the material directly below. Scenarios 3 and 4 are based on the possible failure of deeper seated units that are hydrothermally altered by percolating Crater Lake water or underlain by hydrothermally altered layers. The failure blocks of the two largest collapse scenarios are not directly based on a specific lithological unit as the geology of the lower units of the eastern crater rim were not directly observed. These scenarios were constructed primarily on the basis of the collapse of different volumes of material. This study will look at the collapse and subsequent mass flow of each scenario, initially in the absence of Crater Lake water. As seen in the cross-section below, scenario 3 and 4 would result in the release of large amounts of Crater Lake water if the lake was full during the time of collapse. Crater Lake is currently at a high level, so that any collapse lowering the rim past lake level would result in an outburst flood. A resulting outburst flood could also have the potential to quickly erode soft materials. The study will therefore also simulate scenario 4 with an additional volume, representing the subsequent release of Crater Lake water that would likely occur during current conditions.

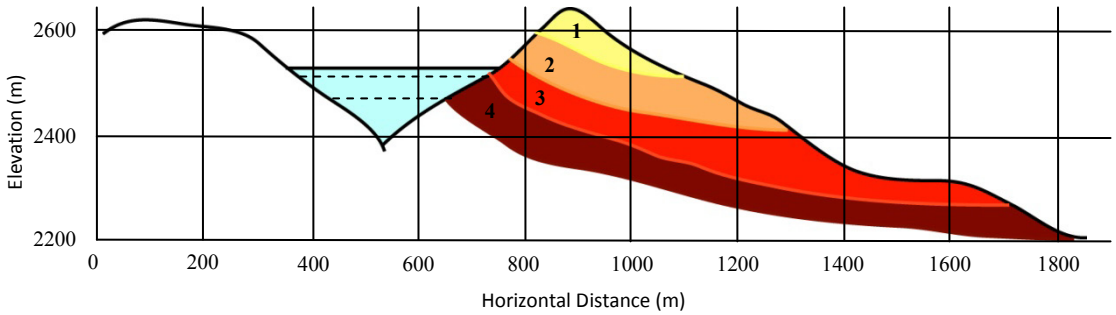

Figure 2.26: Cross-section of the eastern crater rim showing the four scenarios of collapse that will be modelled. Dashed lines represent the portion of the lake that will be released during the collapse of scenario 3 and 4.

Chapter 3: TITAN2D MODELLING AND PARAMETER TESTING

3.1 Introduction:

Volcanic debris avalanches are common mass flow phenomena from large volcanic edifices. They are the result of flank failure and may transform into debris flows with long run outs. Debris avalanches are very mobile, reaching tens of kilometres away from source with extremely high velocities. These events produce devastating impacts on people and property with very little warning. Volcanic hazards from mass flows are generally mitigated by the creation and planning application of hazard-zonation maps that depict areas that are likely to be inundated by future debris avalanches, debris flows and other volcanic processes (Schilling, 1998). The key element in the creation of hazard maps is a detailed geological study of mass flow deposits (Schilling, 1998). However, such observations and detailed recordings have not been made for all potentially hazardous volcanoes (Schilling, 1998). This is due to the difficulty accessing remotely located volcanoes; typically incomplete geological exposures, as well as the partially eroded or reworked nature of mass flow deposits; and the fact that detailed geological field observations are hard to achieve in a timely manner during times of volcanic activity (Schilling, 1998). Hence other means of estimating areas of potential risk from geophysical mass flow events are required. Numerical models and computer simulations can help with the understanding and management of debris avalanches and subsequent debris flows or lahars. In some (albeit rare) situations, numerical models may also be used to help find analytical solutions to problems. They are a description of a system in a mathematical language and enable the prediction of the system's behaviour from a set of parameters and initial conditions. Many types of models include dynamic systems, statistical models, and differential equations. Computer simulations are conducted on a computer program that has been coded to simulate a model of a particular system. Computer simulations have become a useful tool for expressing numerical models and can be used to gain new insights into and predict the performance of systems too complex for analytical solutions. Common flow

characteristics modelled are those that are of concern in hazard assessments, such as flow run out and inundation area. Hydrodynamic flow models like that of FLOW3D, statistical models such as LAHARZ, and granular models like that of DAN and Titan2D have been used to gain a better understanding of mass flow behaviour, forecasting the extent of future mass flow events and aiding in the development of hazard and risk maps and mitigation plans.

3.2 Previous models:

Recent efforts in modelling geophysical mass flows began with Savage and Hutter (1989). They began with equations of mass and momentum balance, using a Mohr-Coulomb constitutive relation (Pitman *et al.,* 2003a). Through scaling arguments, Savage and Hutter (1989) developed a one-dimensional model system based on the shallow water equations to simulate the flow of granular material (Pitman *et al*., 2003a). Pitman *et al*. (2003b) wrote a computer code to numerically solve the resulting equations. They also performed a series of table-top experiments, to extend the model to two-dimensions allowing them to examine flows over more general basal surfaces.

The efforts of Savage and Hutter (1989) were extended by Iverson (1997) to include the effects of pore fluid and later modern shock-capturing numerical techniques were used to solve the model system (Pitman *et al*., 2003a). Gray *et al*. (1999) and Gray (2001) re-derived the governing equations for granular flow over general basal surfaces, and tested his model against experimental avalanches in a rotational drum. Pitman and Tulyakov (1998) wrote a Godunov solver for one-dimensional flows that can incorporate general topographical features into the simulation.

The equations determined by the works of Savage and Hutter (1989) are not frame-invariant and therefore are unsuitable for modelling granular-type flows over 'real' terrain (Patra *et al*., 2005). In recent work, Iverson and Denlinger (2001) derive depth-averaged, frame-invariant equations for fluidized granular masses on three-dimensional terrain (Patra *et al*., 2005). Debris avalanches, debris flows, lahars and other related phenomena consist of particle-fluid mixtures that move across varied topographies. Iverson and Denlinger (2001) proposed that, despite differing mixture

compositions, initial and boundary conditions that may result in varied flow behaviour and deposit characteristics, the same basic forces should govern motion in all of these phenomena.

Models have been created for simulating various types of geophysical mass flows (Sheridan *et al*., 2005), such as: DAN (Hungr, 1995), Delft3D (Delft Hydraulics, 2011) and Titan2D (Patra *et al*., 2005). Flow models such as LAHARZ and Flow3D are statistical and empirical models that are applied to determine flow path and run out on natural terrain (Kover, 1995; Schilling, 1998). These different types of models were built on different assumptions about geophysical mass flows (McKinnon, 2010). Therefore each model has an appropriate usage depending on the problem and each has particular advantages and disadvantages (Sheridan *et al*., 2005).

3.2.1 Flow3D

The Flow3D model was developed by Kover (1995). It uses a detailed topographic database of the volcano for which it closely mimics the trajectories of flows (Saucedo *et al*., 2005). The Flow3D model is based on Coulomb resistance to a sliding block and hence is not a flow model in the strict sense. Flow3D calculates the changes in velocity as the block slides across a Digital Elevation Model (DEM), constructed using a Triangulated Irregular Network (TIN) (Sheridan *et al*., 2005). A gravitational acceleration vector, which is unique to each of the triangles in a TIN, is the driving force of the modelled flows (Sheridan *et al*., 2005). Resistance to flow in the model is calculated using a formula that solves for three empirical parameters: basal friction, internal resistance to flow, and external resistance due to turbulence (Saucedo *et al*., 2005; Sheridan *et al*., 2005). The limitations to this model are: multiple sliding blocks do not interact with each other; volumetric parameters are not included in the input or output data; conservation of mass and momentum are not used in the model; and the accurate measurement of planimetric extent of the flow cannot be obtained from the output (Sheridan *et al*., 2005).

3.2.2 LAHARZ

The LAHARZ model (Schilling, 1998), developed at the United States Geological Survey Cascades Volcano Observatory, was designed to rapidly simulate inundation areas of laharic mass flows. LAHARZ uses an empirical relationship between the planimetric area, cross-sectional area, and volume of debris flows in the Cascade Range to calculate the predicted flow path and deposit inundation of user-specified mass flow run out volumes over a DEM of the local topography (Iverson *et al*., 1998; Schilling, 1998). LAHARZ provides a fast, objective, automated, and reproducible method of risk assessment for future debris flows (Manville *et al*., 2003). LAHARZ, hence, is not a flow model per se and it does not give any information on flow velocity or momentum. Also the empirical relationships of the Cascade Range may not apply accurately to other areas (Stinton *et al*., 2004).

3.2.3 DAN and DAN3D

DAN (Dynamic Analysis) and DAN3D (Hungr & McDougall, 2009) were developed and used for the analysis of landslide run out, in particular, for practical landslide hazard and risk assessment. Both models are based on a system of depth-averaged governing equations derived from the principles of continuum mechanics, which treats the modelled mass as a continuous mass rather than as discrete particles (Hungr & McDougall, 2009). Both of the models use a semi-empirical approach based on the concept of 'equivalent fluid' (Hungr, 1995). The equations behind the two models begin from mass and momentum conservation laws that govern the mechanics of a continuum. These equations were expanded to include boundary conditions and depth averaging with the use of the Leibniz's rule (Hungr & McDougall, 2009). Entrainment of material is accounted for by allowing volume flux across the basal boundary (Hungr & McDougall, 2009). The equations were converted to a Lagrangian coordinate system. DAN is a 1-dimensional model based on a Lagrangian solution of the equations of motion and allows the selection of a variety of material rheologies (Hungr, 1995). DAN3D uses a 2-dimentional form of the same equations as DAN to smooth particle hydrodynamics and calculate run-out along a user-prescribed 3-dimensional DEM (Hungr & McDougall, 2009; McKinnon, 2010).

3.2.4 Delft3D

The Delft3D model is a commercially-available fluid dynamics software suite from Delft Hydraulics (2011). Delft3D solves the Navier-Stokes equations for an incompressible fluid under the shallow water and Boussinesq assumptions (Carrivick *et al*., 2009). The governing equations for Delft3D are the continuity and momentum equations, solving the unsteady shallow water equations in two- (depth-averaging) and three-dimensions (Carrivick *et al*., 2009; Delft Hydraulics, 2011). Delft3D treats the modelled mass as having a fluid density that is 100% water flow. Flow propagation and hydraulic conditions only consider Newtonian behaviour, with no consideration for sediment transport (Carrivick *et al*., 2009).

3.3 Titan2D

Titan2D (Patra *et al*., 2005) is a software application developed by the Geophysical Mass Flow Group at the State University of New York (SUNY) at Buffalo. Titan2D was developed for the purpose of simulating granular flows (primarily debris avalanches and landslides) over digital elevation models (DEMs) of natural terrain. Titan2D combines numerical simulations of flow with digital elevation data of natural terrain supported through a Geographical Information System (GIS) interface such as GRASS. Titan2D is derived from a depth-averaging model for an incompressible Coulomb continuum, a "shallow-water" granular flow (Patra *et al*., 2005). The resulting governing equations are solved using a parallel, adaptive mesh Godunov scheme (Patra *et al*., 2005). Mesh adaptively allows for the concentration of computing power on areas of special interest (Patra *et al*., 2005). Mesh refinement also captures the complex flow features at the leading edge of the flow, as well as at locations where topography changes rapidly (Patra *et al*., 2005). The Titan2D model assumes a volume, pulled down slope by gravity; this momentum is resisted by friction between particles and between particles and the ground. The outputs of Titan2D are flow depth and momentum, which can later be used to compute field observable variables at a specific location, such as run-up height, inundation area and flow time. Titan2D operates via a python scripted Graphical User Interface (GUI); through this interface the user inputs

the parameters needed to run the program successfully: pile dimensions, starting coordinates, internal and basal friction angles, and simulation time. Titan2D requires an initial volume and shape estimate of the starting material for the simulated granular flow. Simulation is computed on a Digital Elevation Model (DEM) of the desired area and results can be displayed through the Titan2D viewer utility or other visualization software packages (i.e. Arc View and TecPlot).

This research used Titan2D to simulate various debris avalanche scenarios originating from the predicted failure of the eastern crater rim of Mount Ruapehu. Numerous preliminary runs were made to constrain the model with realistic limits. Once the model was constrained, successive flow simulations were made with various volumes and the simulated outputs analysed.

3.3.1 Applications of Titan2D

Titan2D has been used for different types of mass flows at locations worldwide such as; modelling block-and-ash flows at Colima volcano, Mexico (Rupp *et al*., 2003; Patra *et al*., 2005); pyroclastic flow modelling of the Soufriere Hills Volcano pyroclastic flow deposits (Widiwijayanti *et al*., 2004); identifying the potential hazard from mass flows at Tungurahua volcano, Ecuador (Sheridan *et al*., 2004); simulating in conjunction with Flow3D, peak avalanches from Mount Rainier (Sheridan *et al*., 2005); pyroclastic flows at Cerro Machin Volcano, Colombia (Murcia *et al*., 2010); and forecasting hazards from Mount Taranaki (Yu *et al*., 2009; Procter *et al*., 2010a).

Titan2D simulated block-and-ash flows from the 1991-1999 eruptions of Colima Volcano, Mexico, with volumes ranging from a few cubic metres to a million cubic metres (Rupp *et al*., 2003). The resulting simulations were compared with the actual deposits, and for a given flow volume, Titan2D approximated the flow path and run-out distance well and the outputs were consistent with field observations (Patra *et al*., 2005).

Past simulations from Flow3D and published field data on the 1963 Little Tahoma Peak avalanches on Mount Rainier, Washington were used to evaluate the Titan2D model (Sheridan *et al*., 2005). The resulting simulations from Titan2D stayed within the mapped extent of the field deposits (Sheridan *et al*., 2005). Titan2D also managed to simulate the small portion of a flow that escaped through a small gap between the crest of the terminal moraine and the lower slopes of Goat Island Mountain (Sheridan *et al*., 2005). Overall the simulations for Titan2D compared favourably with the actual avalanche data (Sheridan *et al*., 2005).

Titan2D was applied to evaluate the possible effects of future pyroclastic density currents from Cerro Machin (Murcia *et al*., 2010). The distribution and thickness of the deposits obtained from the simulations were consistent with the hazard map presented by the Geological Survey of Colombia in 2002.

Titan2D was used to map block-and-ash flow hazards from Mount Taranaki, New Zealand. Before it was applied, it was calibrated by simulating past events (AD 1860 and AD 1755) (Procter *et al*., 2010a). From these, appropriate input parameters were defined with scenarios being created from an acceptable range of parameters. The study resulted in a suite of potential areas likely to be inundated by a future block-and-ash flow under the present-day terrain, which helps in the production of hazard zones (Procter *et al*., 2010a).

3.4 Previous modelling of Ruapehu mass flows:

Vignaux and Weir (1990) presented a mathematical model of the motion of lahars. They used a kinematic wave model to calculate lahar propagation and travel speeds. The kinematic wave model equates gravitational accelerations to frictional losses. Vignaux and Weir (1990) applied the model to all recorded lahar flows from Mount Ruapehu at the time, and managed to satisfactorily describe all lahars generated by a single explosive mechanism. They successfully calculated lahar discharges and travel

times of past lahars generated by single seismic events. However, describing lahar decay and rheological changes were found to be difficult (Vignaux & Weir, 1990).

Stevens *et al.* (2002) investigated the effects of Digital Elevation Model (DEM) errors on the performance of a volcanic flow model designed to delineate areas at risk from lahar inundation, LAHARZ. Two DEMs of southern Mount Ruapehu were used; the first was derived from digitised 1:50 000 topographic maps while the second was derived from an airborne C-band Synthetic Aperture Radar (SAR) interferometry obtained using the NASA AIRSAR system (Stevens *et al*., 2002).

After the LAHARZ model was run over both DEMs, it was found that predicted flow paths on sleeper slopes of >4° (where drainage channels are deeply incised) were generally in agreement for both DEMs (Stevens *et al*., 2002). However, over shallow slopes of <4°, where channels are shallow and tend to meander (ring plain), flow path prediction in both DEMs encountered problems. This was due to interpolation errors and forestry masking the true topography (Stevens *et al*., 2002). Stevens *et al*. (2002) found that areas of inundation predicted by the LAHARZ model were affected by DEM quality and resolution (fig. 3.1).

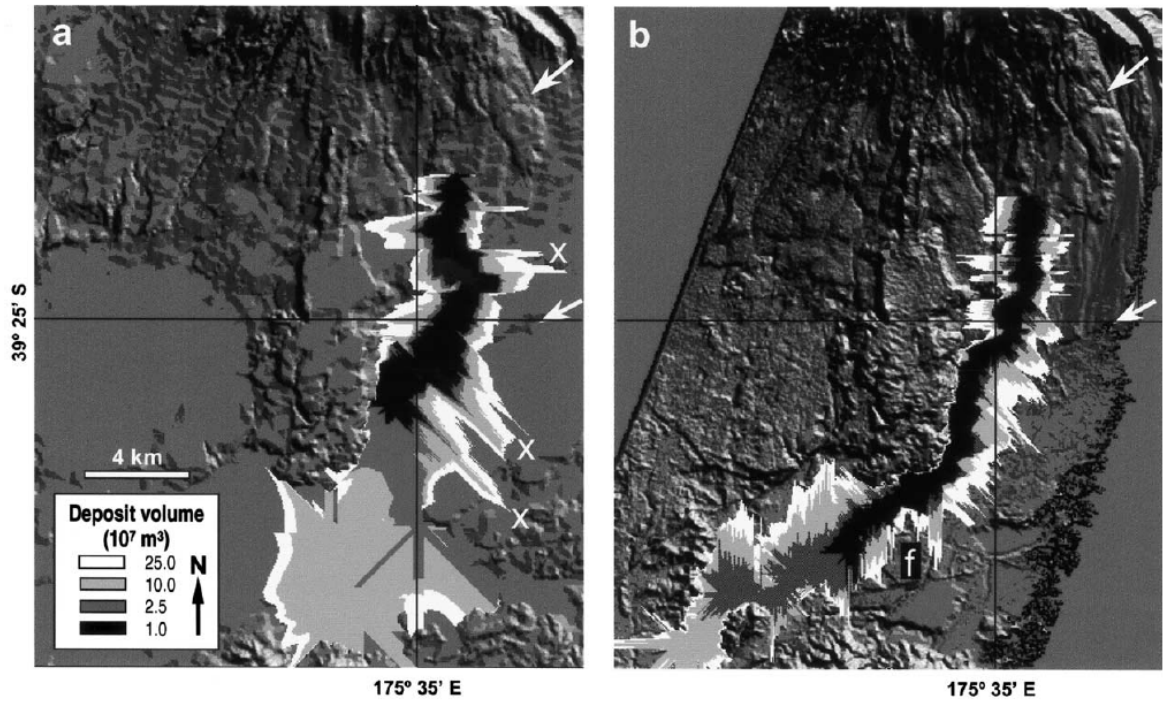

Figure 3.1: Predicted lahar inundation using the same starting position in (a) the LINZ DEM, and (b) the TOPSAR DEM, plotted over shaded relief images of the respective DEMs at the same scale. Arrows indicate the major fault scarps, and the Tahatekapua lava flow is in the centre of each DEM. 'X' indicates areas in the LINZ DEM where the lahar inundation has spread unreasonably far laterally, coinciding with flat spots in the DEM. 'f' denotes an area of forest in the TOPSAR DEM, which is incorrectly interpreted as a high relief obstacle to the lahar deposition (Stevens *et al*., 2002).

Stevens *et al*. (2002) concluded that digital elevation data at the spatial resolution and relative accuracy of the NASA SRTM (Shuttle Radar Topography mission) data will be a valuable and reasonably reliable asset for future risk assessment. Even though it was not addressed in the study, Stevens *et al*. (2002) noted that changes in topography at volcanoes due to deposition and erosion following large-scale lahars and other volcanic processes are another source of error in digital elevation data. Existing flow paths may change significantly as a result; therefore repeat surveys at volcanoes were recommended.

Manville *et al.* (2003) used LAHARZ to simulate debris avalanches with volumes ranging three orders of magnitude at Mount Ruapehu. From this they demonstrated the advantages and disadvantages of the program. Utilising a 20 m DEM, they attempted to simulate the debris avalanche that emplaced the 9.5 ka Murimotu Formation (Palmer & Neall, 1989) on the north western ring plain of Mount Ruapehu. The

simulated deposit was slightly displaced to the east of the actual formation, which was inferred to be due to the modern topography already including the deposit being simulated, changing its course. During the evaluation of the LAHARZ software Manville *et al.* (2003) modelled four different volume based scenarios of likely future debris avalanches at Mount Ruapehu (table 3.1). Based on geological evidence the likely origin of these events was Pyramid Peak, the south-eastern crater rim. Four failure surfaces were determined and volume scenarios calculated.

Scenario	Cone height (m)	Cone radius (m)	Cone volume (x 10^6 m^3)	Crater Lake (x 10^6 m^3)	10 % dilation factor (x 10^6 m^3)	Total debris avalanche volume (x 10^6 m^3)	Whangaehu channel (75%) (x 10^6 m^3)	Northern tributary (25%) (x 10^6 m^3)
1	326	653	146	9	16	171	126	45
2	282	565	95	9	10	114	84	30
3	217	435	43	9	5	57	42	15
4	161	322	17.5	9	2	28.5	21	7.5

Table 3.1: Volumes of debris avalanche LAHARZ scenarios for Pyramid Peak collapse (Manville *et al*., 2003).

The largest event involved the collapse of the entire Pyramid Peak due to a deep-seated failure reaching the bottom of the lake (Manville *et al*., 2003). The dilation of the material was set at 10% and assumed to occur on the Whangaehu Fan. It was also assumed that 75% of the material would be directed into the main Whangaehu channel and 25% directed into a northern tributary.

Manville *et al.* (2003) found that the resulting simulation (fig. 3.2) of the debris avalanche that was directed into the main Whangaehu channel travelled 20 km downstream from the proximal hazard zone boundary at the fan apex, with the Rangipo fault scarp diverting it to the south. The portion of the flow that was directed into the northern tributary of the Whangaehu River spontaneously avulsed into the upper Waikato catchment, apparently across a low drainage divide, and entered into the Tongariro River catchment. Manville *et al.* (2003) stated that this was a realistic result from an event of this size. The largest scenario inundated an area of ~62 km^2 and the smallest scenario ~19 km^2. The average deposit thicknesses were found to be ~4 m and ~2 m respectively.

The main limitation of LAHARZ was that it did not take velocity and momentum effects into account, or account for flow transformations (Manville *et al*., 2003).

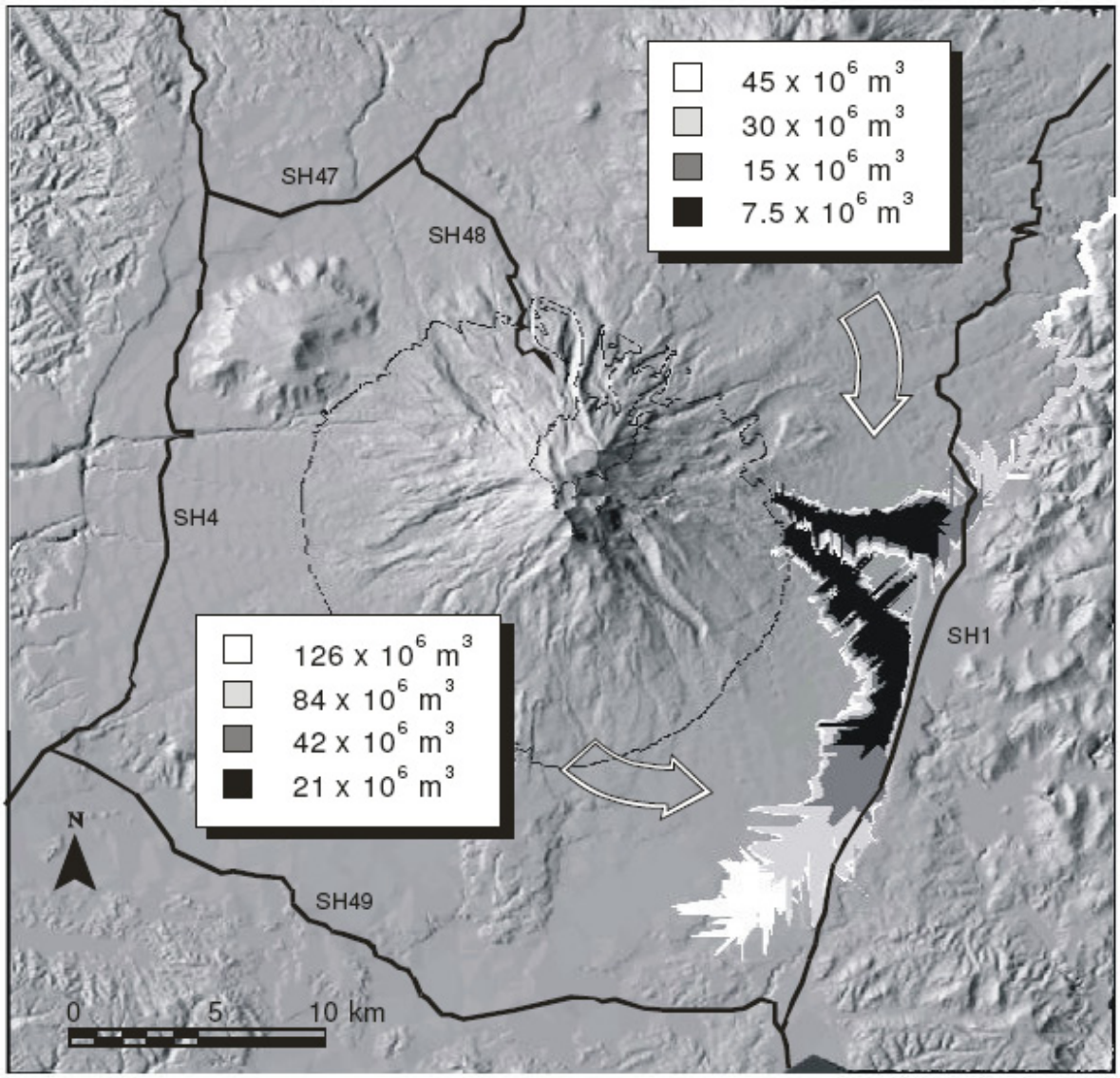

Figure 3.2: Results of Pyramid Peak collapse models simulated by LAHARZ (Manville *et al*., 2003).

Fagents and Baloga (2005) developed a mathematical description of lahar propagation over digital topography using an elementary model of lahar transport dynamics. Their approach was used to derive flow parameters though each topographic increment of digital terrain, and thereby investigating the sensitivity to topographic resolution of flow-front advance rates and transit times. They applied the model using parameters typical of large volume (10^6 to 10^7 m^3), long run-out (25-50 km) lahars at Mount

Ruapehu. As the analysis aimed to isolate the effects of topographic resolution on calculating transit times, they used a continuous, analytic slope model to represent volcano topography, and discretize it to produce a sequence of inclined planes, rather than use a real DEM of Ruapehu's flanks, which would contain irregularities that would engender new problems themselves. Fagents and Baloga (2005) found that transit-time predictions are sensitive to the number of increments into which the flow path can be divided by the available topographic data. For this example, accurate transit-time prediction is ensured by taking approximately 200 equally spaced horizontal intervals (DEM of 250 m horizontal resolution or 10 m contours). They also state that irregular topography cannot be modelled as a drop in elevation over a run-out distance (H/L) as this will result in significant errors in transit-time predictions.

Carrivick *et al*. (2009) used Delft3D, a fluid dynamics model to analyse the 18th March 2007 dam break lahar at Mount Ruapehu. The intent of the study was to address quantification of those flow conditions most important for hazard management, i.e. stage and travel time, because they were considered to govern inundation zones and effective warning times.

Delft3D considers an end-member case of lahars i.e. one where the fluid density is that of a 100% water flow. Flow propagation and hydraulic conditions only consider Newtonian behaviour; therefore there is no consideration of sediment transport (Carrivick *et al*., 2009). The major results of the study were computations of inundation area, time to inundation, peak flow depth variation and flow velocity variation. Every 20 minutes these flow properties were described for the entire study area and for each of their key sites.

Carrivick *et al*. (2009) found that the results of the modelled lahar generally compared well with gauged records, historic records and other modelling approaches. However, they found discrepancies with frontal velocity and time to peak stage. There were two main reasons for this. The first was specifying roughness, which arises from slope variations between adjacent computational nodes, and which is also stage-dependent. The second is rapid topographic changes which produce frequent hydraulic jumps for

which the numerical scheme inadequately accommodates. They stated that the overall relationships between topographic and hydraulic variables and pattern of discharge attenuation is similar to that calculated for lahars on other volcanoes, therefore this modelling method can be applied to other sites where hydraulic and high-resolution topographic data are available.

Carrivick *et al*. (2009) noted that spatial and temporal distributed modelling approaches need to be developed to accommodate the variable behaviours of lahars. An example was made of the 18th March 2007 lahar which had an initial volume of 1 x10^{6} m^{3}. Due to bulking, the flow reached a maximum volume of 4 x10^{6} m^{3}. Hence they suggested that the total volume is not of prime importance for determining longitudinal hydraulic variations, as is suggested by some GIS based regression models and some granular flow models.

3.5 Titan2D and Ruapehu:

Titan2D modelling was applied to model the run-out of possible future debris avalanches from the eastern crater rim of Mount Ruapehu. Preliminary runs were simulated in order to determine appropriate input parameters (internal and basal friction angles). These unknown input parameters were found by systematically testing different combinations of the two friction angles and assessing how physically realistic each flow run-out was with respect to actual flow data measured in the field (18th March 2007 lahar). Laboratory experiments by Martelli (2007) provided constraints to the input parameters. The outputs of the flow models were visualised in TectPlot 360 and displayed on the NZMS 260 T20 topographical map and constructed DEMs using ArcView.

3.5.1 Scenarios

Two different series of computational experiments were run on Titan2D. The first series was set up to systematically determine the influence of the volume of collapsed material on flow behaviour. For simplicity the crater was assumed empty in this series. The range in collapse volumes from Pyramid Peak were varied over 1.5 orders of

magnitude and spanned geologically feasible lower and upper limits of material that could potentially collapse (scenarios 1-4 in table 3.2).

In the second series of computational experiments, scenario 4 was to be repeated for the case of a full Crater Lake. In this simulation, which represent the current situation at Mount Ruapehu, the effect of further increasing the mass of collapsing material (the mass of outbursting Crater Lake water) and the effect of increasing the water/solid ratios of the bulk flow on flow run-out behaviour were to be modelled. However, Titan2D was unable to model the entire run-out of two separate collapsing piles at the same time due to the interaction of variable fluid components. Subsequently scenario 4 had to be modelled with only the additional mass of the outbursting Crater Lake water. This additional scenario was labelled scenario 5. This simulation was run to see the effect of the additional collapsing volume on the resulting mass flow. Calculated volumes of Crater Lake water released in scenario 3 and 4 are given in table 3.3.

Scenario	Pile Height (m)	Initial solid vol. fraction	Centre of pile		Major pile radius (m)	Minor pile radius (m)	Orientation (degrees)	Calculated pile volume from Titan2D (m^3)
			Eastings	Northings				
1	45	0.85	2731597	6210478	146.5	130	-18	$1.3x10^6$
2	90	0.85	2731597	6210478	295	205	-18	$8.5x10^6$
3	135	0.85	2731597	6210478	498	262.5	-18	$2.8x10^7$
4	180	0.85	2731597	6210478	655	288.5	-18	$5.3x10^7$
5	202	0.85	2731597	6210478	655	288.5	-18	$6.0 x10^7$

Table 3.2: Summary of the determined input parameters for this study.

Scenario	Lake depth (m)	Min radius (m)	Max radius (m)	Lake volume (m^3)
4	65	228	296	$6.9x10^6$
3	20	228	296	$2.1x10^6$

Table 3.3: The volume of Crater Lake water subsequently released after flank collapse scenarios 3 and 4.

3.5.2 Determining input parameters

Input parameters required for a Titan2D simulation are divided into three categories: computational, numerical/physical, and volumetric in terms of where the initial mass is sourced (fig. 3.3, 3.4, & 3.5). A summary of the input parameters used to produce each simulation in this study are presented in table 3.2.

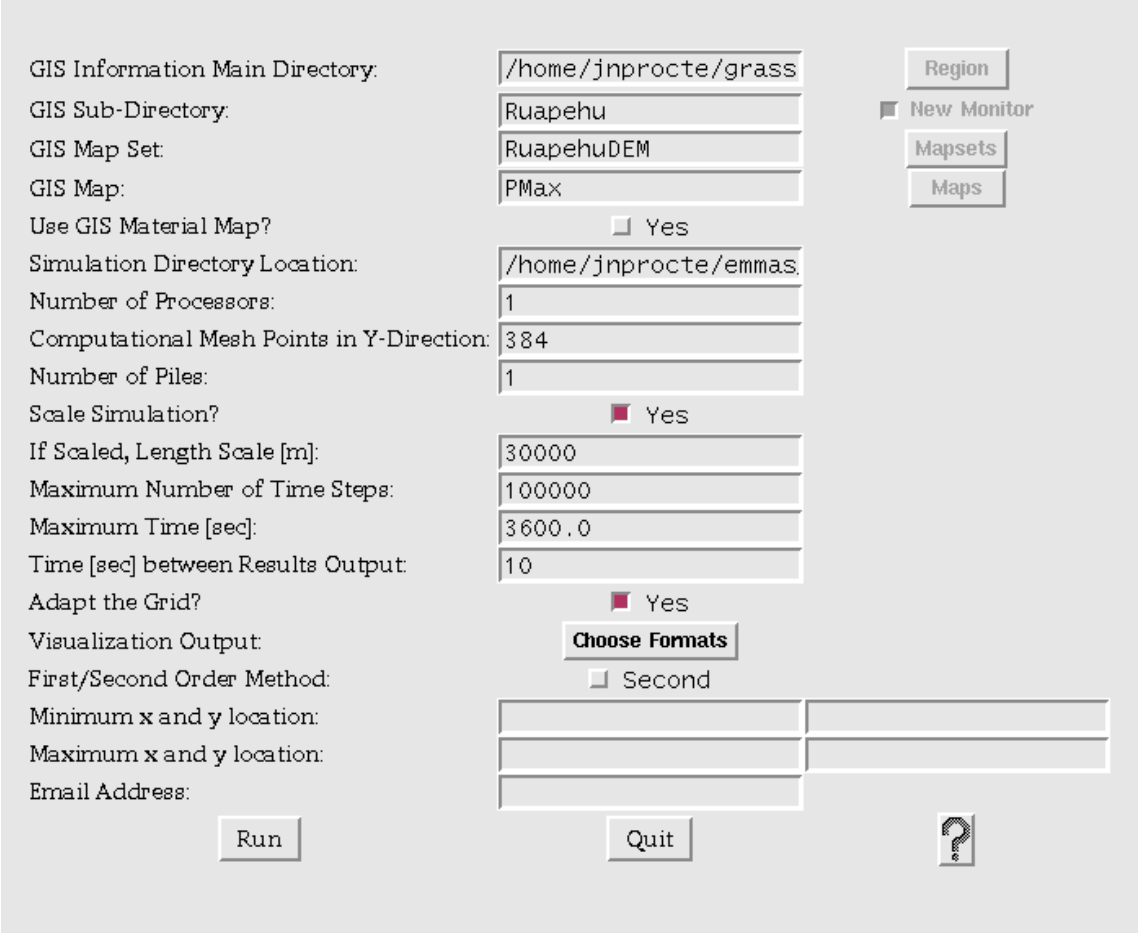

Figure 3.3: Screen shot of the first screen of input parameters for Titan2D tool kit requesting the computational requirements.

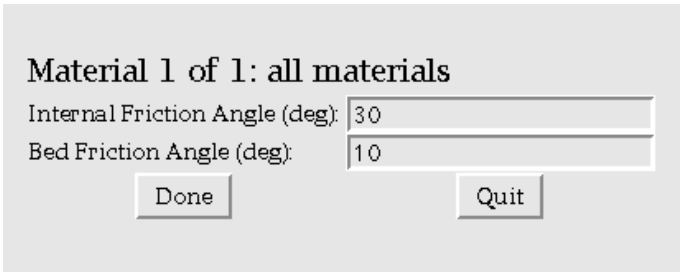

Figure 3.4: Input parameter screen 2, defining the piles internal and basal friction angles.

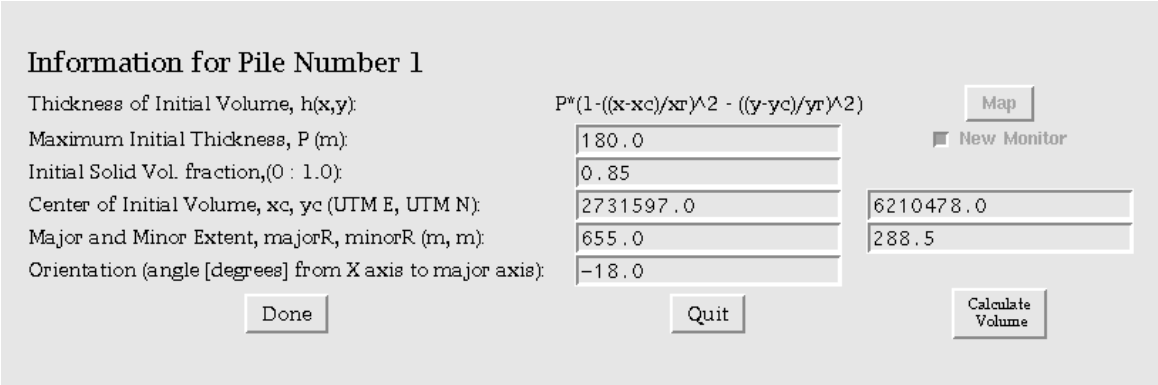

Figure 3.5: Input parameter screen 3, determining pile dimensions and initial volume.

3.5.3 Creating Digital Elevation Model (DEM) surfaces

Digital elevation models were created to provide surfaces for the models to be simulated on and to yield topographic information for the analysis of the resulting simulations, such as elevation, run-out length and location of points of interest. A DEM at 20m resolution of the central North Island from LINZ was used for image display. In addition four DEMs of the eastern rim and the eastern flank area at 10m resolution were created from contour and spot height data to provide further detail for this proximal region. All DEMs were constructed in the ESRI GIS software, ArcMap, from a point file of elevation data, NZMS 260 T20 topomap contours and spot heights from various RTK GPS surveys. Triangular irregular networks (TINs) were constructed from these data sources and converted into GRASS GIS raster formats for the use in Titan2D modelling.

The scenarios simulated by Titan2D in this study represent a range of possible volumes expected to collapse from Pyramid Peak. The volumetrically largest scenario (scenario 4) represents the collapse of the entire eastern rim with a volume of 53 x 10^6 m^3 and a basal area of 6 x10^5 m^2 (fig. 3.6b). This basal area is used to subtract the contained elevation on the DEM, creating a planar failure plane. The initial collapsing pile created in Titan2D was positioned on this failure plane surface, representing the mass that was subtracted from the DEM (i.e. the entire eastern rim). A shape file of the representative basal area for each scenario was created in ArcMap. In turn these shape files were used to construct specific DEMs for each scenario simulated in Titan2D.

3.5.4 Pile dimensions and initial volumes

The initial flow volume was calculated within Titan2D from a user defined starting pile. Input pile dimensions (fig. 3.5) for each scenario were derived from ArcMap shape files, representing the basal area and volume of different portions of the eastern rim (fig. 3.6b). The area of Pyramid Peak was divided into four approximate portions of 25%, 50%, 75%, and 100%, representing each scenario. These shape scenarios were digitised from an orthophoto of Mount Ruapehu (fig. 3.6a) obtained from the Light Detection and Ranging airborne laser scan (LiDAR) Massey University and GNS Science acquired in April 2007, after the 18th March 2007 lahar. This orthophoto, along with the shape files, constructed DEMs and the NZMS 260 T20 topomap, were all used to define the pile dimensions for each scenario (1-4). Scenario 5 is an amalgamation of the mass collapsed in scenario 4 and the calculated volume of the Crater Lake water that would subsequently be released from the collapse of this portion of the eastern rim.

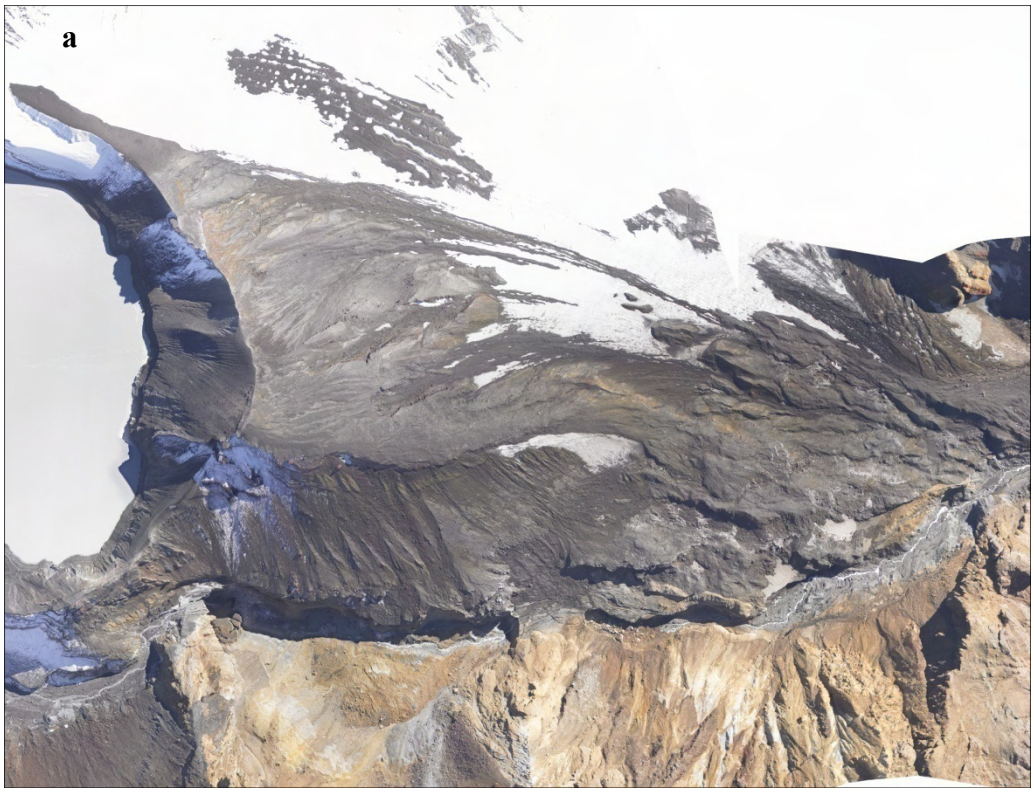

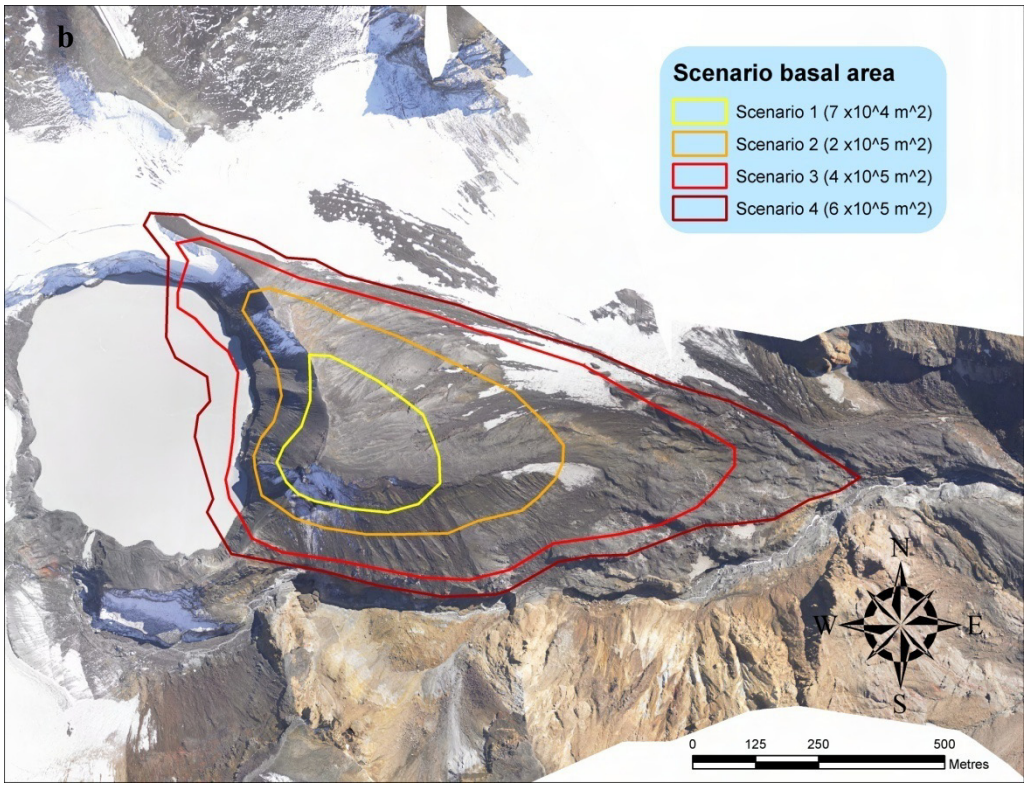

Figure 3.6: a) The Massey University and GNS Science orthophoto, April 2007, used to identify the scenarios of collapse. b) Shape files constructed in ArcMap of the outline representing basal failure planes for recreating the Titan2D initial pile for scenarios 1-4.

3.5.5 Determining friction angles

Internal and basal friction angles are important input parameters for Titan2D. The internal friction angle is the parameter that defines the inter-granular Coulomb force due to velocity gradients normal to flow direction, which varies with flow composition. The basal friction angle is the parameter that defines the resisting force at the base of the flow due to Coulomb friction (Martelli, 2007; Procter *et al*., 2010b).

A wide range of basal friction angles (5-35°) were systematically tested in preliminary Titan2D runs in 5° intervals for constant collapse volumes of c. 47 x 10^6 m^3. This flow had input parameters of 384 computational mesh points, a defined run-out maximum of 30 km, maximum computational time steps of 100,000, with 10 seconds between each output. The basal friction angle was found to significantly affect the flow behaviour and resulting inundation area (fig. 3.7). The most physically realistic results were found with angles of 5° and 10°. In modelling block-and-ash flows on Mount Taranaki, Procter *et al*. (2010a) found that basal friction angles between 15-25° best

matched historic deposits. After testing basal friction angles before modelling debris flows at Mount Ruapehu, Procter *et al*. (2010b) found that the best results were from the simulations with angles between 9-12° by comparing previous lahar inundation areas in the Whangaehu channel. Where slopes were less than 9° it was found that flow behaviour changed from notably erosional to depositional. Simulated flows were also seen to be less accurate over DEM slopes of less than 9° as they no longer conformed to topographic depressions and natural drainage paths. From the analysis in this study a fixed basal friction angle of 10° was chosen to be most realistic.

A range of internal friction angles were also tested. However, changes in internal friction angles appeared to only affect flow velocity and only had a minor influence on resulting inundation areas of the simulated flows; hence an optimal angle could not be determined. Therefore, a fixed internal friction angle of 30° was chosen based on the angle-of-repose (30-35°) typical of Ruapehu debris flow sediment (Procter *et al*., 2010b); tilt table experiments by Martelli (2007) also confirmed that internal friction angles of around 33° suited similar sediments.

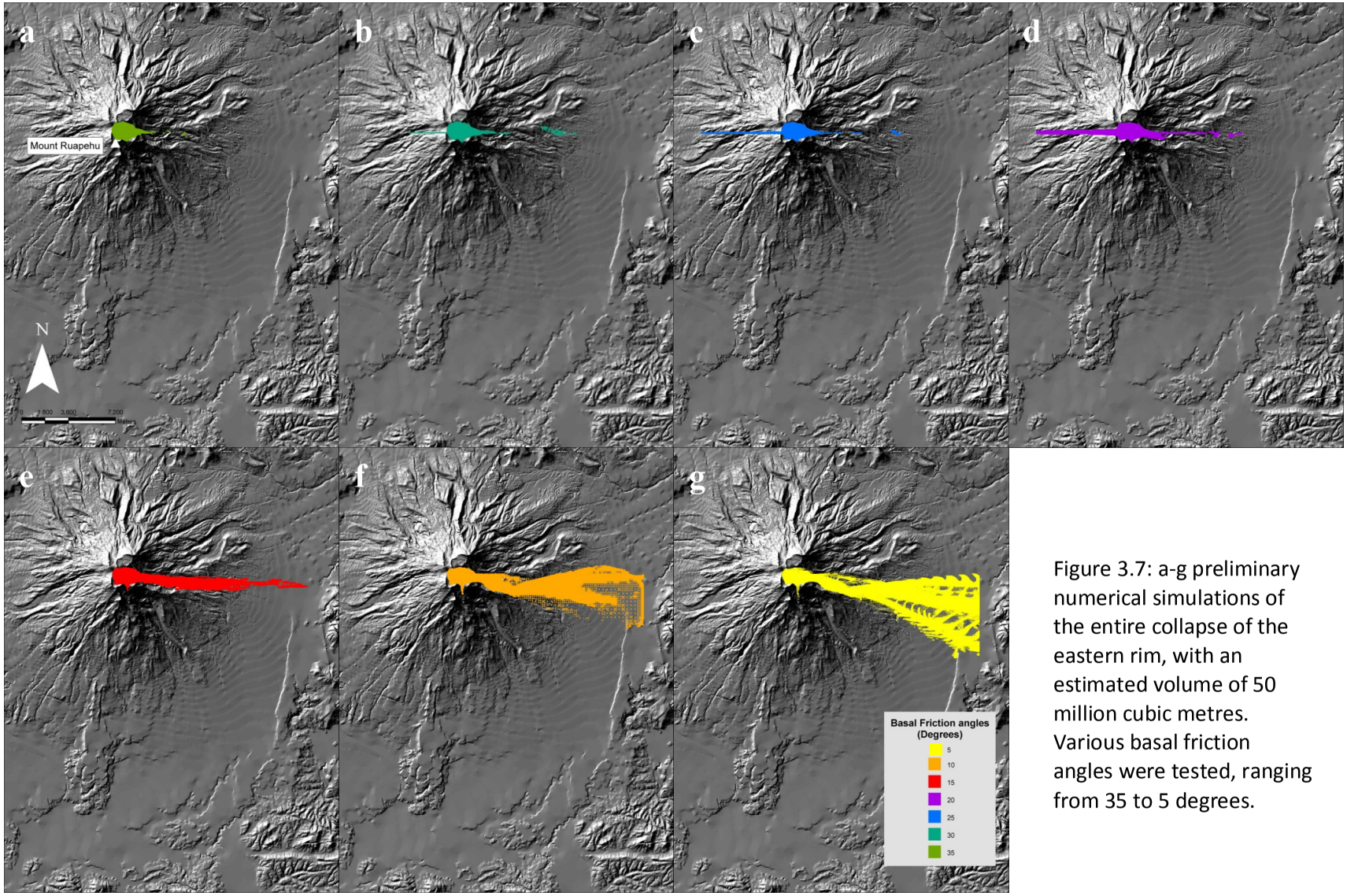

Figure 3.7: a-g preliminary numerical simulations of the entire collapse of the eastern rim, with an estimated volume of 50 million cubic metres. Various basal friction angles were tested, ranging from 35 to 5 degrees.

3.6 Resulting Titan2D simulations and outputs:

The total inundation areas of the scenarios modelled are displayed in figures 3.9, 3.11, 3.13, 3.15, and 3.17. The simulation data were plotted in ArcMap to define and compare inundation areas, run-out lengths and flow path. The output data from Titan2D were displayed in ArcMap by converting the Tectplot output file into comma-delineated text files. The text files were imported into ArcMap as x, y point data and then exported as point based shape files. These were in turn converted into rasters where the maximum flow pile height was used as the interpreted attribute. The modelled flows were also displayed in an AVI movie format through Tectplot 360. This provided a good visual aid in describing flow behaviour over time. Separate time step files were also analysed in Tectplot 360 to provide flow front location and average velocity over time. This was later used to calculate frontal velocities and flow arrival times.

3.6.1 Whangaehu River channel

At the base of the southern flank of Pyramid Peak lie the headwaters of the Whangaehu River (fig. 3.8). Water is supplied to the catchment from the Crater Lake outlet and known springs further downstream. The Whangaehu River flows in a steep bedrock gorge, which bifurcates approximately 2km downstream. The northern path is a deeply entrenched narrow gorge, while the southern channel is broader and is usually dry. These two paths meet up again at a confluence ~6 km from Crater Lake. At a site called the “chute” the channel splits again before emerging out onto the braided Whangaehu Fan. The Whangaehu Fan (from 1300 m in elevation) is 4.5 km wide and 6 km long, truncated to the west by the 50 m high Rangipo Fault scarp (fig. 3.8) (Cronin *et al*., 1999). At the apex of the fan an artificial bund has been constructed to prevent a large break-out lahar from over flowing into northern catchments that lead into the Tongariro River and then Lake Taupo (Procter *et al*., 2010b). 17 km from Crater Lake the braided channels on the Whangaehu Fan join together to form a single meandering channel at the foot of the Rangipo fault scarp. The river then travels south-westward towards the road and rail bridges at Tangiwai, 39 km downstream.

The Whangaehu River remains a single meandering channel until it reaches the coast 155 km from source. These geomorphic features are crucial in determining flow path.

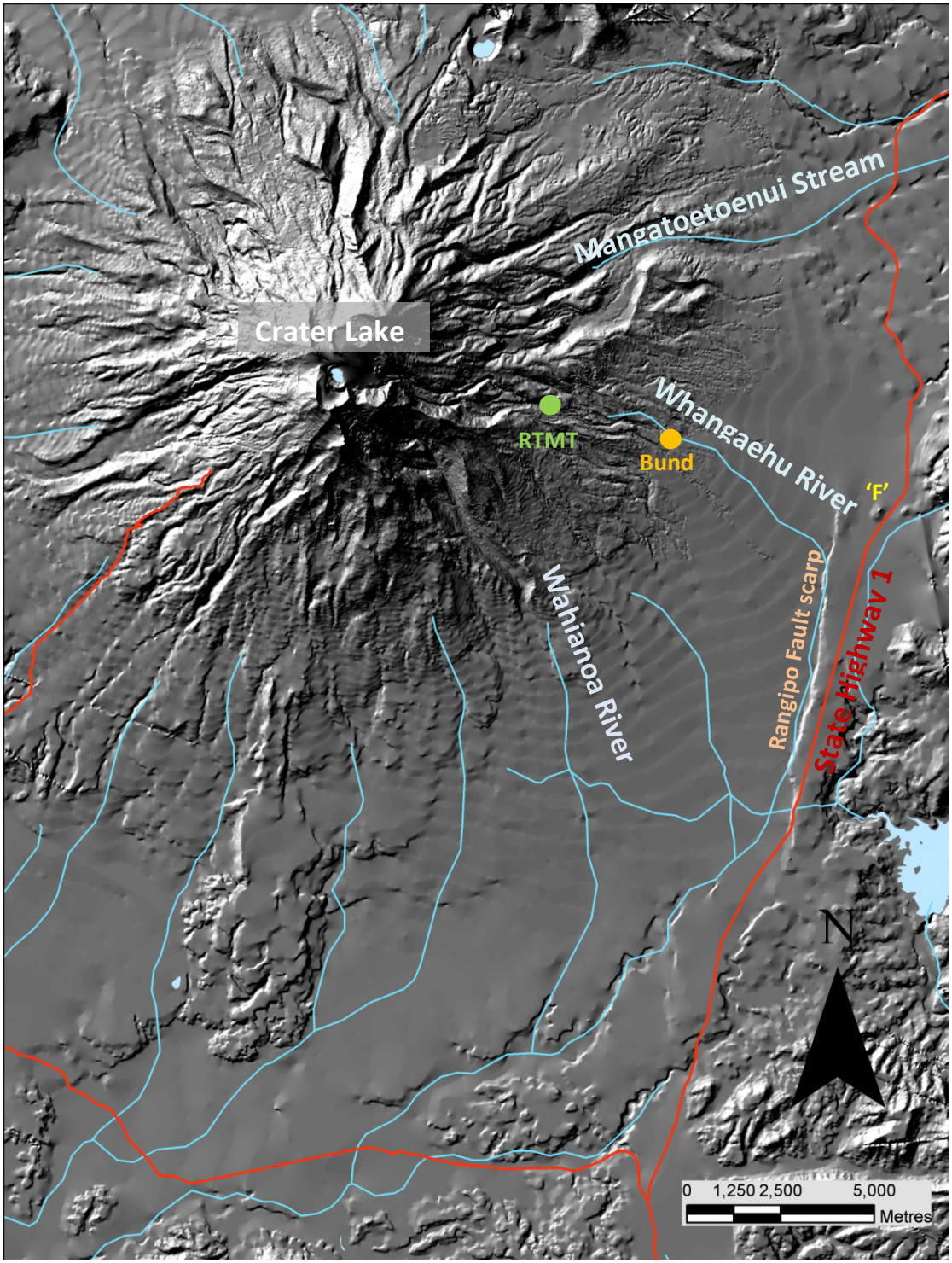

Figure 3.8: Location map of catchments and other features on the eastern side of Mount Ruapehu. RTMT represents 'Round the Mountain Track' and 'F' represents a small mound named 'Feature Foxtrot'.

The Whangaehu Catchment is the drainage path most often affected by past lahars; however, lahars have also been generated in the Whakapapa, Mangaturuturu, Wahianoa, and Mangatoetoenui Catchments (Cronin *et al*., 1999). The following are general observations made from the resulting debris avalanche scenarios simulated in this study with Titan2D.

3.6.2 Scenario 1: 2.5% of the entire eastern rim.

A portion of the collapsing pile pools into Crater Lake, while the rest falls to either side of the remaining Pyramid Peak structure (fig. 3.10). These two portions then join at the base of Pyramid Peak before continuing down the Upper Whangaehu River channel. The flow can be seen moving from side to side down the channel as it runs up the valley walls. Near the Round the Mountain Track (RTMT) (fig. 3.9) a large portion of this flow travels straight across the fan seemingly no longer constrained by the channel topography, while the rest of the flow continues down the normal stream flow path to the southeast onto the Whangaehu Fan (fig. 3.9), reaching the boundary of the NZ Army training area ~9 km from source with a flow height of ~0.5 m. The eastward portion of the flow continues towards the main road reaching 12 km from source, north of the NZ Army training area with a flow height of ~0.5 m. The simulated 1.3 x10^6 m^3 debris avalanche had a total inundation area of ~6.6 km^2 and a maximum run-out length of 12 km. The flow height ranged between 45-4.9 m.

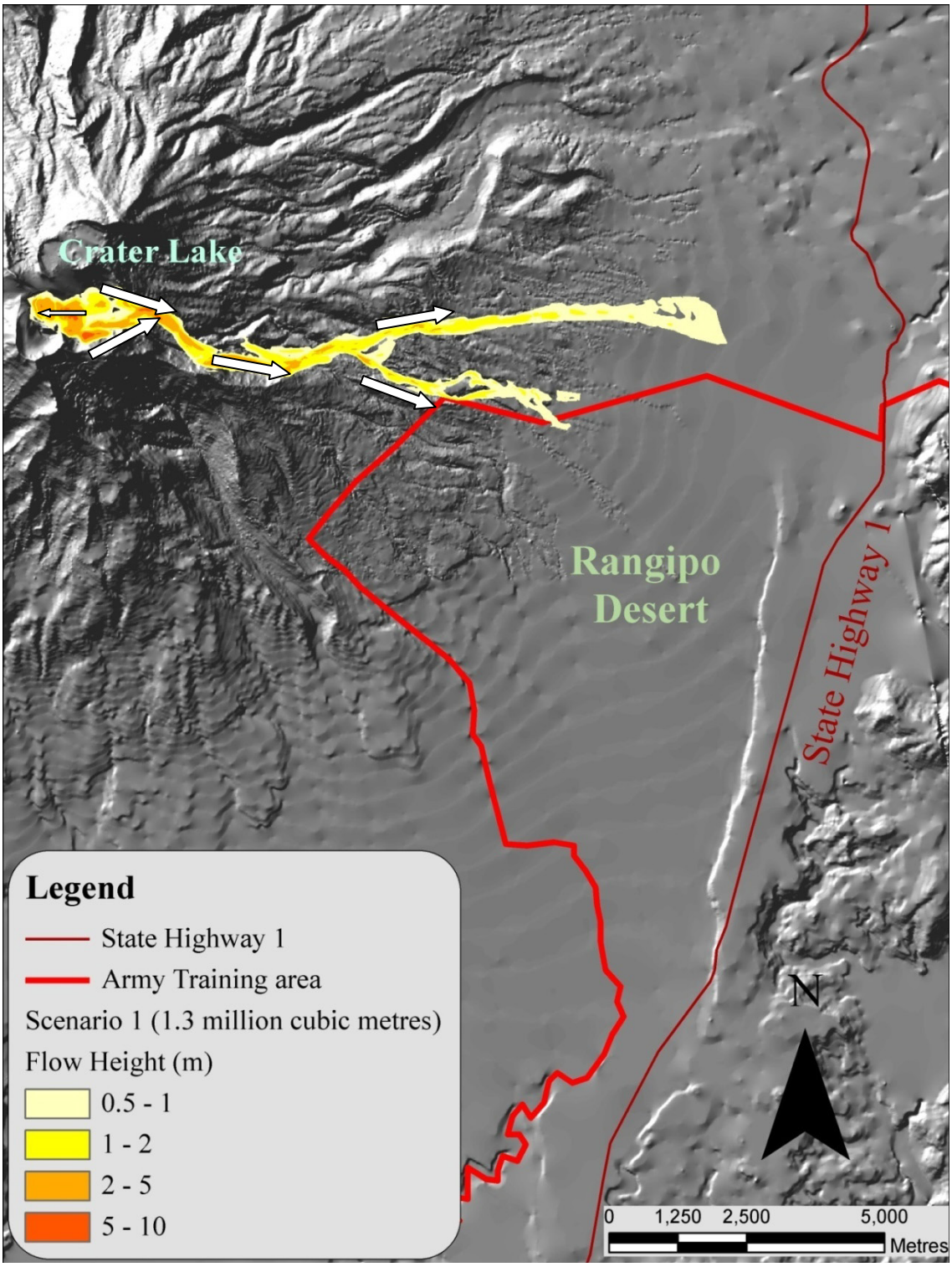

Figure 3.9: Output for scenario 1. Inundation area where the flow reached >0.5 m. The white arrows showing flow direction.

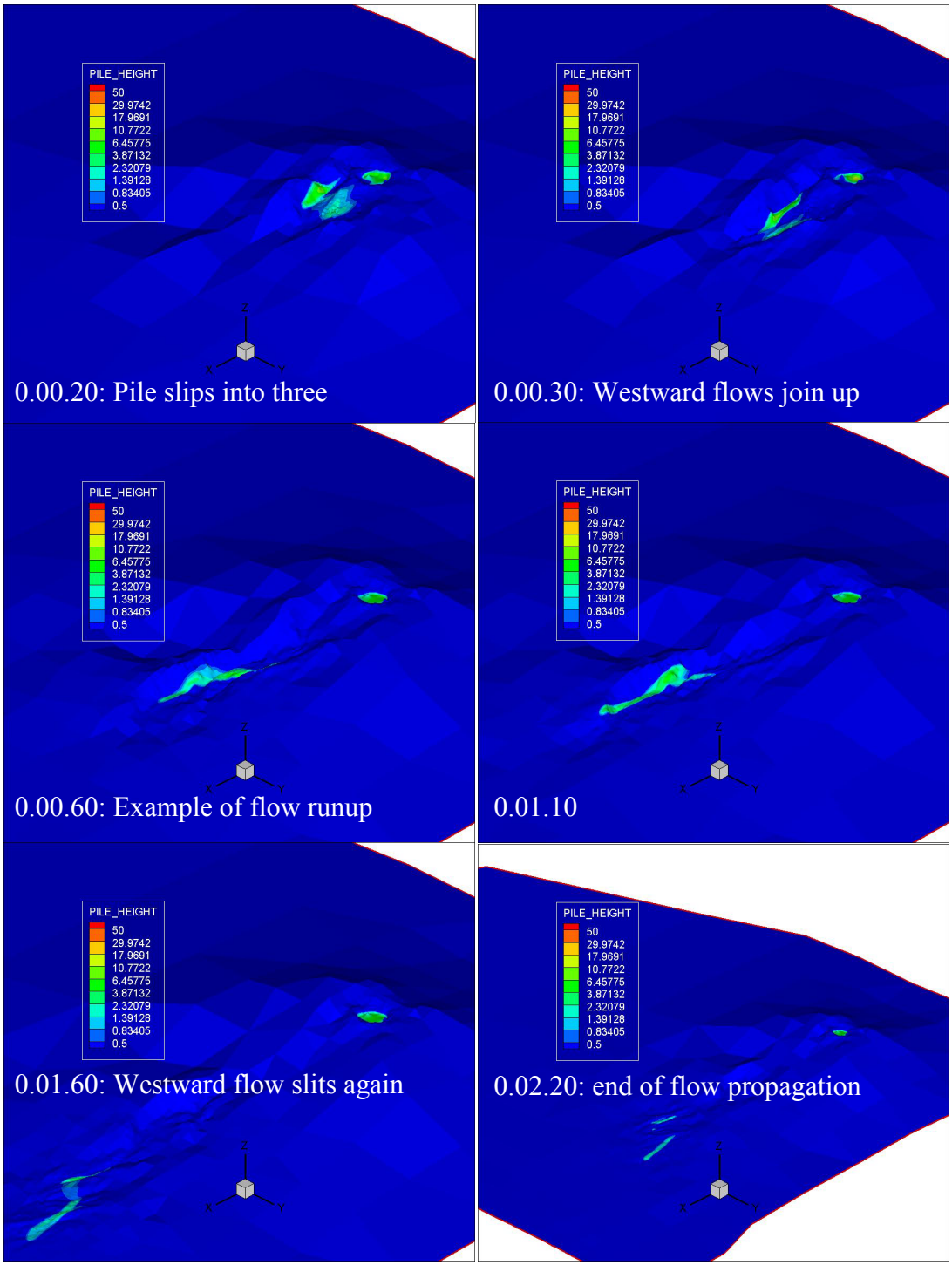

Figure 3.10: Scenario 1. Time steps (hours.minutes.seconds)of the simulated flow. Pile height in metres.

3.6.3 Scenario 2: 15% of the entire eastern rim.

A portion of the pile slumps into the Crater Lake then overflows at the natural lake outlet. The rest of the pile flows from the Pyramid Peak area, with a portion of it running up the southern wall of the gorge (fig. 3.12). This occurs as the pile in the model collapses like a pile of sand rather than sliding initially as a cohesive block. This may not be realistic for all types of volcanic collapse events. The flow continues down the Upper Whangaehu River channel, also running up the valley walls on its way downstream. While the main part of the flow travels down the usually dry southern channel, a portion of the tail end of the flow is diverted into the deeper gorge to the north, and then meets up with the main flow again. After this point the majority of the flow is no longer confined by the normal drainage channel and spreads eastward across the Whangaehu Fan towards the main road (fig. 3.11). A smaller portion of the flow stays within the normal drainage channel travelling ~9 km from source. The eastward portion of the flow reaches ~13.5 km from source before reaching the northern end of the Rangipo Fault scarp where it continues a further 2.5 km south. The simulated 8.5 x10^6 m^3 debris avalanche had a total inundation area of ~24.9 km^2 and a maximum run-out length of 16.1 km. The flow height ranged between 85-20.6 m.

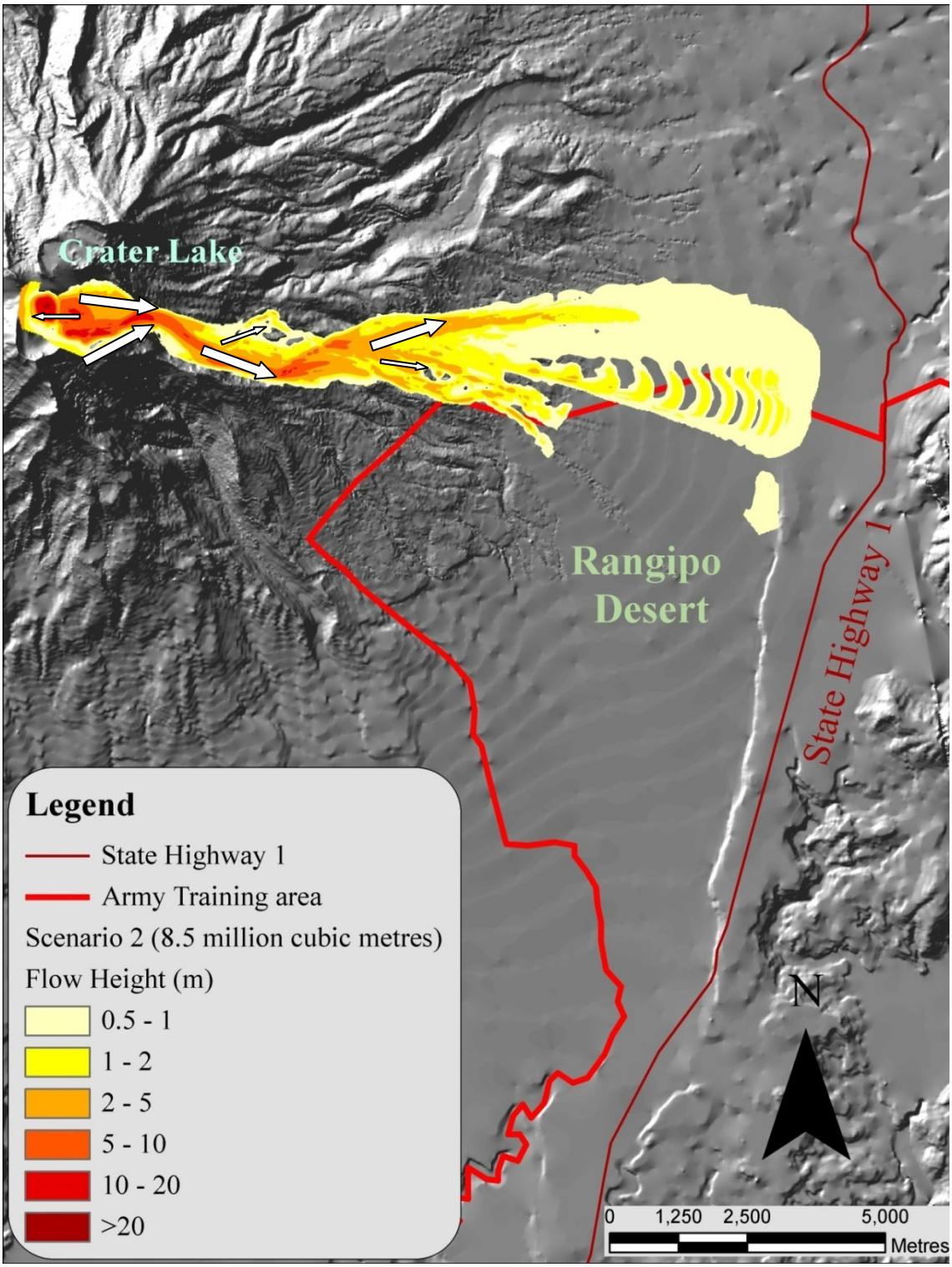

Figure 3.11: Output for scenario 2. Inundation area where the flow reached >0.5 m. White arrows showing flow direction.

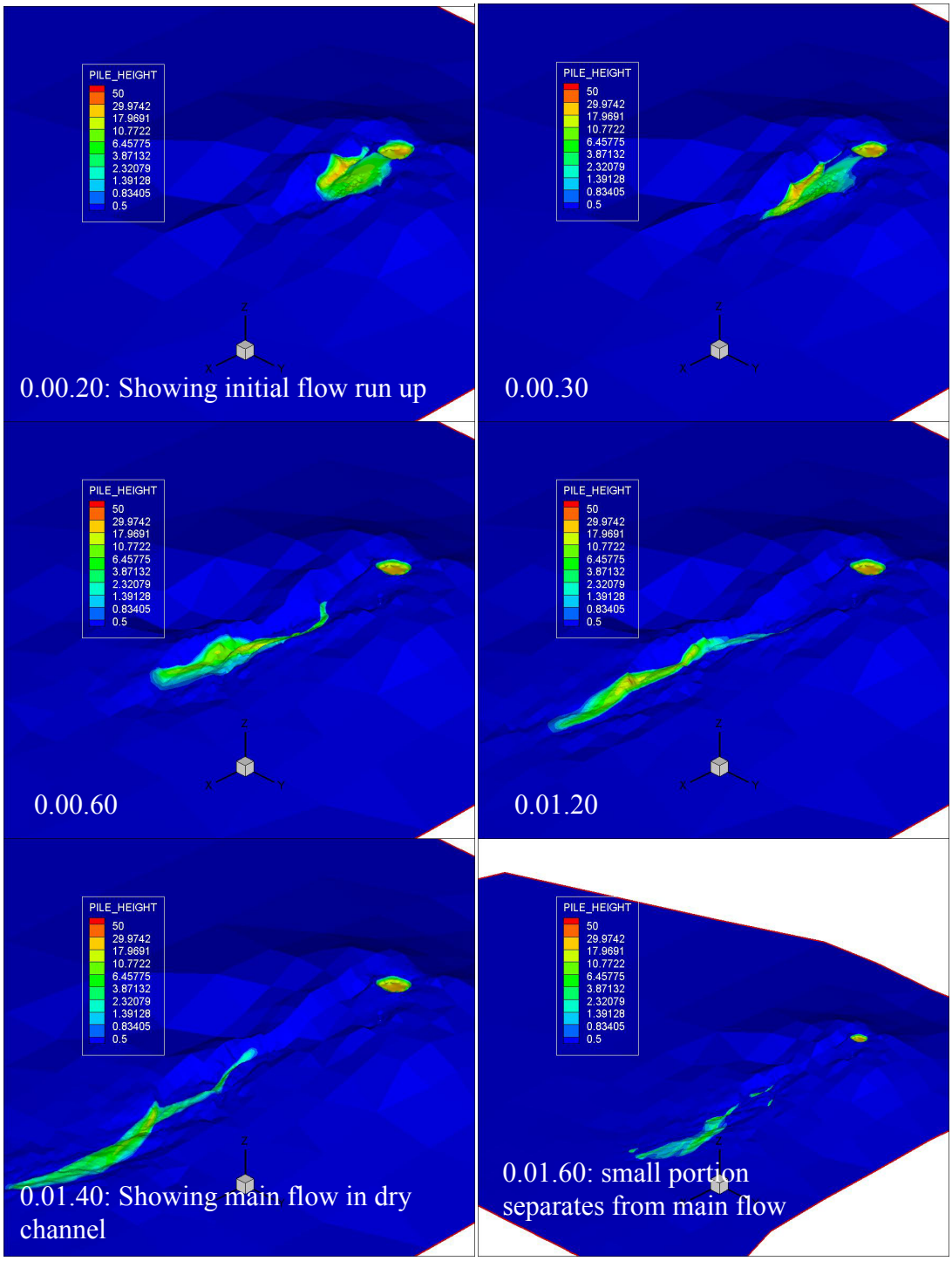

Figure 3.12: Scenario 2. Time steps (hours.minutes.seconds)of the simulated flow. Pile height in metres.

3.6.4 Scenario 3: 50% of the entire eastern rim.

The pile collapses into Crater Lake and also to either side of the remaining Pyramid Peak structure. A small portion of the simulated flow over-tops a saddle in the southern ridge, flowing into the Wahianoa River (fig. 3.14). Another part overtops the valley side to the north sending material into the headwaters of the Mangatoetoenui Stream. This could be occurring as there is still the topographic barrier of the lower portion of Pyramid Peak directing the flow to either side. Meanwhile the main flow makes its way down the Upper Whangaehu channel, running up valley walls and jumping from normal drainage paths to abandoned channels and back again. Like scenario 2, the main flow travelled down the normally dry channel, while a small portion flows down the steep northern gorge prior to meeting again before the RTMT and Chute. The momentum seems to carry the flow over the natural drainage path across the fan to the east (fig. 3.13). A small portion of the mass travels along the normal stream flow path to the south east ~10 km, diverting at the chute into two parallel flows. The flow continues to spill out over the fan to the east ~14 km from source then travels south another ~8 km to reach the Rangipo Fault scarp. Some of the flow pools up on top of the scarp around the feature "Foxtrot" (fig. 3.8), a small observation hill, and to the north. The simulated 2.8 $x10^7$ m^3 debris avalanche had a total inundation area of ~43.9 km^2 and a maximum run-out length of 21.8 km. The flow height ranged between 131-31.7 m.

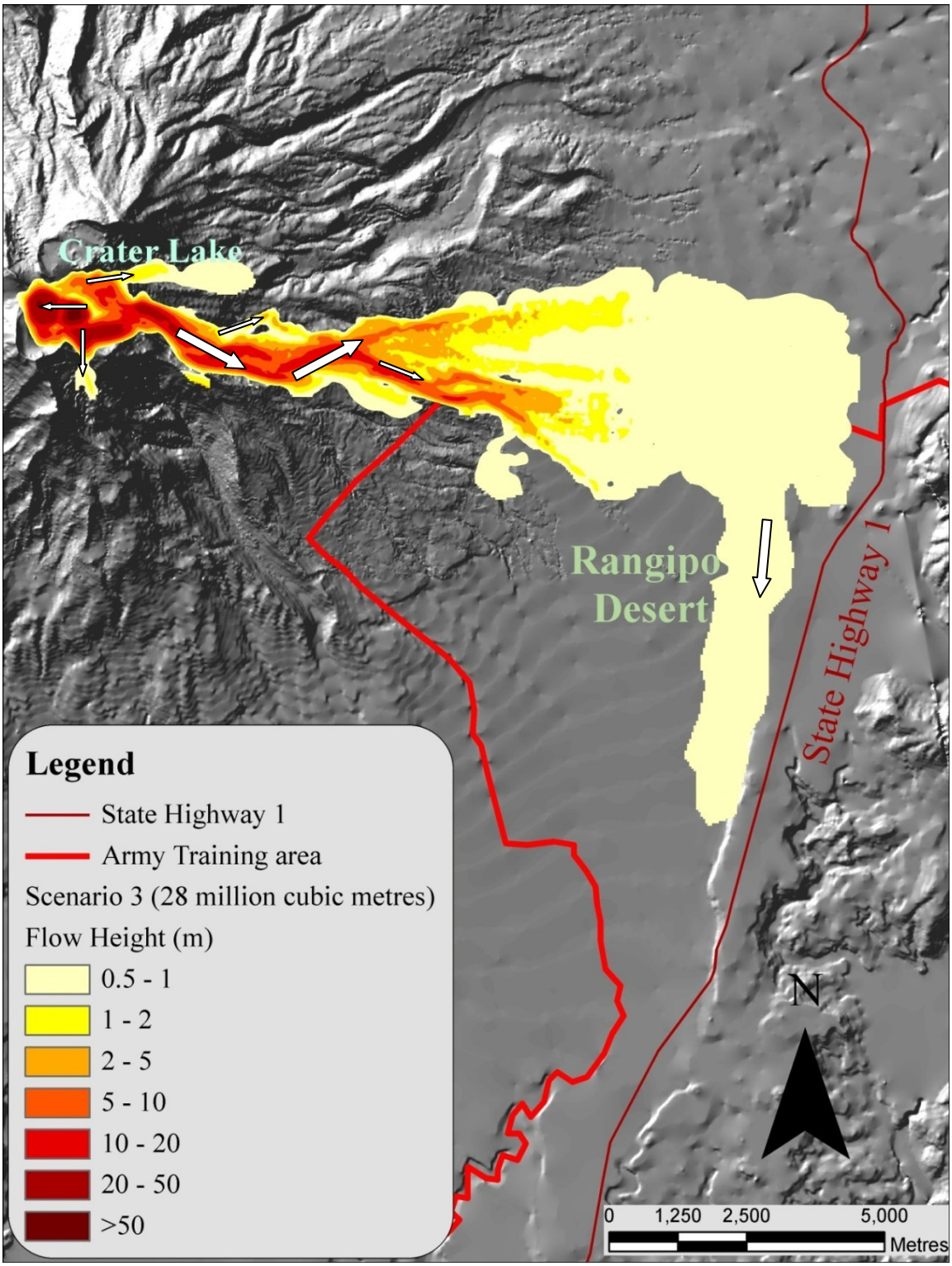

Figure 3.13: Output for scenario 3. Inundation area where the flow reached >0.5 m. White arrows showing flow direction.

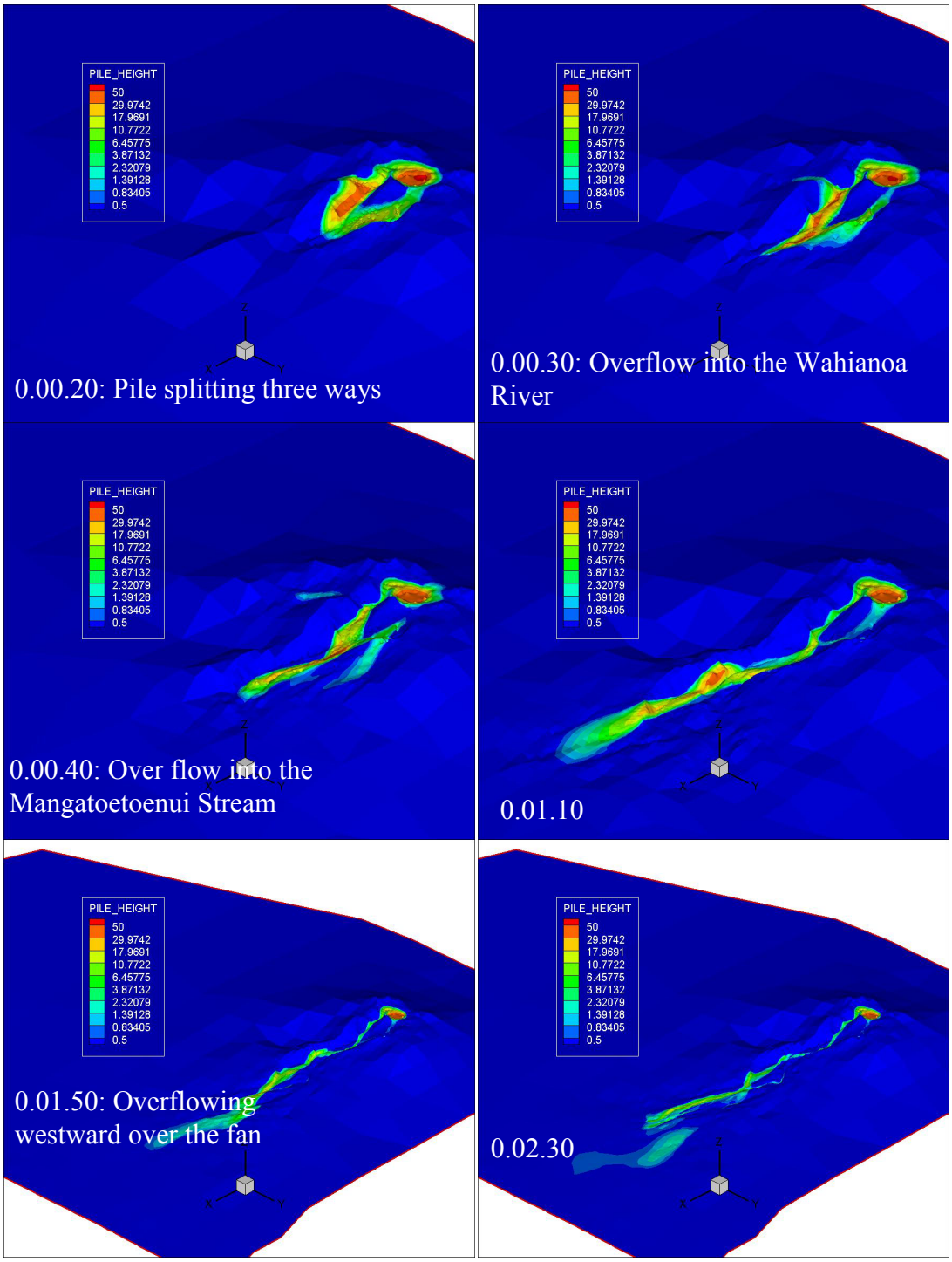

Figure 3.14: Scenario 3. Time steps (hours.minutes.seconds)of the simulated flow. Pile height in metres.

3.6.5 Scenario 4: 100% of the entire eastern rim.

The collapsing pile totally inundates the Crater Lake area and with no remaining eastern rim to obstruct the flow, it therefore travels as a single mass down the Whangaehu Channel. Like scenario 3 the southern gorge wall cannot contain the collapsing pile of material as it runs up and over a saddle into the Wahianoa River (fig. 3.16). None of the flow makes it into the Mangatoetoenui Stream. The volume of this flow seems to be too much for the natural channels and valleys to accommodate as it over tops all channels and inundates an area to the north of both the southern dry channel and deep northern gorge. As the bulk of the flow passes, the tail becomes confined again by the main drainage pattern and abandoned channels. These channels remain occupied for some time after the main flow passes, with the slow release of material from the natural lake outlet from the portion of the mass that collapses into Crater Lake. The flow front continued onto the Whangaehu Fan, spreading like a fan as it travels east (fig. 3.15). A small portion follows the natural stream flow into the Whangaehu River but soon gets lost in the spreading material. The flow manages to flow up over the northern portion of the Rangipo Fault scarp ~14.5 km from source before being diverted to the south ~8 km. The simulated 5.3 $x10^7$ m^3 debris avalanche had a total inundation area of ~54.1 km^2 and a maximum run-out length of 21.9 km. The flow height ranged between 178-6.6 m.

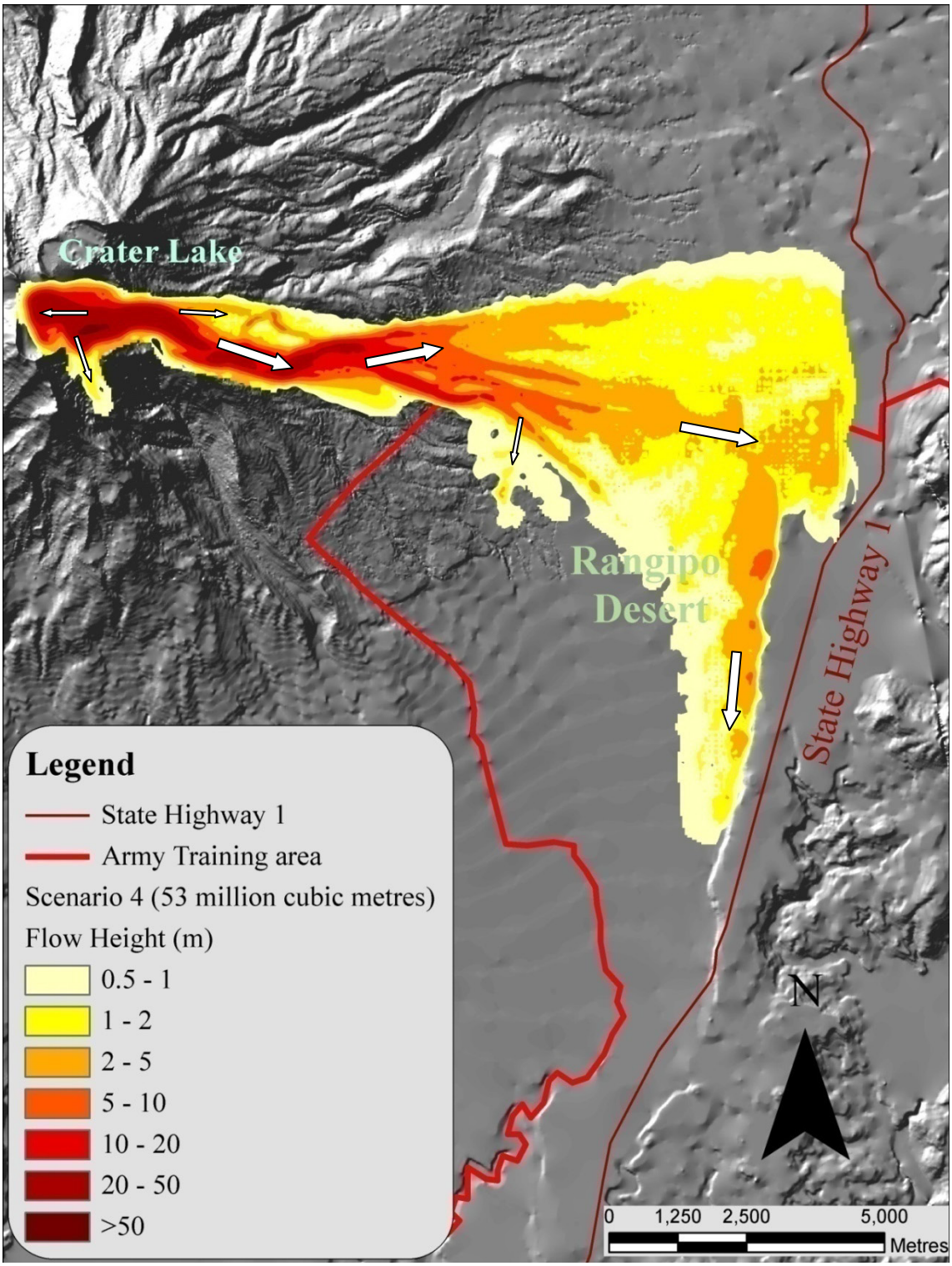

Figure 3.15: Output for scenario 4. Inundation area where the flow reached >0.5 m. White arrows showing flow direction.

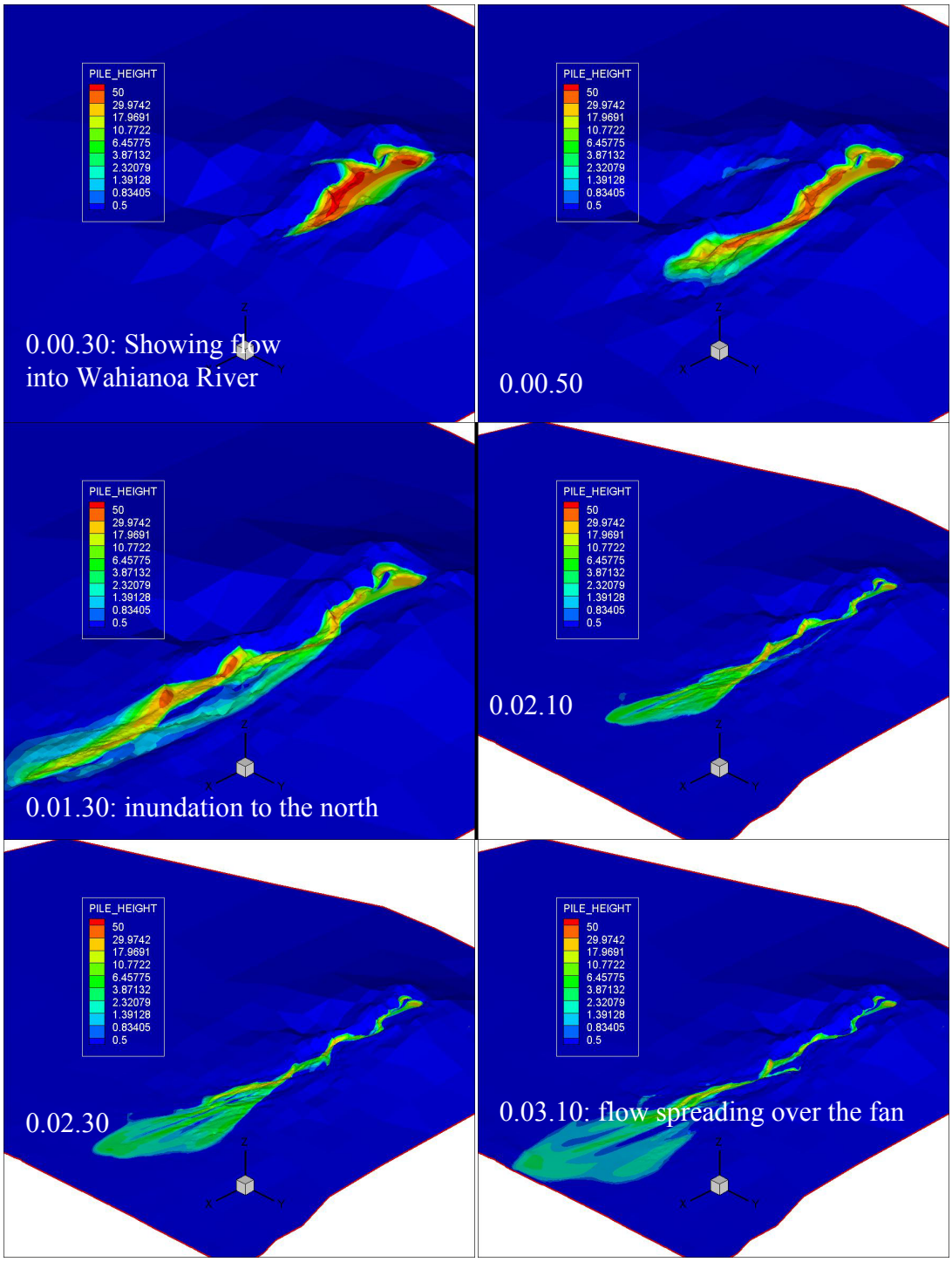

Figure 3.16: Scenario 4. Time steps (hours.minutes.seconds)of the simulated flow. Pile height in metres.

3.6.6 Scenario 5: 100% of the entire eastern rim and Crater Lake water.

Overall scenario 5 behaved much the same as scenario 4, although it had greater flow heights and a larger area inundated in some places (fig. 3.17). A portion of the collapsing material travels further down the upper parts of the Wahianoa River catchment than in scenario 4 (fig. 3.18). A greater amount of material also pooled around 'Feature Foxtrot' (fig. 3.8), inundating a little more of State Highway 1 than the simulated flow in scenario 4. The northern, eastern and southern extent of the simulated flow did not significantly exceed that of the extents of scenario 4. The only location that had any significant increase in inundation was that of the north western corner of the Army training area in the Rangipo Desert. The simulated 6.0×10^7 m^3 debris avalanche had a total inundation area of 56.1 km^2 and a maximum run-out length of 22.2 km. The flow height ranged between 202-6.2 m.

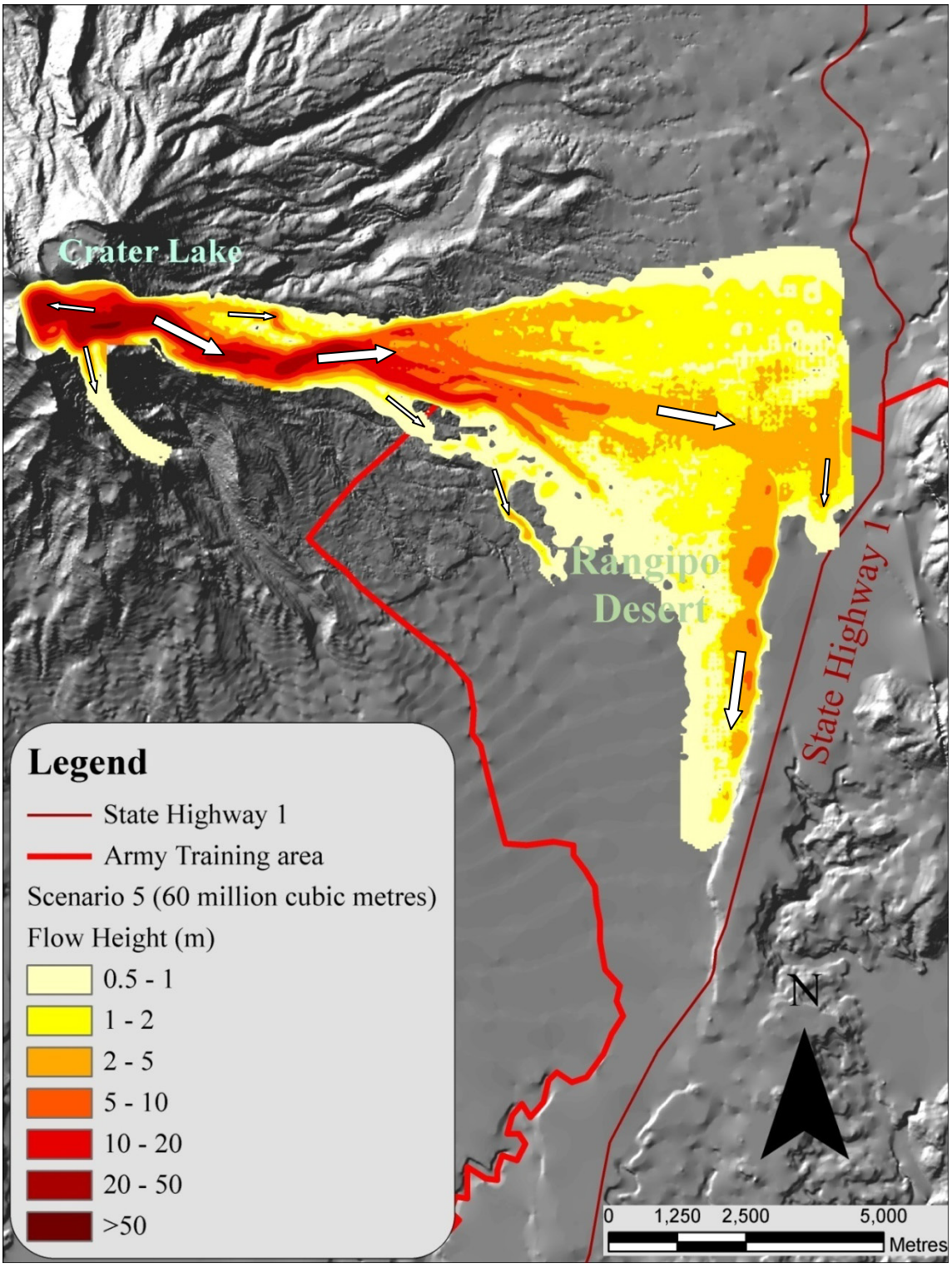

Figure 3.17: Output for scenario 5. Inundation area where the flow reached >0.5 m. White arrows showing flow direction.

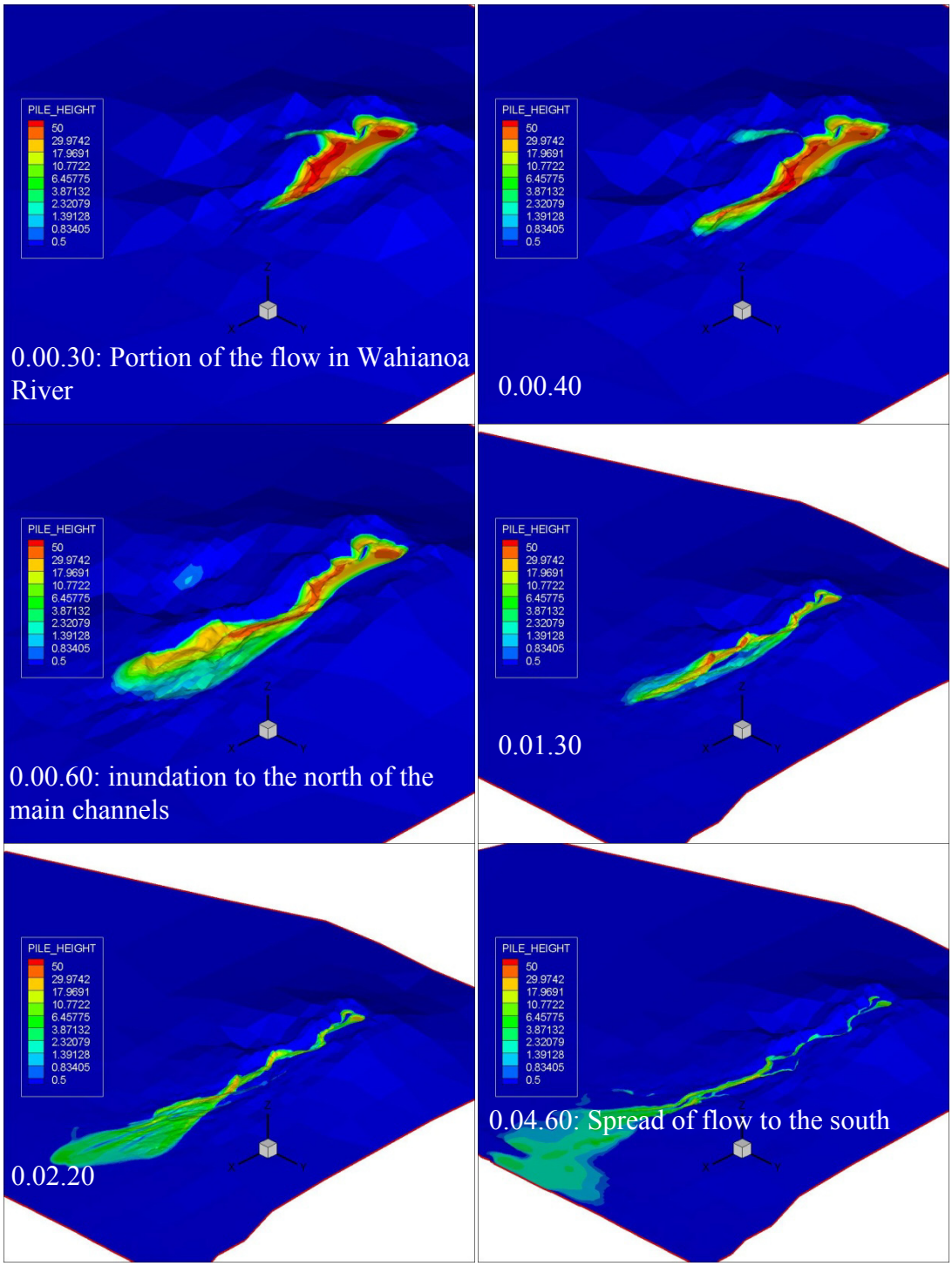

Figure 3.18: Scenario 5. Time steps (hours.minutes.seconds)of the simulated flow. Pile height in metres.

3.6.7 Overall simulated flow properties of scenarios 1-5.

Scenario	Initial volume (m^3)	Inundation area (km^2)	Run-out length (km)	Max pile height range (m)	Average velocity (m/s) Max Min	Max frontal velocity (m/s)
1	$1.3x10^6$	6.6	12	45 – 4.9	37.1 – 2.6	63
2	$8.5x10^6$	24.9	16.1	90 – 20.6	40.5 – 2.7	74
3	$2.8x10^7$	43.9	21.8	135 – 31.7	34.8 – 3.3	94
4	$5.3x10^7$	54.1	21.9	180 – 6.6	50.5 – 1.4	94
5	$6.0 x10^7$	56.1	22.2	202 – 6.2	51.1 – 1.5	95

Table 3.4: Result summary for all scenarios.

The average and frontal flow velocities were calculated (fig. 3.19 (a-e)). Overall it can be considered that both frontal and average flow velocities have a similar pattern of behaviour over distance and time for each scenario. The location of peak velocities and where velocities started to decrease were also determined. Although the velocity values differ from scenario to scenario, the increase and decrease patterns are similar across all scenarios with a relatively sharp increase peaking at ~7500-9000 metres from source, an undulating plateau and then a sharp decrease around 11000-14000 metres from source. Scenarios 2-4 seem to have peak flow speeds around 9000 m from source, which is near the bund site and the base of the volcano with cone slopes changing from 15° to 9°. As the flow hits the flatter terrain of the Whangaehu Fan the flows starts to slow down as expected. The flows of scenario 2-4 seem to plateau then dramatically decrease in speed around 14000 m from source. This is around the location of the power lines to the west of the main road. This is also where the eastward direction of the flows is stopped by the Rangipo Fault and diverted to the south.

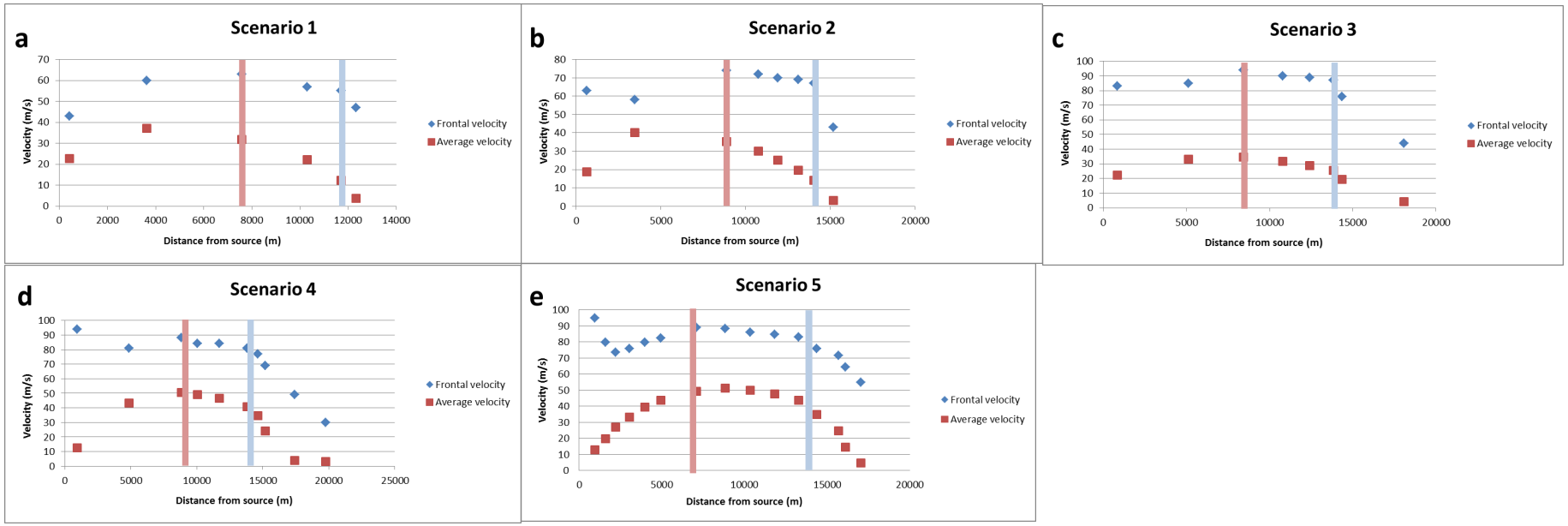

Figure 3.19: (a-e) Graphs showing the frontal and average flow velocities of each simulated flow scenario. Red lines marking peak velocities and blue lines marking where there is a sudden decrease in velocity.

In all scenarios the pile collapsed in three directions: west into the Crater Lake basin, north onto the saddle of the Whangaehu Glacier, and south into the natural drainage channel, before recombining and making its way down the Whangaehu channel. As the volume of the collapsing pile increases, the space available to accommodate the material in the Crater Lake area and to either side of Pyramid Peak decreases. This lead to material overflowing into the Mangatoetoenui Stream and the Wahianoa River in scenario 3. However, in scenarios 4 and 5 the collapsing material did not flow into the Mangatoetoenui Stream. The reason for this is uncertain. However, it seems that once the entire eastern rim collapses the material is no longer directed to the north or south of the remaining Pyramid Peak structure as occurred in scenarios 1 to 3. Hence the difference in the topography could have affected the behaviour of these flows.

The main portion of all flows modelled in this study tend to flow down the southern dry channel and then migrate out of the channel before the chute and continue eastward out over the Whangaehu Fan (fig. 3.20). The flow seems to be carried by momentum and is no longer confined by channel topography. At this stage the flow is also still accelerating down the slope nearing its peak velocity; therefore it is less likely to be controlled by topographic features.

As flow volume and height increases, it becomes less confined by topography and is no longer confined to natural drainage channels. Flows begin to slosh down the eastern flank valley walls, ignoring channel sinuousity and flowing into other abandoned drainage paths. Even though the flows are less confined it seems that the flows are still generally guided in the direction of topographic lows. This differential behaviour of debris avalanches depending on volume was also discussed in Palmer *et al*. (1991); it was observed that larger flows tend to fan out where smaller flows are confined to topographic lows (channels).

The minimun average flow velocities and lowest recorded maximum pile heights (table. 3.4) for simulated flows increase from scenario 1-3 as initial volume increases. However, these measures decrease from scenario 3-5 where the flows have greater initial volumes. A suggested reason for this is that smaller flows are more confined by

channels where higher velocities and flow inundation heights can be achevied. Once flow volumes are too large, all of the flow can no longer be accommodated by drainage paths, resulting in portions of the flow overflowing onto higher and flatter topography and decreasing average flow velocities and lowest recorded pile heights. This in turn could suggest that larger flows would have shorter flow paths down the flanks of the volcano due to the decreased sinuosity.

All of the simulated flows seemed to inundate the portion of the Whangaehu Fan north of the Whangaehu River. It has also been observed that the maximum eastern extent of some flows is abrupt and not in the vicinity of the Rangipo Fault scarp. This represents an unexpected result. It was considered to be a problem where the flow was reaching the extent of the DEM; however, the flow stops before the DEM ends, confirming that the scarp is still providing a barrier to a portion of the flow mass. Another suggested explanation was that the flow length specified in the inputs was too short, yet when this was doubled the flow still repeated the pattern. The computational grid could have picked up the elevation increase caused by the hill country near the edge of the DEM to the northeast of the scarp and where the grid is less refined, and projected the slope westward. An additional explanation is when the DEM and grid are not perfectly square, the model can place many points to the edge of this square area to maintain the overall even distribution of computational points over the area.

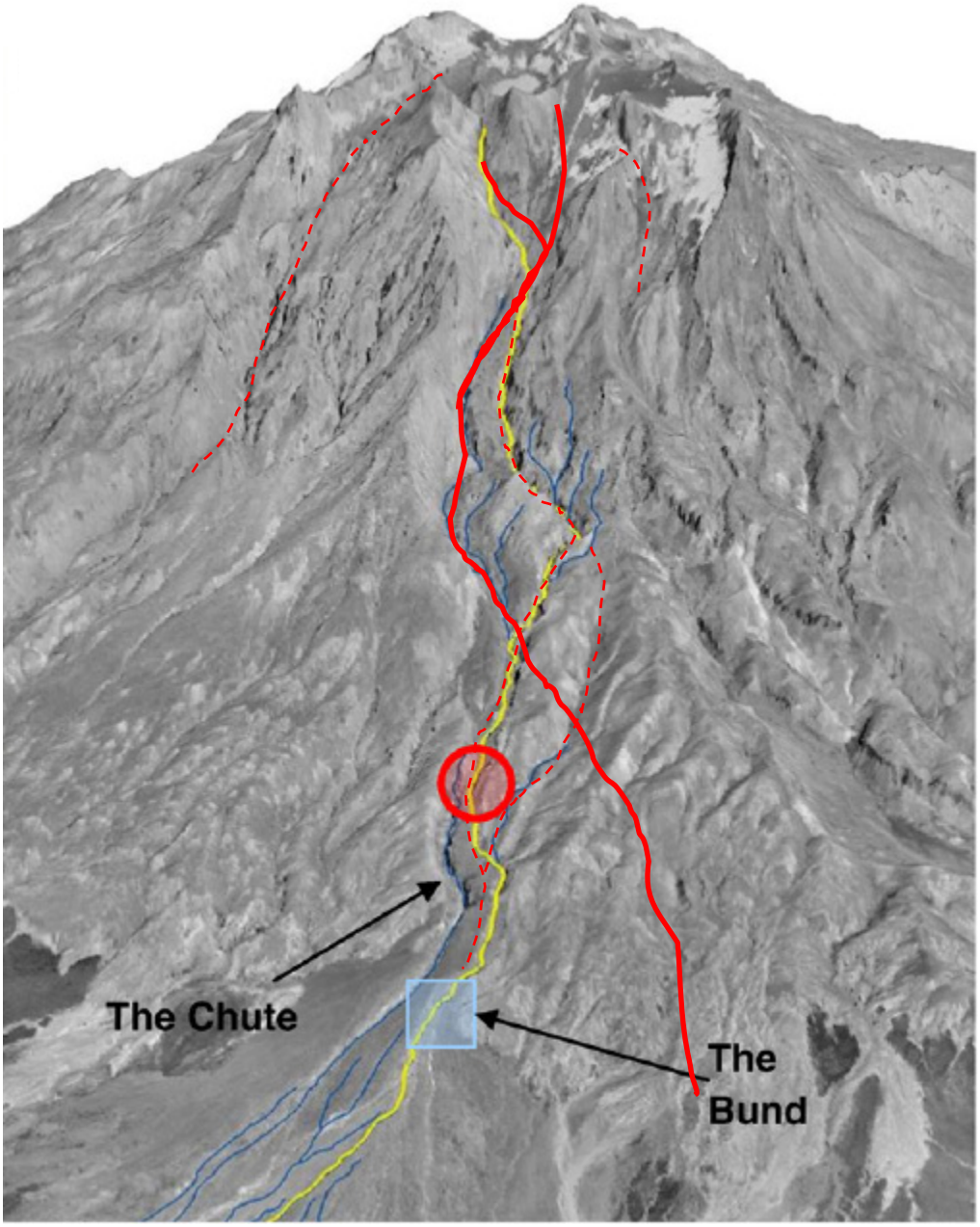

Figure 3.20: The Upper Whangaehu channel showing the main flow path (yellow) and the modelled debris avalanche path (red). The bulk of the modelled flows follow the bold red where the dashed lines show where smaller portions of the flow have inundated. Figure modified from Procter *et al*. (2010b).

3.7 Discussion:

3.7.1 Comparing Titan2D simulation results with other models

The only other study that has looked at modelling the collapse of the eastern crater rim of Mount Ruapehu is that of Manville *et al.* (2003). Due to vast differences in numerical basis and computational methodology, it was impossible to directly compare all aspects of this study with that earlier work. Like this study, however, Manville *et al.* (2003) defined four scenarios of possible volumes of collapsing material from Pyramid Peak. As seen in the two cross-sections below, the geometry of the four principle scenarios in the two studies differ due to different geological interpretations. Manville *et al.* (2003) also included the entire volume of the Crater Lake in each scenario (~9 x10^6 m^3) even though the collapse of scenario 3 and 4 does not result in the entire collapse of the eastern crater wall. Despite these differences, the resulting flows of similar overall volume were compared (table 3.5).

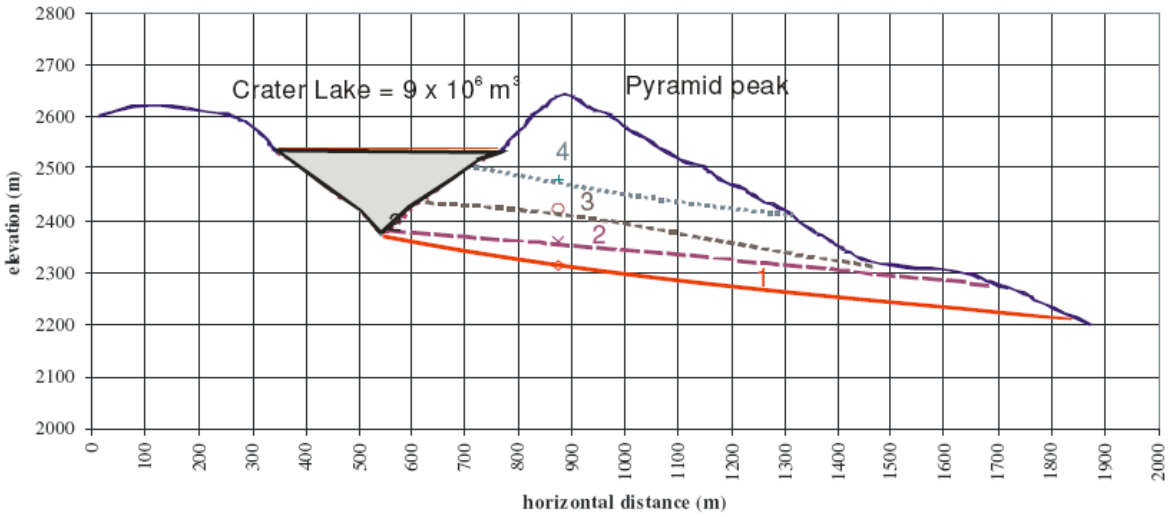

Figure 3.21: Cross-section of four collapse scenarios from Manville *et al.* (2003).

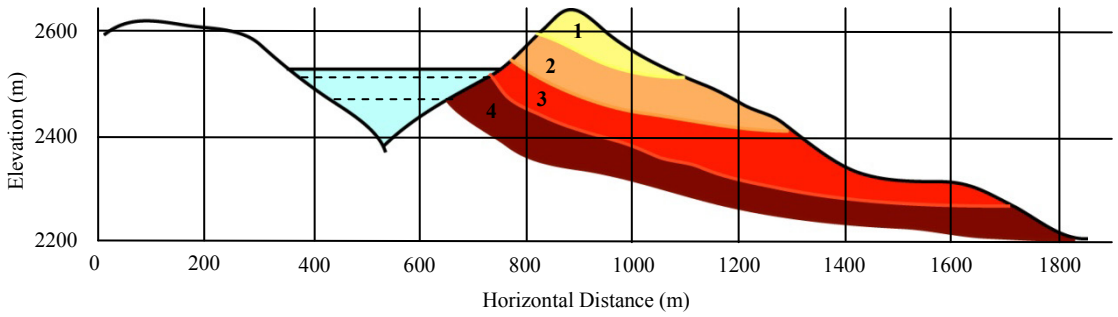

Figure 3.22: Cross-section of four collapse scenarios defined in this study.

Study	Manville *et al* (2003)		This study	
Scenario	4	3	3	4
Flow volume (m^3)	28.5 $x10^6$	57 $x10^6$	28 $x10^6$	53 $x10^6$
Pile height (m)	161	217	135	180
Pile radius (m)	322	435	262.5-498	288.5-655
Run-out length (km)	23.4	26.7	21.9	21.8

Table 3.5: Comparison of pile parameters and model outputs.

Despite the differences outlined above, there are some similarities in the overall run-out distance of the resulting flows. Manville *et al.* (2003) manually split the flow into two once the flow reached the Whangaehu Fan, with 75% following the natural drainage path down the Whangaehu river and 25% flowing eastward across the fan towards the main road following upper tributaries of the Whangaehu and Mangatoetoenui Stream drainage routes. The flows in this study also automatically split into two main parts. However, the main part of the simulated debris avalanche tended to flow eastward over the fan rather than down the Whangaehu River as suggested in Manville *et al.* (2003). The eastward extent of the flows simulated by both models, where the volumes are comparable, is both around 14-15km from source. All flows reach the northern end of the Rangipo Fault scarp close to or on State Highway 1. However, the flows from LAHARZ continued north eastward into the Tongariro River with larger volumes (Manville *et al.*, 2003), where flows from Titan2D pooled around the eastern extent then flowed south into the Whangaehu River, guided by the Rangipo Fault scarp. The two flows from this study reached a total (eastern extent plus the southern extent) run-out length of ~22 km from source, whereas the flows from Manville *et al.* (2003) of similar volumes reached lengths of ~23-27 km from source. The longer run-out lengths could be due to the main part of the flow in LAHARZ flowing down the Whangaehu River, whereas in Titan2D only the minor portion of the flow follows this path. It could also be a result of the manual adjustment and user intervention. The inherent differences in how each model simulates flows must not be discounted as an explanation for the observed differences.

Carrivick *et al.* (2009) did not model debris avalanches from Mount Ruapehu, but reconstructed the dam break 2007 lahar which had an initial volume of around 1.3 million cubic metres, similar to that of the volume of scenario 1 in this study. Carrivick

et al. (2009) used Delft3D, a fluid dynamics model, to analyse the flow. Like Titan2D, Delft3D does not account for bulking or changes in flow behaviour. Delft3D differs, however, by modelling flows as 100% water (Newtonian Fluid). The resulting flow from Carrivick *et al.* (2009) is depicted in figure 3.23 below.

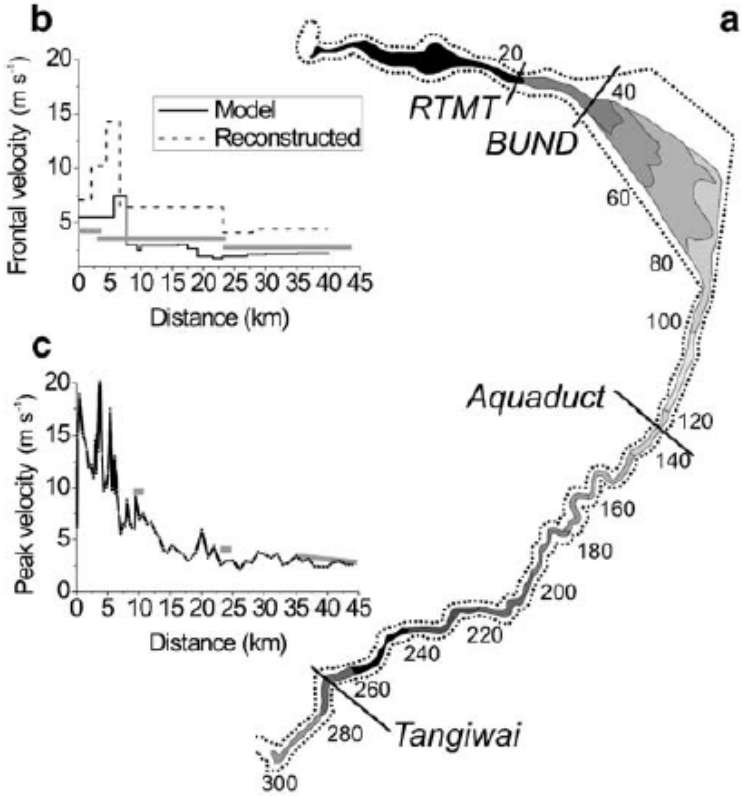

Figure 3.23: a) Represents a progression of inundation over time (minutes) in time steps of 20 minutes, each displayed in a different shade. b) Variation in mean frontal velocity over distance in kilometres. c) Modelled longitudinal variation in peak main body velocity (Carrivick *et al.* 2009).

The resulting flow travelled east 1.4 km before bifurcating as observed in this study with Titan2D. However, Carrivick *et al.* (2009) stated that most of the flow was contained by the northern gorge, rather than the wider southern channel Titan2D simulated in this study. The lahar modelled in Carrivick *et al.* (2009) travelled through the Whangaehu gorge and across the Whangaehu Fan, not spreading too far north of the Whangaehu river channel. The lahar then travelled a further 22 km southwest down the Whangaehu River to the Tangiwai bridge, an additional ~24 km than that of scenario 1 in this study. This is probably due to the difference in the nature of the flows being modelled, where one flow is assumed to be 100% water and the other ~85% solid material. Carrivick *et al.* (2009) calculated a mean frontal velocity of 6.5 m/s

and a peak velocity of 19.6 m/s. In this study, very high frontal velocities were found, ranging between 43 and 63 m/s. The average velocities seemed to be closer to that found in Carrivick *et al.* (2009), with a mean average velocity of 14.4 m/s and a range of 37.1-2.6 m/s. These differences are inherently due to modelling debris avalanches in relation to debris flows. Within Delft3D a high degree of user input was required, with sections of channel being modelled individually due to the model being unable to computationally simulate flows down a complex large terrain.

3.7.2 Comparing Titan2D simulation results with past recorded events

Following the 1995/1996 eruptions, 9 m of tephra was deposited on the south crater rim, blocking the former outlet of the lake (Procter *et al.,* 2010c). As Crater Lake began to refill, a sudden lake-breakout lahar was anticipated and the resulting hazard of such an event was assessed. This assessment was hindered, however, by an unknown factor of bulking (Procter *et al*., 2010c). This is how much an initial volume may increase through the entrainment of sediment and/or water to generate lahars with long run-outs (Procter *et al*., 2010c). Subsequent research found that bulking factors for Ruapehu were estimated at 3-5 times that of the initial flow (Procter *et al*., 2010c).

Full dam collapse occurred on the 18th March 2007 during a rainstorm at around 11.18 am, releasing 1.3 x10^{6} m^{3} of water down the Whangaehu gorge (Procter *et al*., 2010c). This volume is the same as that of scenario 1 in this study. Even though these flows both have the same initial volume and similar starting locations the resulting flow parameters differed vastly. Recorded flow parameters from the 2007 dam-break lahar and the simulated flow outputs from Titan2D are compared in table 3.6.

Flow	2007 Dam-break lahar (Procter *et al* (2010c)	Scenario 1 simulation (This study)
Flow volume (m^{3})	1.3 x10^{6}	1.3 x10^{6}
Flow height (m) 6.9 km from source	9	2-5
Average velocity (m/s)	9-10	14.4
Run-out length (km)	200	12

Table 3.6: Comparing scenario 1 and 18th March 2007 lahar flow parameters. Dam-break lahar data from Procter *et al.* (2010c).

The differences in the two flows in table 3.6 are possibly due to the differences in the solid/liquid ratio, with scenario 1 being initially ~85% solid material (debris avalanche) and the 2007 lahar being initially nearly all lake water (hyperconcentrated flow), this leads to different flow behaviours. The differences in the flow parameters above could also represent the problems with applying Titan2D. Titan2D cannot show the changes in flow composition downstream as the flow entrains material and/or water, changing the flow rheology. Titan2D also does not allow for bulking or debulking. Even though the 2007 lahar had an initial volume of 1.3 $x10^6$ m^3 it bulked to a peak volume of around 4.4 $x10^6$ m^3 at ~6 km from source, a bulking factor of around 3.3 (Procter *et al*., 2010c). Therefore, this could mean that the flows modelled in this study could reach greater volumes than that of the initial volume of material collapsing. If the simulated debris avalanche reaches catchments that contain water or if it picks up snow and ice, the behaviour of the flow could change dramatically leading to each scenario modelled in this study reaching greater run-out distances and impacting greater areas than predicted by Titan2D.

3.7.3 Comparing Titan2D simulation results with mapped flow deposits

Geological evidence shows that a similar failure of hydrothermally altered flank material on this side of the volcano has occurred before. The Mangaio Formation (fig. 3.24) represents a debris-avalanche event occurring c. 4600 yrs BP (Donoghue & Neall, 2001). It is characterised by abundant white hydrothermally altered lithic clasts in a clay-textured matrix (Donoghue & Neall, 2001). It has been suggested that the Formation is derived from the failure of hydrothermally altered flank rocks and not associated with eruption activity due to the absence of tephras directly overlying and underlying the deposit (Donoghue & Neall, 2001). The possible source of the debris avalanche is the highly (hydrothermally) altered Wahianoa Formation near Pyramid Peak, which makes up much of the south eastern flank of Mt Ruapehu.

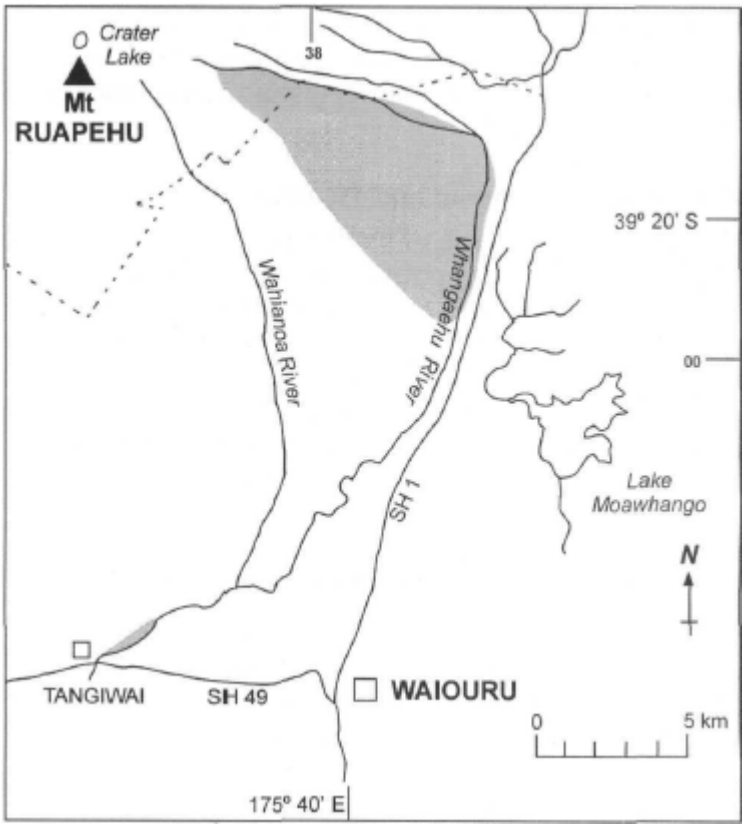

Figure 3.24: Generalised distribution of the Mangaio Formation (c. 4600 yr BP) on the south-eastern ring plain of Mount Ruapehu. From Donoghue and Neall (2001).

The estimated preserved volume of the Mangaio Formation is ~34 x10^6 m^3 (Donoghue & Neall, 2001), suggesting it could have been formed by a crater rim collapse event between that simulated in scenario 3 and 4 of this study. The Mangaio Formation is thought to cover most of the north eastern Rangipo Desert, bounded to the north by the Whangaehu River and tributary channels, and to the east by the Northern Rangipo Fault scarp. The southern extent was obscured, but Donoghue and Neall (2001) found distal facies downstream as far as Tangiwai, giving a greater run-out distance than that of both scenario 3 and 4. This again shows that Titan2D may underestimate run-out lengths due to the inability to measure change in flow behaviour from the entrainment of material and/or water.

The Mangaio Formation was found to overtop a portion of the Rangipo Fault scarp (~14 km from source) and an estimated flow velocity was calculated at ~18 m/s (Donoghue & Neall, 2001). At this point, the flow in scenario 3 had an average velocity of 19.5 m/s and a frontal velocity of 76 m/s. The flow in scenario 4 had an average flow velocity of around 34.6-24.1 m/s and a frontal velocity of 77-69 m/s at this point. This

comparison of velocities and the comparison of velocities with the 2007 dam break lahar and other modelled flows at Ruapehu show that Titan2D produces reasonable average flow velocities when compared to flows of a similar volume and solid fraction but seems to produce very fast frontal velocities, which may not be realistic. However, these parameters have never been measured or observed in actual debris avalanches at this distance from source.

Through the studies of Donoghue (1991), Cronin and Neall (1997) and Donoghue and Neall (2001) on the evolutionary history of the north and south western ring plain of Mount Ruapehu it can be seen that flows have migrated from the north to the south and back again over time. This is due to changes in topography and elevation from erosion and deposition of the flows themselves and other influences such as climate, faulting, lavas, moraines and man-made structures. From the formations described in Donoghue and Neall (2001), it can be seen that there has been a successive build up of the south-eastern ring plain, possibly pushing subsequent flows to the north (fig. 3.25). From the total inundation area of the simulated debris avalanches in this study, it looks as though this trend may continue. The implication of this is an increased likelihood of future flows getting into upper catchments and therefore an increased probability of flows reaching the Tongariro River.

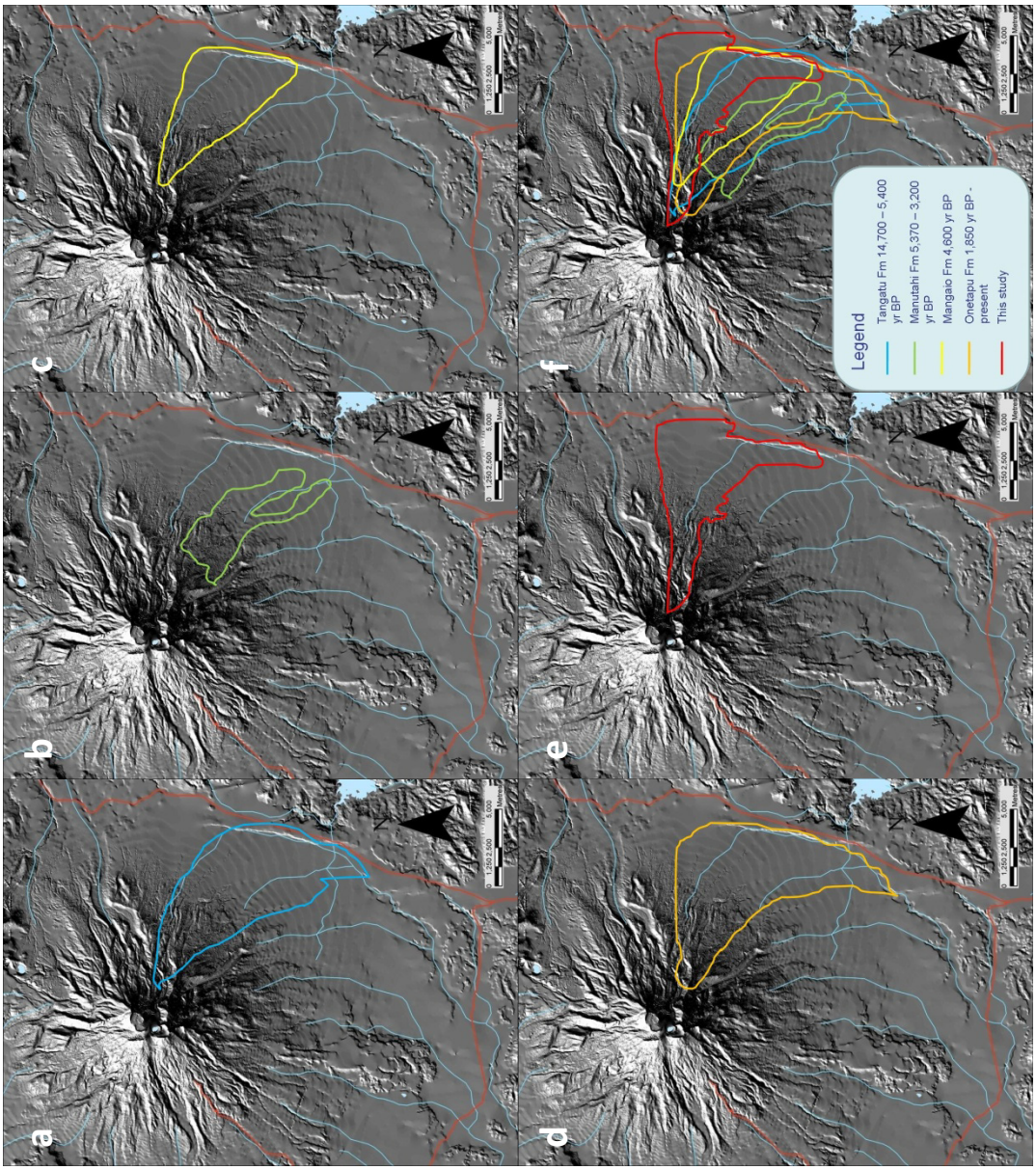

Figure 3.25: (a-f) Migration of deposits that make up the south eastern ring plain of Mount Ruapehu. Deposit outlines derived from Donoghue and Neall (2001).

Chapter 4: HAZARD IMPLICATIONS

4.1 Introduction:

It is widely recognised that the collapse of the eastern crater rim of Mount Ruapehu is a possibility. Hazard and stability studies (Hodgson & Houghton, 1995; Hancox *et al*., 1997; DOC, 1999) mention that a collapse and resulting mass flow or debris avalanche is a real hazard at Mount Ruapehu; however, a detailed and quantitative hazard analysis of this scenario has never been undertaken. Volcanic debris avalanches are known hazardous phenomena that results from a failure on a volcanic edifice. They can transform into debris flows with long run-outs reaching up to tens of kilometres away from source. These mass flow events can have devastating effects on people and property with little warning. Hazard-zonation maps are created to mitigate the impacts of volcanic mass flows. The maps display areas that are likely to be inundated by future mass flows and other volcanic processes. The key element in the creation of such hazard maps is from geological studies of geophysical flow deposits (Schilling, 1998). In the case of Mount Ruapehu, only two avalanche deposits (Murimotu Formation, 9,500 ka (Palmer & Neall, 1989) and Mangaio Formation, 4,600 ka (Donoghue & Neall, 2001) have been identified, displaying a relatively low frequency of occurrence. No direct observations of a large sector collapse have been witnessed on New Zealand stratovolcanoes. Prehistoric deposits of debris flows have been studied but due to erosion and successive burial the full extent of the event is masked. From the resulting computer simulation of the collapsing eastern crater rim of Mount Ruapehu, this study will discuss the hazard implications of each scenario on the surrounding area. The study will also attempt to create a hazard map encompassing any possible collapse event, taking into account the subsequent hazards from the possible transition of the collapsing mass into a debris avalanche and lahar.

4.2 Historical hazards and impacts:

The most devastating historic volcanic-related mass flow event in the region was the 1953 Tangiwai disaster that killed 151 people when the Wellington-Auckland Express train plummeted into the river after a lahar destroyed the rail bridge at Tangiwai (O'Shea, 1954). The lahar was a result of the break out of Crater Lake, which was temporarily dammed by glacial ice (Johnston & Neall, 1995). Crater Lake eruptions in 1969 and 1975 caused lahars which damaged ski fields and scientific equipment on the summit and northeast flank of the volcano (Hodgson & Houghton, 1995). The lahar in 1975 also damaged the Wahianoa aqueduct and Mangaio tunnel, parts of the Tongariro Power Scheme under construction at the time (Hodgson & Houghton, 1995), but no road or rail bridges were damaged downstream (Hancox *et al*., 1997). The most recent and most studied lahar event is that of the March 2007 Crater Lake break-out lahar. On the 18th March 2007 the rising Crater Lake breached a weak tephra dam, deposited by the 1995-96 eruptive sequence, releasing 1.3 x10^{6} m^{3} of water within hours (Procter *et al*., 2010c). The dam was eroded down to a stable lava outlet, after ~11% of the total volume of the lake was drained (Kilgour *et al*., 2010). The lahar flooded around the Tangiwai memorial, topped a small farm access bridge and severely damaged a footbridge on the RTMT that crosses the Whangaehu River. Other than that, there was no significant damage to road and rail bridges and no loss of life.

Three ski fields are situated on the flanks of Mount Ruapehu. There can be up to 10,000 skiers present on the slopes of Mount Ruapehu during the winter months (Kilgour *et al*., 2010). If a future event affected these highly visited areas of volcano, the consequences could be disastrous. The main observed effects of lahars on the immediate and surrounding area have been: the destruction of rail and road bridges, disruption of water supplies, and the disruption of electricity supplies (Hodgson & Houghton, 1995). Debris avalanches, debris flows and lahars can have a great affect on primary industry and manufacturing, agriculture, forestry, tourism, natural resources, infrastructure and communications.

In 1990 Tongariro National Park was declared a World Heritage Area for having outstanding natural properties and cultural values (DOC, 1999). Mount Ruapehu alone

has great international scientific importance and along with Crater Lake has extremely high scenic values (DOC, 1999). The Army Training Group puts an extremely high value on the long range views and the desert-like nature of the terrain (DOC, 1999). The Tongariro National Park also plays an important cultural role in the traditions of Maori people, particularly Ngati Tuwharetoa, Ngati Rangi, and Te Atihaunui-a-paparangi (DOC, 1999). Tongariro National Park is a significant area for recreation and tourism. Ruapehu specifically is nationally important for skiing, with two of three ski fields being of international standard (DOC, 1999). Many other forms of recreation that take place in the area include: tramping, climbing, ski mountaineering, hunting, nature study, photography and multisports. The major attraction of the region is the diversity of environments including bare volcanic mountains, open valleys, desert-like terrain, alpine herbfields, tussock and shrublands, and a variety of forests and rivers (DOC, 1999). This means that the area is visited by people all year round.

Due to the importance of this area, a greater understanding of how to live with and respect the natural environment is required. For people to be able to live within a volcanic landscape they need to understand the environment and the hazards that come with it. Public education activities, including hazard maps, increase hazard knowledge and responsiveness (Leonard *et al*., 2008). Therefore, the production of hazard-zonation maps based on scientific research and monitoring and the dissemination of these maps to the public and visitors to the National Park would help decrease the impact of future hazards. Hazard maps not only show areas that are at the greatest risk from a specific hazard, but they also provide a basis for land use management and human occupation.

Due to the infrequent nature of debris avalanche events at Mount Ruapehu, the chance of their occurrence in the near future is seen as low, and they are often overlooked as a significant hazard to plan for. The hazards that occur frequently such as lahars are well acknowledged with their likely impacts on the surrounding area mapped and the likely magnitude of their impact quantified (fig. 4.1). There is a noticeable absence in the depiction of the possible impact a debris avalanche event could have on the surrounding area.

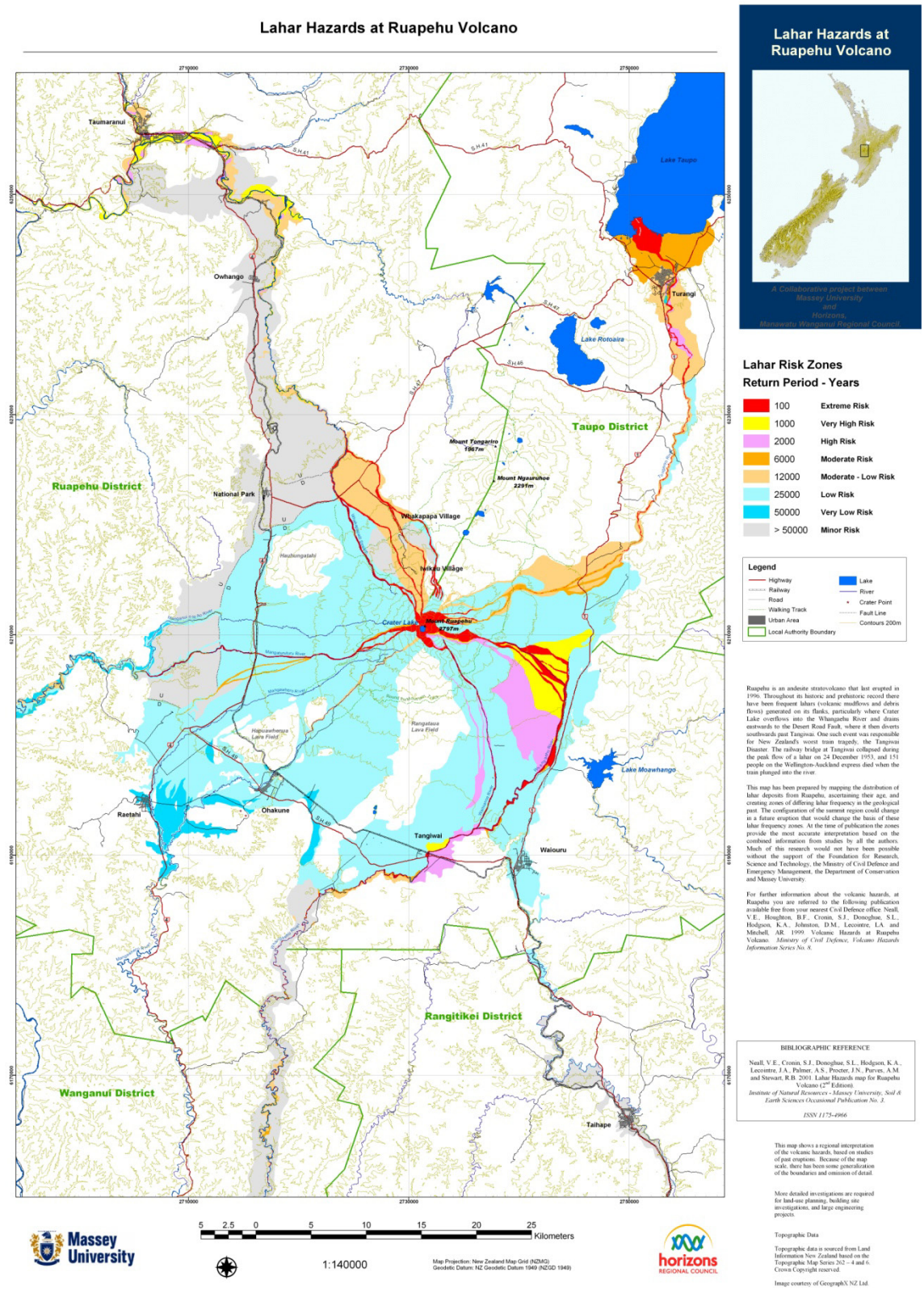

Figure 4.1: Hazard map for lahars at Mount Ruapehu, constructed by Neall *et al*. (2001).

Debris avalanches are mentioned as a possible volcanic hazard at Mount Ruapehu in many publications (Hodgson & Houghton, 1995; Hancox *et al*., 1997; DOC, 1999; Neall *et al.*, 1999) and some have modelled the resultant mass flow from a possible collapse of the eastern crater rim (Manville *et al*., 2003).

4.3 Hazard implications from this study:

Debris avalanches simulated in this study mainly impact the eastern region of Mount Ruapehu and surrounding ring plain, which includes recreational locations such as the New Zealand Alpine Club hut, Tukino Club ski field, RTMT, and Rangipo hut. The New Zealand Alpine Club hut is a small climbing hut at 2000m on a bluff overlooking the headwaters of the Whangaehu River (DOC, 1999). This hut may be out of reach from lahars but was inundated by each mass flow resulting from the collapse scenarios modelled in this study. Tukino club ski field is located 1700-1900 m on the divide between the Tongariro and Whangaehu catchments (DOC, 1999). It may be out of reach from all but the largest lahars but was inundated by the debris avalanche flow resulting from the two largest collapse scenarios in this study. The RTMT crosses the Whangaehu River valley near 1500 m contour and the footbridge over the river is likely to be greatly impacted by a range of possible collapse events of the eastern crater rim. Rangipo hut in this study was not directly impacted by any scenario modelled. The direct impacts of each simulated scenario are depicted in figures. 4.2-4.6 and tables 4.1-4.5.

4.3.1 Direct impacts of each simulated debris avalanche scenario

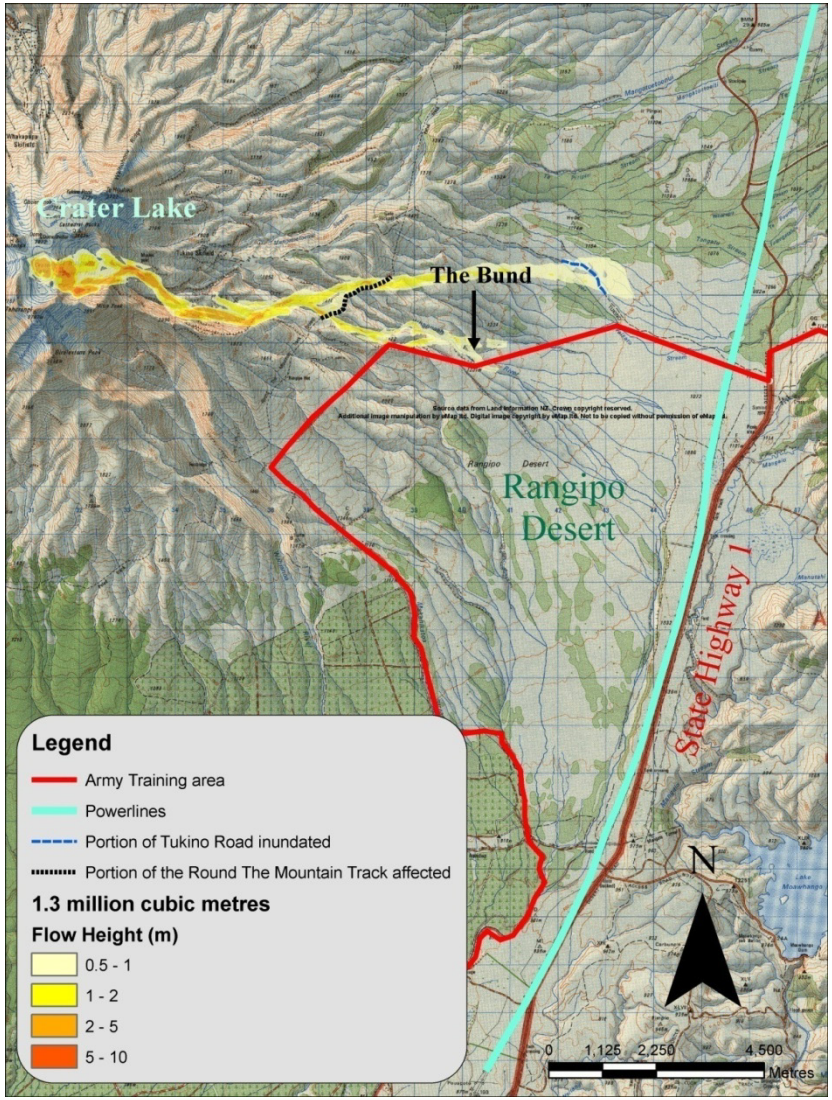

Location	Impact
Alpine ski hut	Inundated by up to 5 m of flow
Round the Mountain Track	1832 m of the Round The Mountain Track inundated with up to 2 m of flow
Bund	Inundated with up to 1 m of flow
Upper Whangaehu catchment	Likely to be impacted
Upper Waikato Stream	Likely to be impacted
Tukino Road	1254 m of Tukino Road inundated with a flow height of up to 1 m
Army Training area	Barely impacts the north western boarder of Army land in the Rangipo Desert.

Table 4.1: Impacts of scenario 1 on the surrounding area.

Figure 4.2: Inundation area and maximum flow heights of scenario 1, 1.3 million cubic metres (2.5% of the entire eastern rim).

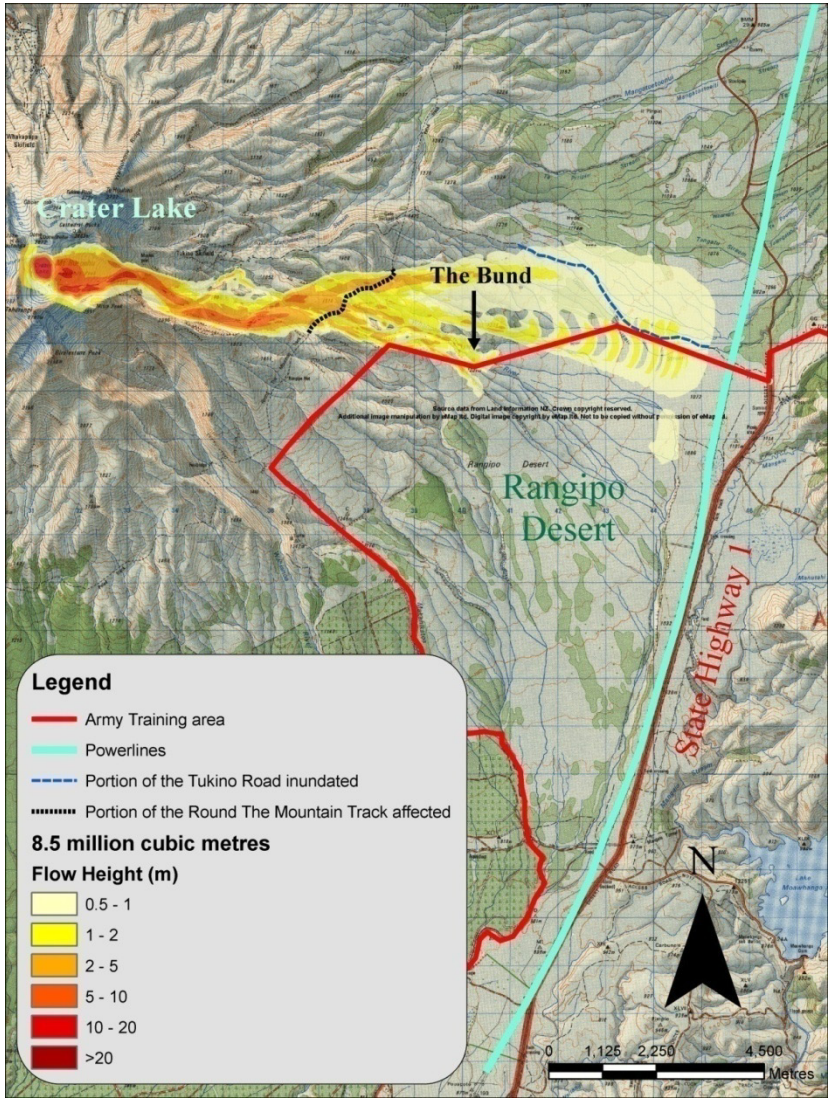

Location	Impact
Alpine ski hut	Inundated by up to 10 m of flow
Tukino Village	Possible hazard to the southern region
Round the Mountain Track	2433 m of the Round The Mountain Track inundated with up to 5 m of flow
Bund	Inundated with up to 2 m of flow
Upper Whangaehu catchment	Likely to be impacted
Upper Waikato Stream	Likely to be impacted
Tukino Road	4755 m of Tukino Road inundated with a flow height of up to 2 m
Army Training area	Slight impact of the north western and northern limit of the Army land in the Rangipo Desert

Table 4.2: Impacts of scenario 2 on the surrounding area.

Figure 4.3: Inundation area and maximum flow heights of scenario 2, 8.5 million cubic metres (15% of the entire eastern rim).

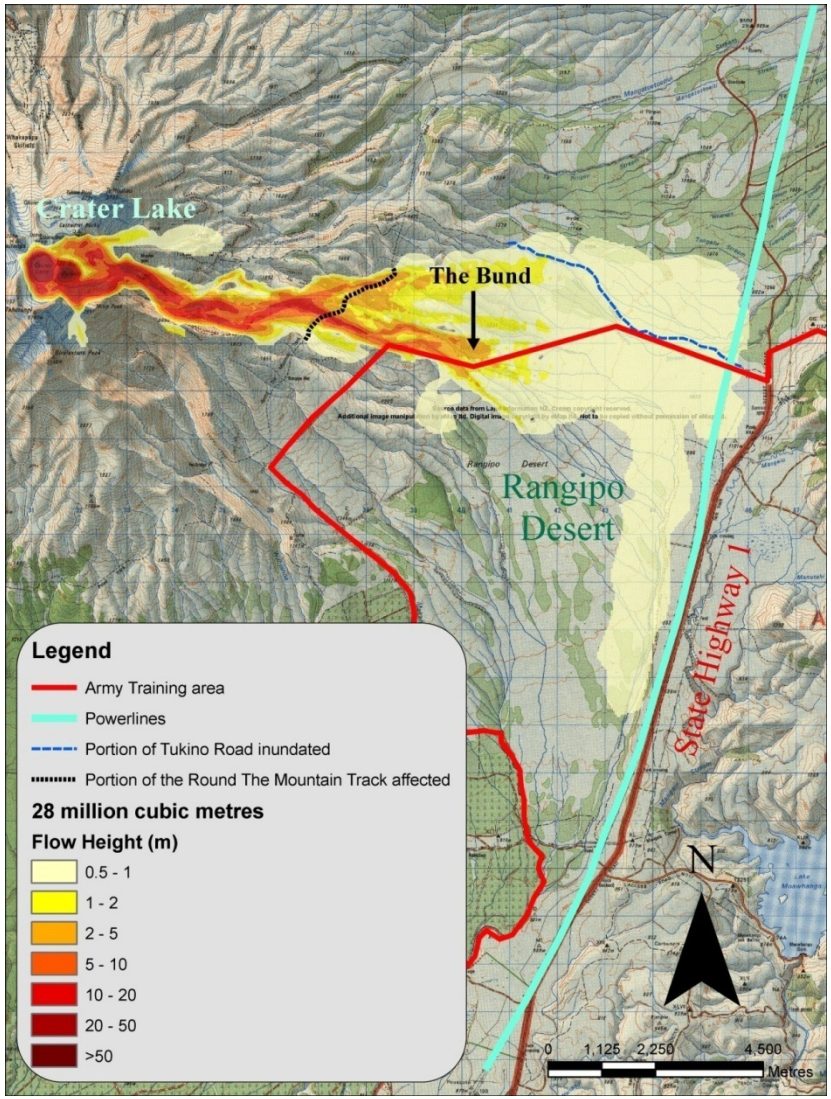

Location	Impact
Alpine ski hut	Inundated by up to 50 m of flow
Tukino ski field and village	Large impact on the Tukino ski field, likely inundation of up to 1 m of flow. An inundation of flow up to 1 m is likely to affect the western and southern portion of the Tukino Village
Round the Mountain Track	2733 m of the Round The Mountain Track inundated with up to 20 m of flow
Bund	Inundated with up to 5 m of flow
Upper and mid sections of the Whangaehu catchment	Impacted
Upper Waikato Stream	Impacted
Tukino Road	5847 m of Tukino Road inundated with a flow height of up to 2 m
Army Training area	Northern and eastern portions of the Army land in the Rangipo Desert will be affected, including some tracks off State Highway 1
Powerlines	2837 m section of powerlines paralleling State Highway 1 will be inundated with up to 1 m of flow at their base
Tangatu Stream	Small regions affected

Table 4.3: Impacts of scenario 3 on the surrounding area.

Figure 4.4: Inundation area and maximum flow heights of scenario 3, 28 million cubic metres (50% of the entire eastern rim)

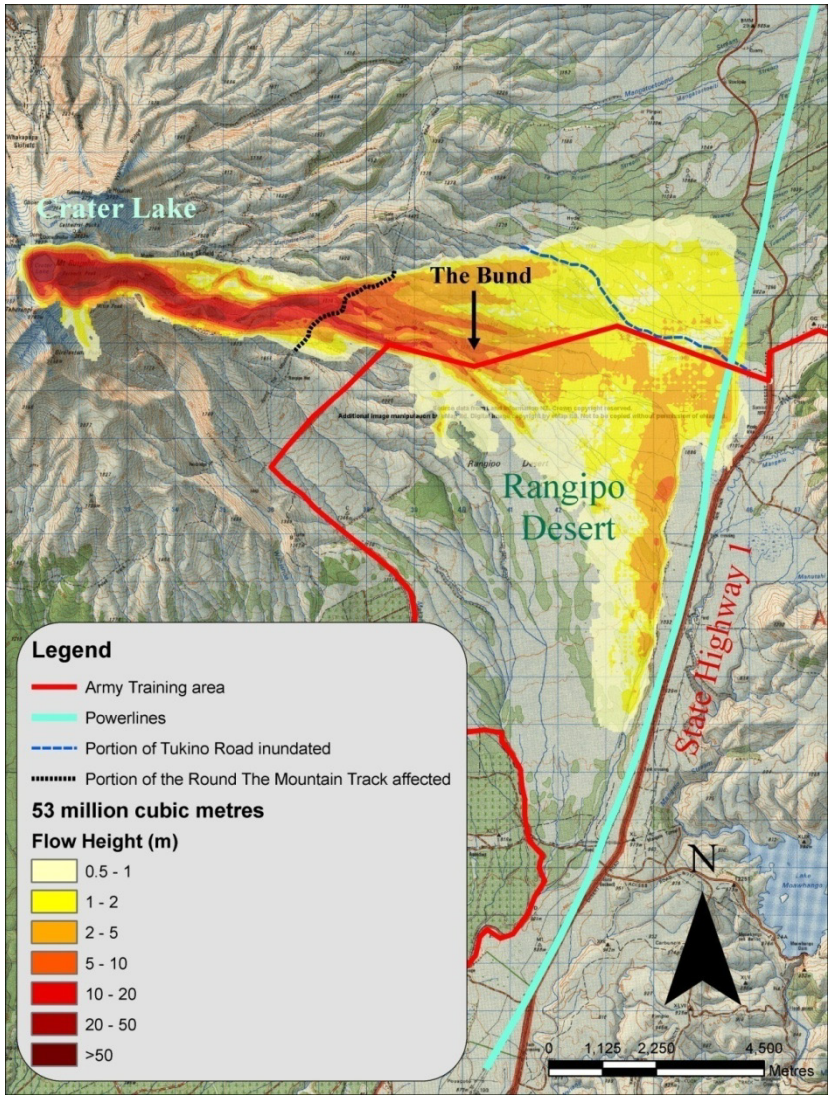

Location	Impact
Alpine ski hut	Inundated by up to 50 m of flow
Tukino ski field and village	Large impact on the Tukino ski field, likely inundation of up to 5 m of flow. An inundation of flow up to 2 m is likely to affect the western and southern portion of the Tukino Village
Round the Mountain Track	2927 m of the Round The Mountain Track inundated with up to 20 m of flow
Bund	Inundated with up to 10 m of flow
Upper and mid sections of the Whangaehu catchment	Impacted
Upper Waikato Stream	Impacted
Tukino Road	5847 m of Tukino Road inundated with a flow height of up to 5 m
Army Training area	Northern and eastern portions of the Army land in the Rangipo Desert will be affected, including some tracks off State Highway 1
Powerlines	3489 m section of powerlines paralleling State Highway 1 will be inundated with up to 5 m of flow at their base
Tangatu Stream	Small regions affected
State Highway 1	A small portion near the Paradise Valley Road turnoff and also part of the picnic area about 700 m north is likely to be inundated with up to 1 m of flow.

Table 4.4: Impacts of scenario 4 on the surrounding area.

Figure 4.5: Inundation area and maximum flow heights of scenario 2, 53 million cubic metres (100% of the entire eastern rim).

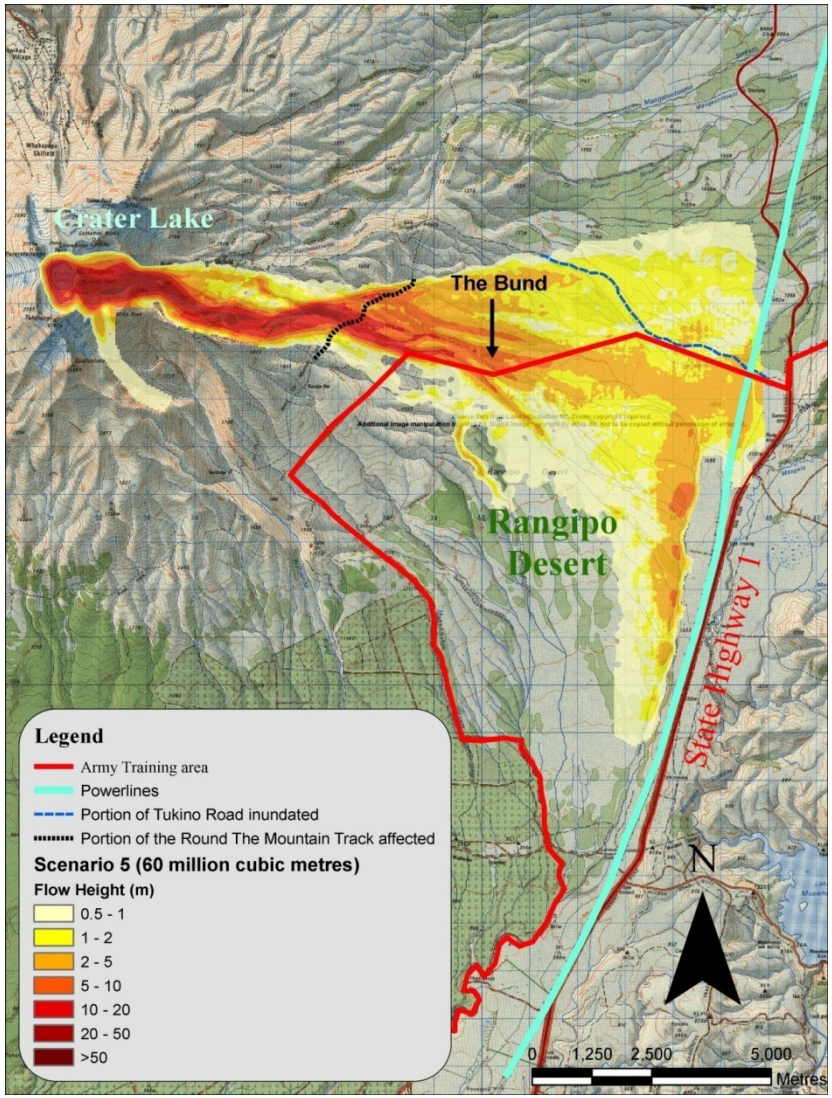

Location	Impact
Alpine ski hut	Inundated by up to 50 m of flow
Tukino ski field and village	Large impact on the Tukino ski field, likely inundation of up to 5 m of flow. An inundation of flow up to 2 m is likely to affect the western and southern portion of the Tukino Village
Round the Mountain Track	2927 m of the Round The Mountain Track inundated with up to 20 m of flow
Bund	Inundated with up to 10 m of flow
Whangaehu catchment	Impacted
Upper Waikato Stream	Impacted
Tukino Road	5847 m of Tukino Road inundated with a flow height of up to 5 m
Army Training area	Northern and eastern portions of the Army land in the Rangipo Desert will be affected, including some tracks off State Highway 1
Powerlines	3894 m section of powerlines paralleling State Highway 1 will be inundated with up to 5 m of flow at their base
Tangatu Stream	A flow of up to 2 m inundates a small portion of the Tangatu Stream and Wharepu Stream, which leads into the Tongariro River
State Highway 1	A small portion near the Paradise Valley Road turnoff and also part of the picnic area about 700 m north is likely to be inundated with up to 1 m of flow.

Table 4.5: Impacts of scenario 5 on the surrounding area.

Figure 4.6: Inundation area and maximum flow heights of scenario 2, 8.5 million cubic metres (100% of the entire eastern rim and 7 million cubic metres of Crater Lake).

Any subsequent lahars and debris flows would likely impact a greater area further from source. In this case the likely areas affected would be the Whangaehu outwash fan, southern Rangipo desert, western Desert Road corridor, lower reaches of the Whangaehu catchment and northern catchments leading into the Tongariro River and Lake Taupo. Ecosystem and species values, surrounding communities, infrastructure and economic values are aspects of this area at risk of a collapse event and subsequent mass flows. The area includes two nationally and regionally important North Island rivers, the Whangaehu and the Tongariro, and the nationally important Lake Taupo (DOC, 1999). The headwaters of the Tongariro River, and hence Lake Taupo originate on the north eastern side of Mount Ruapehu. The Tongariro River has a high water quality important for recreation, trout spawning, blue duck habitat, hydroelectricity and scenic values (DOC, 1999). This could all be at risk from a major lahar resulting from the collapse of the eastern rim. With ~40,000 people per year (DOC, 1999) visiting the river to fish, an event as such could also be life threatening. Lake Taupo is also important for recreation, water supplies, and trout fishing and is the source of the Waikato River. It is the largest freshwater lake in Australasia and a major landscape feature in the central North Island (DOC, 1999).

The towns of Turangi and Waiouru are located at the distal ends of the likely affected regions along the Tongariro and Whangaehu River catchments respectively. Transport routes crossing these rivers and their head waters include State Highways 1, 49 and Tukino Road. The main trunk railway and bridges cross the Whangaehu River at Tangiwai along with fibre-optic cables for communication systems (DOC, 1999). Powerlines carrying electricity for the national grid run along the eastern side of Ruapehu. The area also has national and regional economic importance through power generation (including Rangipo and Tokaanu Power Stations), Tangiwai timber milling, Tranz Rail facilities, and general tourism (DOC, 1999). In planning mitigation schemes for the 2007 lahar, DOC (1999) estimated that the total economic cost of the direct damage of such an event with no intervention would reach into the millions of dollars. The lahars from the 1995-1996 eruptions damaged the hydroelectrical powerstation from ash being washed into the Tongariro River. The estimated cost of loss of

generation was > $12 million and the cost to replace the turbine blades was ~$6 million (Johnston *et al*., 2000). It is not only the damage that mass flows can cause that costs but mitigation plans can have economic impacts too. In the lead up to the 2007 March lahar there was a lot of time and money spent on mitigation plans such as: risk assessments, alarm system and response, Bund structure, and strengthening of State Highway 49 bridge (~$4.1 million) (Keys & Green, 2008). To minimise unnecessary expenditure and ensure that the money that is spent is targeted at the most important locations, such mitigation measures must be based on the best scientific knowledge of the potential damage mass flows can cause.

4.4 Combined hazard map comprising all possible scenarios:

Due to the vast natural, cultural, and economical values of this region it is important to know where these likely affected areas will be. From the inundation areas of scenarios 1-4 and inferred flows from the subsequent breakout of Crater Lake likely in scenarios 3 and 4 if the lake is full and transitional flows (debris flow and lahar) from the possible entrainment of snow, ice and stream water in all scenarios, a hazard map was constructed (fig. 4.7). It is split into two hazard zones. Zone 1: the area likely to be directly impacted from a dry debris avalanche resulting from the collapse of the entire eastern crater rim. The boundary of this zone is based on model outputs. Zone 2: the additional area possibly affected by transitional flows from the entrainment of snow, ice, and stream water and/or the area likely to be impacted by debris flows and/or lahars as a result of the subsequent release of Crater Lake water after the collapse of the eastern crater rim. The boundaries of this zone are indicative of possible flow paths, but not based directly on model outputs. The affected areas of zone 2 were inferred from the path of the modelled debris avalanches in this study and areas affected by lahars in the past, especially those lahars that resulted from dam of rim collapse (Neall *et al*. 1999; Cronin *et al*., 1997).

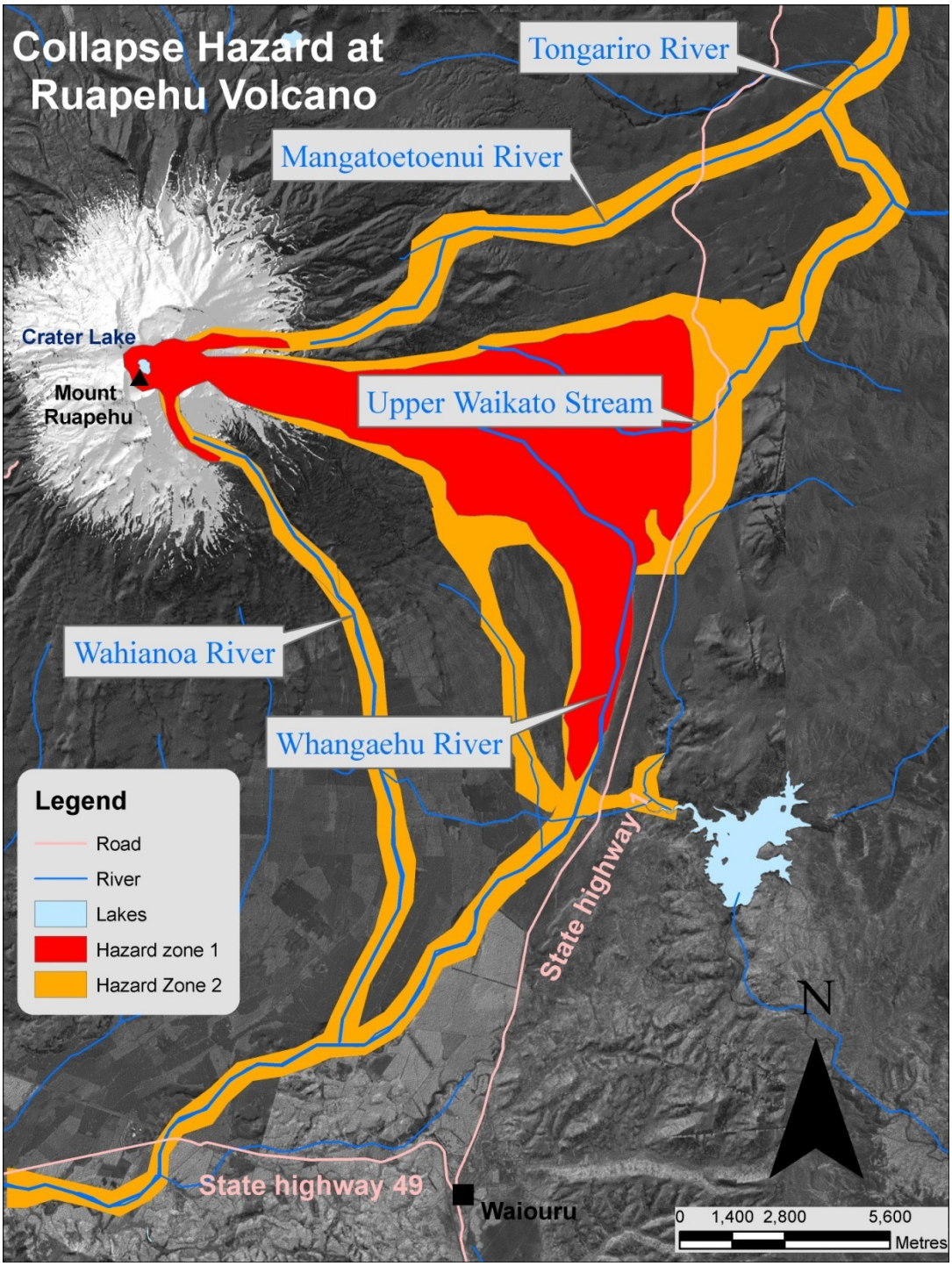

Figure 4.7: Hazard-zone map for the entire collapse of the eastern crater rim, including areas likely to be affected by the subsequent debris avalanche and possible lahars.

From this, it is proposed that current volcanic hazard assessment of lahars integrate the potential for unanticipated mass flows from a collapse scenario at Mount Ruapehu. Debris flows and lahars resulting from a volcanic collapse are less well known than lahars formed by the melting of snow and ice by hot volcanic material, water

released from a crater lake or remobilised unconsolidated volcanic material by rainfall runoff, but their resulting impacts are comparable (Scott *et al*., 2001). A volcanic collapse can result in a debris avalanche with limited run-out potential; however, the run-out potential of the mass flow may increase several fold by entraining water and/or sediment beyond the volcano, increasing its volume and run-out (Scott *et al*., 2001). Due to mass flow transformations downstream from source, the same collapse event could have varied impacts due to changes in flow rheology and hence behaviour. Transformation of a failed mass into a debris flow is a common occurrence at volcanoes such as Mount Rainier and Mount Baker in the Cascade Range (Scott *et al*., 2001).

Lahars at Mount Ruapehu have been generated mainly by eruptions but they have also been caused by non-eruptive events such as the displacement of Crater Lake water from inflowing material and by the collapse of the lake outlet or crater rim (Hancox *et al*., 1997; Procter *et al*., 2010c). Partial and total Crater Lake rim collapses are two mechanisms seen to trigger large lahars at Mount Ruapehu (Lecointre *et al*., 2004). In the case of the collapse scenarios in this study, lahars could result from the addition of melting snow and ice or incorporation of stream water into the resultant debris avalanche mass. Lahars could also be formed by the breakout of water from the Crater Lake. When a debris avalanche flows into the existing lake it may displace a large amount of water, causing a flood of water that can entrain avalanche and loose pyroclastic material. The collapse of a significant section of the crater rim could also result in the release of Crater Lake water.

Chapter 5: DISCUSSION AND CONCLUSION

This study agrees with past stability studies of the eastern crater rim (Hancox *et al*., 1997; Hancox, 2001) that the Pyramid Peak area has been relatively stable since historic observations started and this area is likely to remain stable in current conditions due to its broad nature. The Stump Saddle and J Peak regions seem to be the most unstable as they have been altered the most over time and contain a number of rim faults/fractures. The structural integrity of the entire eastern rim, however, could be altered by an increase in low magnitude events (volcano-seismic activity or phreatic eruptions), or occurrence of a greater magnitude event (extensive magmatic intrusion or an explosive eruption), or simply a change in the hydrothermal system increasing the weathering and weakening of the eastern crater rim and increased pressure put on the crater wall from the Crater Lake or pore water. This continual decline in crater rim strength combined with a small collapse from Stump Saddle, J Peak or the erosion of supporting lava units could result in a subsequent failure of a larger portion of, or the entire, eastern rim complex. Although a large collapse is not likely at present, the continual weakening of the eastern crater rim means that the likelihood may increase over time. If there is the knowledge that a collapse event could be possible at Mount Ruapehu, people should be educated and prepared.

The collapse scenarios in this study were used to depict what could happen if the eastern rim failed. A range of collapse volumes were simulated by Titan2D to model the different sized events that were possible. The first two scenarios (1 and 2) are based on the failure of the upper flanks of the eastern crater, which would be conditioned by the failure of the supporting bands of lava like that of the Pyramid member and Coffin member. The two largest scenarios (3 and 4) are based on the possible failure of deeper seated units that are hydrothermally altered by percolating Crater Lake water. A subsequent scenario (5) was simulated to see the effect of the addition of released Crater Lake water on the resulting mass flow in scenario 4. These scenarios have volumetrically covered the possible failure events likely to occur from the eastern crater rim. What these scenarios did not account for were bulking and debulking. This is because simulating the complex and varied rheological

transformation that can occur within mass flows is beyond the capabilities of Titan2D. The computation took up to a couple of days to model these collapse scenarios, a limitation from only using a single-processor workstation combined with a complex terrain and channel morphology. Computer modelling of mass flows can never replace the importance of geological mapping and the study of historic mass flow events in the creation of hazard maps. This information is also vital for computational modelling inputs. However where this information is unavailable, mass flow simulations provide a reliable indication of flow path and areas of inundation in proximal and medial regions.

Like past events such as glaciations and eruptions that produce structures including medial moraines or lava flows (Cronin & Neall, 1997), the simulated debris avalanche scenarios and resulting deposits will alter the landscape, changing the course of future lahars and debris flows, and therefore changing the hazardscape. The resulting deposit of a debris avalanche may block rivers or the Crater Lake outlet, reorganising existing drainage patterns. This could result in further flooding from rising water levels and subsequent rapid release of dammed water. Not only would it increase the sediment supply but it would fill up valleys and channels, decreasing the volume that can be accommodated. This could lead to increased overflowing and therefore inundation of lahars into unwanted areas. A mitigation structure such as the Bund would decrease in effectiveness as the area around is aggraded or the structure itself removed. Topographic changes upstream of this structure could also increase the chance of such flows overtopping channels, cancelling out the remaining effectiveness of the structure. The Crater Lake outlet currently drains directly into the Whangaehu Catchment, resulting in the river being susceptible to lahars. If this route is blocked or altered during a collapse event due to erosion or deposition of material (decreasing the channel accommodation), future lahars could be directed into other catchments.

Over the evolutionary history of the ring plain flows have migrated from the north to the south and back again. This is due to changes in topography and elevation from erosion and deposition of volcanic material and other influences such as climate, faulting, and moraines. From the formations described in Donoghue and Neall (2001) it can be seen that these flows are building up the south-eastern ring plain pushing

subsequent flows north. From the inundation area of the simulated debris avalanches in this study, it looks as though this trend is to continue. The implication of this is an increased likelihood that volcanic mass flows will be directed into catchments that flow into the Tongariro River. Currently the Mangatoetoenui Stream is the largest contributor of lahars into the Tongariro River, and during the 1995/1996 eruptions the only lahars to enter the Tongariro River travelled down the Mangatoetoenui Stream (Cronin *et al*., 1997). If lahars and debris flows continue to migrate northward, more tributaries of the Tongariro (i.e. Upper Waikato Stream) could contribute to lahar hazards in the Tongariro River and surrounding area.

Due to the alteration of the landscape and mitigation features like that of the Bund, from past events and future events simulated in this study, no subsequent volcanic mass flow can be treated the same as the previous one. A hazard plan for future mass flows need to be unique for each event. These plans also need to be altered to accommodate changes made by these events on the landscape. This is not only seen in the evolution of the build up of the eastern ring plain of Mount Ruapehu but also in the modelling of the debris avalanche that emplaced the 9.5 Ka Murimotu Formation (Palmer & Neall, 1989) by Manville *et al*. (2003). From using topographic information that already included the deposit of the modelled flow, the inundation area of the same flow was significantly displaced to the east of the actual formation (Manville *et al*., 2003). Therefore, due to the significant effect topography has on the behaviour of mass flows, any subsequent event of a similar magnitude may not behave in the same manner as the previous; therefore it may not replicate similar patterns of inundation, erosion or deposition.

5.1 Conclusion

This study initially set out to create a quantitative scenario based hazard forecast for a collapse event of the eastern crater rim of Mount Ruapehu. This included the application of a granular continuum computational modelling technique to forecast the possible hazards from a collapse event in a New Zealand setting and the defining of the resulting impacts on the surrounding area. The study originally aimed to: produce a new detailed map of the eastern crater rim, especially Pyramid Peak; quantify the three-dimensional geometry, state of alteration and failure conditions of key geologic units comprising the eastern rim to define and characterise potential failure planes; determine the volumes of collapsing material and define possible scenarios of collapse; and apply Titan2D to compute flow run-out, diversion, inundation, velocity and mass transport collapse volumes for the range of likely collapse scenarios.

The geological study resulted in a basic map of the Pyramid Peak area. The mapping of the eastern crater rim was based largely on aerial photography. The major limitations of mapping using aerial photographs are that the formations are inferred from purely visual features such as colour, texture and the dipping of beds. Weathering can cause false coloured boundaries within the same unit of material. Bedding is also hard to determine on a highly erodible landscape. Another limitation is that aerial photographs of Mount Ruapehu are generally only taken after an eruption, when most of the area is covered in fresh ash that is eroded soon after. Therefore, much work is needed to confirm any suggestions made in this study on the geology. Due to the lack of information of the lower geological units that make up the eastern crater rim, the structure of the rim was inferred from surface geological interpretations and by other studies (Hancox *et al*., 1997; Hales, 2000; Hancox, 2001). The geology identified in this study provided enough information to determine key lithologic units in the eastern rim structure to define volume scenarios for collapse simulations to be modelled by Titan2D. The main conclusions from the results of this study were:

- Larger collapses are likely to be conditioned by weak hydrothermally altered layers lower in the eastern rim sequences.

- The Pyramid Peak region of the eastern crater rim seems to be stable at the current time. However, with the ongoing erosion and hydrothermal alteration to both the inner and outer crater walls the likelihood of a collapse will increase over time.
- Debris flows, lahars and avalanches on the eastern ring plain are currently migrating northward, a concern for the Tongariro River catchment.
- The Bund will likely be completely inundated by any substantial collapse event from the eastern rim of Mount Ruapehu. The resulting mass flows also seem to avulse into northern catchments upstream of the Bund.
- The Mangatoetoenui, Upper Waikato, Tongariro and Whangaehu River catchments could be greatly affected by a sudden collapse of the eastern rim and any subsequent lahar events.

A more detailed study of the eastern rim needs to be completed to define the structure and stability of lower units that were unable to be studied here. Continual monitoring of the stability of the eastern rim of Mount Ruapehu is recommended and the potential impact of a possible collapse event needs to be included into current hazard maps and mitigation plans.

REFERENCES:

Abaconda Management Group (AMG) (2009). Mount Ruapehu. Guide to Mt. Ruapehu, New Zealand. http://mt-ruapehu.com/category/weather-ruapehu/ (10/03/2011).

Adobe Systems Inc. (2011). Adobe Illustrator. CS2 12.0.0. www.adobe.com.

Allan, A. S. R., Baker, J. A., Carter, L., Wysoczanksi, R. J. (2008). Reconstructing the Quaternary evolution of the world's most active silica volcanic system: insights from an ~ 1.65 Ma deep ocean tephra record sourced from Taupo volcanic zone, New Zealand. *Quaternary Science Reviews* 27: 2341-2360.

Beck, A. C. (1950). Volcanic Activity at Mount Ruapehu from August to December, 1945. *New Zealand Journal of Science and Technology* B31: 1-13.

Carrivick, J. L., Manville, V., Cronin, S. J. (2009). A fluid dynamics approach to modelling the 18th March 2007 lahar at Mt. Ruapehu, New Zealand. *Bulletin of Volcanology* 71: 153-169.

Cassidy, J., Ingham, M., Locke, C. A., Bibby, H. (2009). Surface structure across the axis of the Tongariro Volcanic Centre, New Zealand. *Journal of Volcanology and Geothermal Research* 179: 233-240.

Christenson, B. W., Reyes, A. G., Young, R., Möbis, A., Sherburn, S., Cole-Baker, J., Britten, K. (2010). Cyclic processes and factors leading to phreatic eruption events: Insights from the 25 September 2007 eruption through Ruapehu Crater Lake, New Zealand. *Journal of Volcanology and Geothermal Research* 191: 15-32.

Christenson, B. W. and Wood, C. P. (1993). Evolution of a vent-hosted hydrothermal system beneath Ruapehu Crater Lake, New Zealand. *Bulletin of Volcanology* 55: 547-565.

Cole, J. W. (1990). Structural control and origin of volcanism in the Taupo volcanic zone, New Zealand. *Bulletin and Volcanology* 52: 445-459.

Cole, J. W., Graham, I. J., Hackett, W. R., Houghton, B. F. (1986). Volcanology and petrology of the Quaternary composite volcanoes of Tongariro volcanic centre, Taupo volcanic zone. *In* Late Cenozoic Volcanism in New Zealand, Vol. 23. I. E. M. Smith. *Bulletin, Royal Society of New Zealand*: 224-250.

Cole, J. W. (1978). Andesites of the Tongariro volcanic centre, North Island, New Zealand. *Journal of Volcanology and Geothermal Research* 3: 121-153.

Cronin, S. J. (1996). Late Quaternary volcanic stratigraphy within a portion of the northeastern Tongariro Volcanic Centre. Unpublished PhD Thesis. Massey University, Palmerston North. 181 pages.

Cronin, S. J. and Neall, V. E. (1997). A late Quaternary stratigraphic framework for the northeastern Ruapehu and eastern Tongariro ring plains, New Zealand. *New Zealand Journal of Geology and Geophysics* 40: 185-197.

Cronin, S. J., Neall, V. E., Lencointre, J. A., Hedly, M. J., Loganathan, P. (2003). Environmental hazards of fluoride in volcanic ash: a case study from Ruapehu volcano, New Zealand. *Journal of Volcanology and Geothermal Research* 121: 271-291.

Cronin, S. J., Neall, V. E., Lecointre, J. A., Palmer, A. S. (1999). Dynamic interations between lahars and stream flow: A case study from Ruapehu volcano, New Zealand. *Geological Society of America Bulletin* 111: 28-38.

Cronin, S. J., Neall, V. E., Palmer, A. S. (1997). Lahar history and Hazard of the Tongariro River, Northeastern Tongariro Volcanic Centre, New Zealand. *New Zealand Journal of Geology and Geophysics* 40: 383-393.

Cronin, S. J., Neall, V. E., Palmer, A. S. (1996). Geological history of the north-eastern ring plain of Ruapehu volcano, New Zealand. *Quaternary International* 34-36: 21-28.

Dade, W. B. and Huppert, H. E. (1998). Long-runout rockfalls. *Geology* 26: 803-806.

Delft Hydraulics (2011). Downloading Delft3D user manuals. http://delftsoftware.wldelft.nl/index.php?option=com_docman&task=cat_view&gid=39&Itemid=61 (02/05/2011).

DOC (1999). Environmental and risk assessment for mitigation of the hazard from Ruapehu Crater Lake report prepared for the Ministry of Conservation. Department of Conservation, Turangi/Taupo Conservancy. April 1999.

Donoghue, S. L. (1991). Late Quaternary volcanic stratigraphy of the southeastern sector of Mount Ruapehu ring plain New Zealand. Unpublished PhD Thesis. Massey University, Palmerston North.

Donoghue, S. L. and Neall, V. E. (2001). Late Quaternary construction history of the southeastern Ruapehu ring plain, New Zealand. *New Zealand Journal of Geology and Geophysics* 44: 439-466.

Donoghue, S. L. and Neall, V. E. (1996). Tephrostratigraphy studies at Tongariro Volcanic Centre, New Zealand: An overview. *Quaternary International* 34-36: 13-20.

Donoghue, S. L., Neall, V. E., Palmer, A. S., Stewart, R. B. (1997). The volcanic history of Ruapehu during the past 2 millennia based on the record of Tufa Trig tephras. *Bulletin of Volcanology* 59: 136-146.

Donoghue, S. L., Neall, V. E., Palmer, A. S. (1995). Stratigraphy and chronology of late Quaternary andesitic tephra deposits, Tongariro Volcanic Centre, New Zealand. *Journal of the Royal Society of New Zealand* 25: 115-206.

Drost, F., Renwick, J., Bhaskaran, B., Oliver, H., McGregar, J. (2007). A simulation of New Zealand's climate during the Last Glacial Maximum. *Quaternary Science Reviews* 26: 2505-2525.

ESRI Inc. (2011). ArcGIS 9.2 Software. www.esri.com.

Fagents, S. A. and Baloga, S. M. (2005). Calculation of lahar transit times using digital elevation data. *Journal of Volcanology and Geothermal Research* 139: 135-146.

Froggatt, P. C. and Lowe, D. J. (1990). A review of late Quaternary silicic and some other tephra formations from New Zealand: their stratigraphy, nomenclature, distribution, volume, and age. *New Zealand Journal of Geology and Geophysics* 33: 89-109.

Gamble, J. A., Price, R. C., Smith, I. E. M., McIntosh, W. C., Dunbar, N. W. (2003). $^{40}Ar/^{39}Ar$ geochronology of magmatic activity, mamga flux and hazards at Ruapehu Volcano, Taupo Volcanic Zone, New Zealand. *Journal of Volcanology and Geothermal Research* 120: 271-287.

Gamble, J. A., Wood, C. P., Price, R. C., Smith, I. E. M., Stewart, R. B., Waight, T. (1999). A fifty year perspective of magmatic evolution on Ruapehu Volcano, New Zealand: verification of open system behaviour in an arc volcano. *Earth and Planetary Science Letters* 170: 301-314.

Genesis Energy (2010). Scheme description of Tongariro. http://www.genesisenergy.co.nz/genesis/index.cfm?0E58E2D9-FD4C-675E-C3DF-9E9681D507DF (07/03/2011).

Gibson, W. and Morgan, P. G. (1927). The Geology of the Egmont subdivision. *New Zealand Geological Survey Bulletin* 29: 92 p.

Graettinger, A. H., Manville, V., Briggs, R. M. (2009). Depositional record of historic lahars in the upper Whangaehu Valley, Mt. Ruapehu, New Zealand: implications for trigger mechanisms, flow dynamics and lahar hazards. *Bulletin of Volcanology* 72(3): 279-296.

Graham, I. J., Cole, J. W., Briggs, R. M., Gamble, J. A., Smith, I. E. M. (1995). Petrology and petrogenesis of volcanic rocks from Taupo Volcanic Zone: a review. *Journal of Volcanology and Geothermal Research* 68: 59-87.

Graham, I. L., and Hackett, W. R. (1987). Petrology of calc-alkaline lavas from Ruapheu and related vents, Taupo volcanic zone, New Zealand. *Journal of Petrology* 28: 531-657.

Grange, L. I. (1931). Conical Hills on Egmont and Ruapehu Volcanoes. *New Zealand Journal of Science and Technology* 12: 376-384.

Gray, J. M. N. T. (2001). Granular flow in partially filled slowly rotating drums. *Journal of Fluid Mechanics* 441: 1-29.

Gray, J. M. N. T., Wieland, M., Hutter, K. (1999). Gravity-driven free surface flow of granular avalanches over comlex basal terrain. *Proceedings of the Royal Society, London Series A* 455: 1841-1874.

Gregg D. R. (1960). The geology of Tongariro Subdivision. *New Zealand Geological Survey Bulletin* 40: 152 p.

Grim, R. E. (Editor) (1968). Clay mineralogy (2nd edition). McGraw-Hill Inc.

Hackett, W. R. (1985). Geology and petrology of Ruapehu volcano and related vents. Unpublished PhD Thesis. Geology Department. Wellington, Victoria University of Wellington: 303-312.

Hackett, W. R., and Houghton, B. F. (1989). A facies model for a Quaternary andesitic composite volcano: Ruapehu, New Zealand. *Bulletin of Volcanology* 51(1): 51-68.

Hales, T.C., (2000). The geology of the summit area, Mt Ruapehu. Unpublished BSc Hons Thesis, Canterbury University.

Hancox, G. T. (2001). Report on inspection of 'J' Peak area of Ruapehu crater rim, 25 April 2001. *GNS Client Report 43009B.10 (report prepared for DOC, Turangi, June 2001).*

Hancox, G. T., Nairn, I.A., Otway, P.M., Webby, G., Perrin, N. D., Keys, J. R. (1997). Stability assessment of Mt Ruapehu crater rim following 1995-1996 eruptions. *GNS Client Report 43605B (Open File report prepared for DOC Turangi, June 1997).*

Hayashi, J. N. and Self, S. (1992). A comparison of pyroclastic flow and debris avalanche mobility. *Journal of Geophysical Research* 97 (B6): 9063-9071.

Healy, J., Lloyd, E. F., Rishworth, D. E. H., Wood, C. P., Glover, R. B., Dibble, R. R. (1978). The eruption of Ruapehu, New Zealand, on 22 June 1969. *New Zealand Department of Scientific and Industrial Research Bulletin* 224: 88 p.

Heim, A. (1932). Bergsturz und Menschenleben, Fretz und Wasmuth, Zürich, p.218.

Hobden, B. J., Houghton, B. F., Lanphere, M. A., Nairn, I. A. (1996). Growth of the Tongariro volcanic complex: New evidence from K-Ar age determinations. *New Zealand Journal of Geology and Geophysics* 39: 151-154.

Hodgson, K. A. (1993). Later Quaternary lahars from Mount Ruapehu in the Whangaehu River valley, North Island, New Zealand. Unpublished PhD thesis, Massey University, Palmerston North, New Zealand, Vol.1. 256 pages.

Hodgson, K. A. and Houghton, B. F. (1995). Manawatu-Wanaganui Regional Council Volcanic Hazard Assessment. *GNS Client Report 71415D.11.*

Hodgson, K. A., Lecointre, J. A., Neall, V. E. (2007). Onetapu Formation: the last 2000 yr of laharic activity at Ruapehu volcano New Zealand. *New Zealand Journal of Geology and Geophysics* 50: 81-99.

Houghton B. F., Latter, J. H., Hackett W. R. (1987). Volcanic hazard assessment for Ruapehu composite volcano, Taupo Volcanic Zone, New Zealand. *Bulletin of Volcanology* 49: 737-751.

Hungr, O. (1995). A model for the runout analysis of rapid flow slides, debris flows and avalanches. *Canadian Geotechnical Journal* 32: 610-623.

Hungr, O. and McDougall, S. (2008). Two numerical models for landslide dynamic analysis. *Computers and Geosciences* 35: 978-992.

IDM Computer Solutions Inc. (2011). UltraEdit Professional text/HEX Editor, version 14.20.1.1008. www.ultraedit.com.

Inoue, A. (1995). Formation of clay minerals in hydrothermal environments. In: Velde, B. (Editor), Origin and mineralogy of clays: clays and the environment. Springer. 268-329.

Iverson, R. M. (1997). The physics of debris flows. *Reviews of Geophysics* 35 (3): 245-296.

Iverson, R. M. and Denlinger, R. P. (2001). Flow of variably fluidized granular material across three-dimensional terrain 1. Coulomb mixture theory. *Journal of Geophysical Research* 106: 537-552.

Iverson, R. M., Schilling, S. P., Vallance, J. W. (1998). Objective delineation of lahar-inundation hazard zones. *Geological Society of America Bulletin* 110: 972-984.

Johnston, D. M. and Neall, V. E. (1995). Ruapehu Awakens: the 1945 eruption of Ruapehu. *The Science Centre and Manawatu Museum Scientific Monograph No. 1.*

Johnston, D. M., Houghton, B. F., Neall, V. E., Ronan, K. R., Paton, D. (2000). Impact of the 1945 and 1995-1996 Ruapehu eruptions, New Zealand: An example of increasing societal vulnerability. *Geological Society of America Bulletin* 112 (5): 720-726.

Keys, H. J. R. and Green, P. M. (2008) Ruapehu Lahar New Zealand 18 March 2007: Lessons for Hazard Assessment and Risk Mitigation 1995-2007. *Journal of Disaster and Research* 3(4): 284-296.

Kilgour, G., Manville, V., Pasqua, F., Graettinger, A., Hodgson, K. A., Jolly, G. E. (2010). The 25 September 2001 eruption of Mount Ruapehu, New Zealand: Direct ballistics, surtseyan jets, and ice-slurry lahars. *Journal of Volcanology and Geothermal Research* 191: 1-14.

Kover, T. P. (1995). Application of a digital terrain model for the modelling of volcanic flows: a tool for volcanic hazard determination. MA Thesis. University at Buffalo, Buffalo, New York.

Lecointre, J. A., Hodgson, K.A., Neall, V. E., Cronin, S. J. (2004). Lahar-Triggering Mechanisms and Hazard at Ruapehu Volcano, New Zealand. *Natural Hazards* 31: 85-109.

Lecointre, J. A., Neall, V. E., Palmer, A. S. (1998). Quaternary lahar stratigraphy of the western Ruapehu ring plain, New Zealand. *New Zealand Journal of Geology and Geophysics* 41: 225-245.

Legros, F. (2002). The mobility of long-runout landslides. *Engineering Geology* 63: 301-331.

Leonard, G. S., Johnston, D. M., Paton, D., Chirstianson, A., Becker, J., Keys, H. (2008). Developing effective warning systems: Ongoing research at Ruapehu volcano, New Zealand. Journal of Volcanology and Geothermal research.

Lowe, D. J., Shane, P. A. R., Alloway, B. V., Newnham, R. M. (2008). Fingerprints and age models for widespread New Zealand tephra marker beds erupted since 30,000 years ago: a framework for NZ-INTIMATE. *Quaternary Science Reviews* 27: 95-126.

Lube, G., Cronin, S. J., Procter, J. N. (2009). Explaining the extreme mobility of volcanic ice-slurry flows, Ruapehu Volcano, New Zealand. *Geology* 37 (1): 15-18.

Manville, V., Stevens, N. F., Heron, D. (2003). Numerical simulation of debris avalanche hazards at Ruapehu: Application of the USGS-LAHARZ GIS-program. *Institute of Geological and Nuclear Sciences*. Science report 2002/16.

Martelli, K. M. (2007). Computer modelling of the potential hazard from scoria and ash flows on Mt. Ngauruhoe, Tongariro volcanic centre, New Zealand. Unpublished Masters Thesis, Massey University, Palmerston North, New Zealand.

McClelland, E. and Erwin, P. S. (2003). Was a dacite dome implicated in the 9,500 BP collapse of Mt Ruapehu? A palaeomagnetic investigation. *Bulletin of Volcanology* 65: 294-305.

McGuire, W.J. (1996). Volcano instability: a review of contemporary issues. In: W.J. McGuire, A.P. Jones and J. Neuberg (Editors), Volcano instability on the Earth and other planets. *Geological Society of London Special Publication*. 110: 1-23.

McGuire, W. J. (2003). Volcano instability and lateral collapse, ***Revista*** 1: 33-45.

McKinnon, M. (2010). Statistical analysis of physical characteristics and model parameters. MA Thesis. University of British Columbia, Vancouver.

Möbis, A. (2010). Understanding the Holocene explosive eruption record of the Tongariro Volcanic Centre, New Zealand. Unpublished PhD Thesis. Massey University, Palmerston North. 344 pages.

Murcia, H. F., Sheridan, M. F., Macias, J. L., Cortes, G. P. (2010). Titan2D simulations of pyroclastic flows at Cerro Machin Volcano, Columbia: Hazard implications. *Journal of South American Earth Sciences* 29: 161-170.

Nairn, I. A., Kobayashi, T., Nakagawa, M. (1998). The ~10 Ka multiple vent pyroclastics eruption sequence at Tongariro Volcanic Centre, Taupo Volcanic Zone, New Zealand: Part 1. Eruptive processes during regional extension. *Journal of Volcanology and Geothermal Research* 86: 19-44.

Nairn, I. A., Wood, C. P., Hewson, C. A. Y. (1979). Phreatic eruptions of Ruapehu: April 1975. *New Zealand Journal of Geology and Geophysics* 22: 155-173.

Nakagawa, M., Wada, K., Thordarson, T., Wood, C. P., Gamble, J. A. (1999). Petrological investigations of the 1995 and 1996 eruptions of Ruapehu volcano, New Zealand: formation of discrete and small magma pockets and their intermittent discharge. *Bulletin of Volcanology* 61: 15-31.

Neall, V. E., Cronin, S. J., Donoghue, S. L., Hodgson, K. A., Lecointre, J. A., Palmer, A. S., Procter, J. N., Purves, A. M., Stewart, R. B. (2001). Lahar Hazards Map for Ruapehu Volcano (2nd edition). *Institute of Natural Resources – Massey University Soil & Earth Sciences Occasional Publication No. 3.*

Neall, V. E., Houghton, B. F., Cronin, S. J., Donoghue, S. L., Hodgson, K. A., Johnston, D. M., Lecointre, J. A., Mitchell, A. R. (1999). Volcanic Hazards at Ruapehu Volcano. *Ministry of Civil Defence, Volcanic Hazards Information Series No. 8.*

Nicol, A. and Wallace, L. M. (2007). Temporal stability of deformation rates: comparison of geological and geodetic observations, Hikurangi subduction margin, New Zealand. *Earth and Planetary Science Letters* 258: 397-413.

O'Shea, B. E. (1954). Ruapehu and the Tangiwai disaster. *New Zealand Journal of Science and Technology* B36: 174-189.

Palmer, B. A. (1991). Holocene lahar deposits in the Whakapapa catchment, northwestern ring plain, Ruapehu volcano (North Island, New Zealand). *New Zealand Journal of Geology and Geophysics* 34: 177-190.

Palmer, B. A. and Neall, V. E. (1989). The Murimotu Formation – 9500 year old deposits of a debris avalanche and associated lahars, Mount Ruapehu, North Island, New Zealand. *New Zealand Journal of Geology and Geophysics* 32: 477-486.

Palmer, B. A., Purves, A. M., Donoghue, S. D. (1993). Controls on accumulation of a volcaniclastic fan, Ruapehu composite volcano, New Zealand. *Bulletin of Volcanology* 55: 176-189.

Palmer, B. A., Alloway, B. V., Neall, V. E. (1991). Volcanic-debris-avalanche deposit in New Zealand – Lithofacies organisation in unconfined, wet-avalanche flows. In: R. V. Fisher and G. A. Smith (Editors), Sedimentation in volcanic settings. *SEPM (Society for Sedimentary Geology) Special Publication* 45: 89-98.

Patra, A. K., Bauer, A. C., Michita, C. C., Pitman, E. B., Sheridan, M. F., Bursik, M., Rupp, B., Webber, A., Stinton, A. J., Namikawa, L. M., Renschler, C. S. (2005). Parallel adaptive numerical simulation of dry avalanches over natural terrain. *Journal of Volcanology and Geothermal Research* 139: 1-21.

Pillans, B., McGlone, M., Palmer, A., Mildenhall, D., Alloway, B., Berger, G. (1993). The Last Glacial Maximum in central and southern North Island, New Zealand: a paleoenvironmental reconstruction using the Kawakawa Tephra formation as a chronostratigraphy marker. *Palaeogeography, Palaeoclimatology, Palaeoecology*, 101: 283-304.

Pitman, E. B. and Tulyakov, S. (1998). Granular debris flows in 1 dimension. UB Math Department report.

Pitman, E. B., Nichita, C. C., Patra, A., Bauer, A., Sheridan, M., Bursik, M. (2003a). Computing granular avalanches and landslides. *Physics of Fluids* 15 (12): 3638-3646.

Pitman, E. B., Nichita, C. C., Patra, A., Bauer, A., Bursik, M., Webb, A. (2003b). A model of granular flows over an erodible surface. *Discrete and Continuous Dynamic Systems-Series B* 3 (4): 589-599.

Price, R. C., Gamble, J. A., Smith, I. E. M., Stewart, R, B., Eggins, S., Wright, I. C. (2005). An integrated model for the temporal evolution of andesites and rhyolites and crustal development in New Zealand's North Island. *Journal of Volcanology and Geothermal Research* 140: 1-24.

Procter, J. N., Cronin, S. J., Platz, J., Patra, A., Dalbey, K., Sheridan, M. F., Neall, V. E. (2010a). Mapping block-and-ash flow hazards based on Titan2D simulations: A case study from Mt. Taranaki, New Zealand. Natural Hazards 53: 483-501.

Procter, J. N., Cronin, S. J., Fuller, I. C., Sheridan, M., Neall, V. E., Keys, H. (2010b). Lahar hazard assessment using Titan2D for an alluvial fan with rapid changing geomorphology: Whangaehu River, Mt. Ruapehu. *Geomorphology* 116: 162-174.

Procter, J. N., Cronin, S. J., Fuller, I. C., Lube, G., Manville, V. (2010c). Quantifying the geomorphic impacts of a lake-breakout lahar, Mount Ruapehu, New Zealand. *Geology* 38 (1): 67-70.

Reyners, M., Eberhart-Phillips, D., Stuart, G., Nishimura, Y. (2006). Imaging subduction from the trench to 300 km depth beneath the central North Island, New Zealand, with Vp and Vp/Vs. Geophysical Journal International 165: 565-583.

Rowland, J. V., Wilson, C. J. N., Gravley, D. M. (2010). Spatial and temporal variations in magma-assisted rifting, Taupo Volcanic Zone, New Zealand. *Journal of Volcanology and Geothermal Research* 190: 89-108.

Rupp, B., Bursik, M., Patra, A., Pitman, E. B., Bauer, A., Nichita, C. C., Saucedo, R., Macias, J. (2003) Simulation of pyroclastic flows of Colima Volcano, Mexico, using the Titan2D program. Geophysical Research Abstracts 5: 12857. European Geophysical Society.

Saucedo, R., Macias, J., Sheridan, M. F., Bursik, M. I., Kamarawski, J. C. (2005). Modelling of pyroclastic flows of Colima Volcano, Mexico: implications for hazard assessment. *Journal of Volcanology and Geothermal Research* 139: 103-115.

Savage, S. B. and Hutter, K. (1989). The motion of a finite mass of granular material down a rough incline. *Journal of Fluid Mechanics* 199: 177-215.

Schilling, S. P. (1998). LAHARZ: GIS programs for automated mapping of lahar-inundation hazard zones. *United States Geological Survey Open-file Report* 98-638, Vancouver, Washington.

Scott, K. M., Macias, J. L., Naranjo, J. A., Rodriguez, S., McGeehin, J. P. (2001). Catastrophic debris flows transformed from landslides in volcanic terrains: mobility, hazard assessment and mitigation strategies. US Geological Survey Professional Paper 1630, 59p.

Sheridan, M. F., Stinton, A. J., Patra, A., Ptiman, E. B., Bauer, A., Nichita, C. C. (2005). Evaluating Titan2D mass-flow model using he 1963 Little Tahoma Peak avalanches, Mount Rainier, Washington. Journal of Volcanology and Geothermal Research 139: 89-102.

Sheridan, M. F., Stinton, A. J., Burkett, B., Patra, A., Nichita, C. C., Pitman, E. B. (2004). Application of Titan2D mass-flow model to potential hazards at Tungurahua Volcano, Ecuador. Geophysical Research Abstracts 6.

Siebert, L., Glicken, H., Ui, T. (1987). Volcanic hazards from Benzymianny- and Bandai-type eruptions. *Bulletin of Volcanology* 49: 435-459.

Stern, T. A. (1986). Geophysical studies of the upper crust within the Central Volcanic Region, New Zealand. *In* Late Cenozoic Volcanism in New Zealand, Vol. 23. I. E. M. Smith. *Bulletin, Royal Society of New Zealand*: 92-111.

Stevens, N. F., Manville, V., Heron, D. W. (2002). The sensitivity of a volcanic flow model to digital elevation model accuracy: Experiments with digitised map contours and interferometric SAR at Ruapehu and Taranaki volcanoes, New Zealand. *Journal of Volcanology and Geothermal Research* 119: 89-105.

Stinton, A. J., Gwenael, D., Burkett, B., Sheridan, M. F., Tharet, J. C., Patra, A. (2004). Titan2D simulated debris flow hazards: Arequipa, Peru. International Symposium on Environmental Software Systems (IESS) Conference Power Point Presentation. In Martelli (2007) Computer modelling of the potential hazard from scoria and ash flows on Mt. Ngauruhoe, Tongariro Volcanic Centre, New Zealand. MA Thesis. Massey University, Palmerston North.

Tecplot Inc. (2011). Tecplot 360. www.tecplot.com.

Thompson, N., Bennett, M. R., Petford, N. (2010). Development of characteristic volcanic debris avalanche deposit structures: New insight from distinct element simulations. *Journal of Volcanology and Geothermal Research* 192: 191-200.

Thorley, W. H. (1920s). Scene with Crater Lake, Mount Ruapehu. http://find.natlib.govt.nz/primo_library/libweb/action/dlDisplay.do?vid=TF&docId=nlnz_tapuhi1290439 (08/09/2010).

Topping, W. W. (1973). Tephrostratigraphy and chronology of late Quaternary eruptives from the Tongariro Volcanic Centre, New Zealand. *New Zealand Journal of Geology and Geophysics* 16 (3): 397-423.

Ui, T., Takarada, S., Yoshimoto, M. (2000). Debris Avalanches. In: H. Sigurdsson, B. Houghton, S. McNutt, H. Rymer and J. Stix (Editors), Encyclopedia of Volcanoes. Academic Press, San Diego. 617-626.

Vallance, J. M. (2000). Lahars. In: H. Sigurdsson, B. Houghton, S. McNutt, H. Rymer and J. Stix (Editors), Encyclopedia of Volcanoes. Academic Press, San Diego. 601-616.

Vignaux, M. and Weir, G. J. (1990). A general model for Mt. Ruapehu lahars. *Bulletin of Volcanology* 52: 381-390.

Villamor, P. and Berryman, K. R. (2006). Late Quaternary geometry and kinematics of faults at the southern termination of the Taupo Volcanic Zone, New Zealand. *New Zealand Journal of Geology and Geophysics* 49: 1-21.

Villamor, P. and Berryman, K. R. (2001). A late Quaternary extension rate in the Taupo Volcanic Zone, New Zealand, derived from fault slip data. *New Zealand Journal of Geology and Geophysics* 44(2): 243-269.

Widiwijayanti, C., Voight, B., Hidayat, D., Patra, A., Pitman, E. B. (2004). Validation of Titan2D flow model code for pyroclastic flows and debris avalanches at Soufrie Hills Volcano, Montserrat, BWI. EOS Trans, AGU, 85 (47), Fall meeting, supplement, Abstract.

Williams, K. (1986). Volcanoes of the south wind: a field guide to the volcanoes and landscape of the Tongariro National Park. Tongariro Natural History Society, Wellington.

Wilson, C. J., Houghton, B. F., McWilliams, M. O., Lanphere, M. A., Weaver, S. D., Briggs, R. M. (1995). Volcanic and structural evolution of Taupo Volcanic Zone, New Zealand: a review. *Journal of Volcanology and Geothermal Research* 68(1-3): 1-28.

Wilson, C. J. N. (1993). Stratigraphy, chronology, styles and dynamics of late Quaternary eruptions from Taupo Volcano, New Zealand. *Philosophical Transactions of The Royal Society of London A* 343: 205-306.

Yu, B., Dalbey, K., Webb, A., Bursik, M., Patra, A., Pitman, E. B., Nichita, C. (2009). Numerical issues in computing inundation areas over natural terrains using Savage-Hutter Theory. *Natural Hazards* 50: 249-267.

APPENDIX (on CD-ROM)

i) Fieldwork Log Book

ii) Lab work

- Lab work excel sheet (grain-size data and clay content)
- Particle Size Distribution Analysis (PSDA) runs
- X-Ray Diffraction (XRD) analysis

iii) Titan2D User Guide (Geophysical Mass Flow Group (GMFG) SUNY Buffalo)

iv) Titan2D input data

v) Simulation videos